NJ-2016-002-4

Design and Fabrication of Orthotropic Deck Details

FINAL REPORT
Vol. IV
February 2016

Submitted by

Sougata Roy, Ph.D.
Former Principal Research Scientist
ATLSS Center
Lehigh University

Soham Mukherjee
Former Research Assistant
ATLSS Center
Lehigh University

NJDOT Research Project Manager
Ms. Priscilla Ukpah

In cooperation with

New Jersey
Department of Transportation
Bureau of Research

DISCLAIMER

“The contents of this report reflect the views of the authors who are responsible for the facts and the accuracy of the data presented herein. The contents do not necessarily reflect the official views or policies of the New Jersey Department of Transportation. This report does not constitute a standard, specification, or regulation. “

TECHNICAL REPORT
STANDARD TITLE PAGE

1. Report No. NJ-2016-002-4	2.Government Accession No.	3. Recipient's Catalog No.
4. Design and Fabrication of Orthotropic Deck Details FINAL REPORT Vol. IV of VII Volumes		5. Report Date February 2016 6. Performing Organization Code
7. Author(s) Roy, Sougata Ph.D. and Soham Mukherjee		8. Performing Organization Report No.
9. Performing Organization Name and Address Advanced Technology for Large Structural Systems (ATLSS) Engineering Research Center, Lehigh University 117 ATLSS Drive Bethlehem, PA 18015		10. Work Unit No. 11. Contract or Grant No.
12. Sponsoring Agency Name and Address New Jersey Department of Transportation PO 600 Trenton, NJ 08625		13. Type of Report and Period Covered 14. Sponsoring Agency Code

15. Supplementary Notes
Volume 4 has 124 pages. All seven volumes total 804 pages.

16. Abstract
The objectives of the research were to verify the design and fabrication of the orthotropic deck details proposed for the lift bridge, for infinite fatigue life. Multi-level 3D finite element analyses (FEA) of the proposed deck were performed to determine the critical stresses at the connections, the corresponding load position, and the deck specimen. To develop cost-effective connection details, three variations of rib-to-floor beam and rib-to-deck plate connection details, including the influence of different fabrication parameters, were explored in full-scale small size mockups. Subsequently, the infinite life fatigue performance of the connection details were evaluated by laboratory testing of a full-scale prototype. The fatigue testing was conducted under simulated rear tandem axle loading of the AASHTO fatigue truck with adequate boundary condition. The prototype testing was runout after 8 million cycles, verifying the infinite life fatigue performance of the deck design.

17. Key Words	18. Distribution Statement
Lift Span, Orthotropic Deck, Rounded Bottom Ribs, Infinite Fatigue Life, Full-Scale Prototype, Fatigue Testing, AASHTO, Run-Out, Cost-Effective, Fabrication.	

19. Security Classif (of this report)	20. Security Classif. (of this page)	21. No of Pages	22. Price
Unclassified	Unclassified	124	

Form DOT F 1700.7 (8-69)

ACKNOWLEDGEMENTS

The authors wish to acknowledge the efforts of the New Jersey Department of Transportation (NJDOT) including the Project Manager Ms. Priscilla Ukpah and Ms. Camille Crichton-Sumners, Manager of the Bureau of Research. The authors thank the Research Selection and Implementation Panel members that included the following NJDOT employees: Ms. Xiaohua Hannah Cheng, Mr. Eddy Germain, Mr. Fred Lovett, Mr. Mahesh Patel, Mr. David Lambert, Mr. Nat Kasbekar, Mr. Eric Kraehenbuehl, Mr. Jayant Dalal, Mr. Vijaykumar Thaker, Ms. Kiranben Patel and Mr. Javier Estradal. These individuals offered valuable comments and suggestions on the research project resulting in an improved product.

Editing of the final report was performed by Dr. Richard Sause, Director of the ATLSS Center.

The research was performed with the assistance of Mr. Xudong Zhao, Mr. Philipp Keller, Mr. Frank Artmont, Mr. Yeun Chul Park and Mr. Juan Tzoc, and the support staff of ATLSS Engineering Research Center and Fritz Engineering Laboratory for their help with successful execution of the project.

The authors would also like to specially thank Mr. Ronnie Medlock, Vice President of Technical Services of High Steel Structures for valuable input on fabrication of this deck and to Dr. John W. Fisher for sharing his vast experience regarding orthotropic decks.

CONTENTS (VOLUME I)

CONTENTS (VOLUME II)

CONTENTS (VOLUME III)

CONTENTS (VOLUME IV)

CONTENTS (VOLUME V)

CONTENTS (VOLUME VI)

CONTENTS (VOLUME VII)

LIST OF FIGURES (VOLUME IV)

LIST OF TABLES (VOLUME IV)

8. FUL-SIZE LABORATORY STUDIES

8.1 Test Setup

The north elevation of the test setup is shown in Figure 335. As discussed earlier, the full-size prototype deck specimen consisting of a deck plate stiffened by five ribs and three floor beams and part of the box girder (referred as edge girder), was tested in a novel test setup with adequate fixtures which was devised based on a multi-level 3D FEA to reproduce the critical stress state of the full bridge deck in the specimen. Refer section 6.3 of Volume III for description of the full-size deck specimen. The fixtures for the specimen were designed to simulate the boundary conditions of the FE model (refer section 6.4.5 of Volume III for the boundary conditions). As discussed earlier, the extensions of the floor beam (floor beam extensions) beyond the deck plate were fabricated separately and are discussed as a part of fixtures in section 8.2.4. The specimen was oriented along the east-west direction of the laboratory as shown in Figure 335 and will be referred accordingly in subsequent texts. The floor beam extensions were bolted spliced to the floor beams and on the other side (north side) were connected to the reaction wall using wall fixtures to simulate the fixed boundary conditions at the end of the floor beams. Wall Columns B-1, C and B-2 (Figure 335) were connected to the west outer, inner and east outer floor beams respectively. The bottom flange of the edge girder was supported on Support Columns A & B at the south side of the specimen aligned with the centerline of the east and the west outer floor beams. The connection between the support columns and the edge girder simulated the pinned boundary condition at the south side of the specimen. The above-deck actuators were hung from an arrangement of two parallel cross beams and one longitudinal loading beam as shown in Figure 335 and Figure 336. Later on, a secondary loading beam (Figure 335) was installed on the top of the primary loading beam to reduce the deflection under the reactions from the above-deck actuators. The bottom flange of the edge girder, aligned with the centerline of the inner floor beam, was supported on an under-deck actuator (Figure 337) that was used for simulating the global displacement boundary condition. As shown in the sectional elevation of the test setup in Figure 337, the under-deck actuator was mounted on the laboratory base through actuator support and was connected to the edge girder bottom flange by actuator connector. Note that the above-deck actuators were not at the inner floor beam location, however they are shown in Figure 337 to show the transverse load disposition. The detail of the fixtures for the prototype deck specimen are discussed in detail in section 8.2. Most of the fixtures were built by Haberle Steel Inc. of Souderton, Pennsylvania, and the rest were used from existing inventory.

Total three hydraulic actuators, two above the deck and one under the deck, were used for applying the load to the prototype deck and for simulating the boundary condition respectively. The details of the actuators are provided in section 8.7.3. The overhead actuators were located 4 ft. (1.2 m) apart, symmetrically 2 ft. on either side of the floor beam as shown in Figure 335. The reason for this loading arrangement is discussed in section 8.7.2. The above-deck actuators to the east and the west side of the specimen will be referred as east actuator and west actuator respectively in subsequent texts. The west actuator was located directly on the transverse splice location (Figure 335).

The above-deck loading simulated the tandem rear axle of an AASHTO fatigue truck in the most critical disposition determined from FEA and the under-deck actuator provided the global displacement boundary condition. The details of the loading and the loading protocol are discussed in section 8.7. At each above-deck actuator location, a spreader beam was installed to distribute the loads from the actuator to the deck via two rectangular loading pads placed 6 ft. (1.8 m) apart in the transverse direction. Each loading pad simulated the contact of a pair of wheels with rubber tires, at each end of an axle.

A W12x190 column was installed beside the under-deck actuator as a safety measure, so that the inner floor beam rested on it when testing was stopped and the under-deck actuator was not hydraulically live. The safety column was anchored to the lab floor through the actuator support for the under-deck actuator. The height of the safety column was 9 in. (229 mm) shorter than the height of the inner floor beam above the laboratory floor. The difference in height was compensated by a 7 in. (178 mm) long stub column which was clamped to the safety column and the remaining gap was compensated by shims. The shims were removed during testing, when the inner floor beam was supported by the live under-deck actuator.

8.2 Test Fixtures

8.2.1 Wall Fixtures

The floor beam extensions were fixed to the north reaction wall by wall fixtures. The wall fixtures are identified as wall columns B-1, B-2 and C in a 3D rendered view of fixtures in Figure 338. The wall fixtures after installation in the lab are shown in Figure 339. Wall columns B-1 and B-2 were different from wall column C and are discussed separately in the following. A typical connection between the wall fixture and the floor beam extension is shown in Figure 340.

Wall Column C

This fixture was fabricated by modifying another fixture which was used in a previous project after modifications. The wall column was fabricated from a W14x398 wide flange section. Existing connection plates were removed and two new connection plates were attached perpendicular to the top flange of the wall column, vertically at 3 ft 4 in (1 m) apart, by CJP welds. The plates were $1^1/_2$ in (38 mm) thick and 1 ft. $1\ ^1/_2$ in (343 mm) long normal to the flange surface. The top flange of the floor beam extension was supported on the top connection plate, and the bottom flange of the floor beam extension was supported on the bottom connection plate (Figure 340). The connection plates were fastened to the top and bottom flanges of the floor beam extension using 1 in (25 mm) diameter A325 bolts. The wall column was fastened to the reaction wall at three elevations using anchor rods that extended through the reaction wall. The height of anchorage of the wall column was decided such that the bottom of the specimen was clear of the pipelines running in the lab. Existing angles from the wall column were removed and two new angles were provided on either side of the floor beam extension, which were welded to the wall column. The outstanding legs of the angles were bolted

to the floor beam extension web using 1 in (25 mm) diameter A325 bolts. The connection between the connection plates and the floor beam extension was designed as a moment connection. The angle-to-floor beam extension connections were designed to carry vertical shear only. All bolted connections between the floor beam extensions and wall column were designed as slip critical.

Wall Columns B1 and B2

This fixtures were fabricated using a W14×426 wide flange section. The outer floor beams were eccentric to the wall anchor locations. So, for providing the fixed connections for the floor beam extensions, a built up I-section of the same depth of the wall columns were connected to the wall columns, to the west side for wall column B-1 and to the east side for wall column B-2. These built-up sections will be referred as wall column extensions in subsequent texts. The wall column extensions didn't extend the full-height of the wall columns. The wall column extensions were fabricated from 1 ½ in. (38 mm) flange plates and 1 in. (25 mm) web plate. The flanges of the wall column extensions were welded to the flanges of the wall columns by CJP weld. Two connection plates were attached perpendicular to the top flange surface of the wall column extensions, vertically at 3 ft 4 in (1 m) apart, by CJP welds. The plates were $1^1/_2$ in (38 mm) thick and 1 ft. $1\ ^1/_2$ in (343 mm) long normal to the flange surface. The floor beam extensions for the two outer floor beams were connected to the wall column extensions. The detail of the connection was similar to the connection between the wall column C and the inner floor beam extension. All bolted connections between the floor beam extensions and wall columns were designed as slip critical.

8.2.2 Support Columns

One support column was provided at each end of the edge girder flange aligned with the two outer floor beams and are identified as support column A and support column B in Figure 338. The support columns after installation in the lab in the lab are shown in Figure 339. Support column A supported the edge girder flange at the east side, while support column B supported the edge girder flange at the west side. The support column fixture consisted of a W12x190 section which was fastened at the bottom to the lab floor using base plate and floor anchors, while at the top was connected to the edge girder flange by a top plate and a sole plate. Elevation of a typical support column fixture is shown in Figure 341. The bottom end of the W12x190 column was welded to a 2 ½ in. thick base plate using PJP weld with 45° bevel on the column, and the base plate was fastened to the lab floor by floor anchors. The top of the column was welded to 2 in. thick top plate using PJP weld with 45° bevel on the column. The top plate was connected to the edge girder flange by a 2 in. thick sole plate and 1 in. (25 mm) diameter A325 bolts. The dimensions of the sole plate was much smaller than top plate to reduce the moment constraint as much as possible.

8.2.3 Under-deck Actuator Fixture

The under-deck actuator was attached to the edge girder flange by using fixture (actuator connector) built from 1 in. (25 mm) thick plates. This fixture is identified as

actuator connector in Figure 337. The height of the fixtures was decided based on the height and the stroke (displacement) of the actuator. The details of the actuators are provided in section 8.7.3. The height of actuator connector was 1 ft. (305 mm). The top clevis of the under-deck actuator was bolted to the actuator connector and the top plate of the actuator connector was bolted to the edge girder bottom flange. The bottom clevis of the under-deck actuator was bolted to a plate fixture identified as actuator support in Figure 338, which was fastened to the lab floor by floor anchors. The height of the actuator support was 10 ¼ in.

8.2.4 Floor Beam Extensions

The floor beam extensions were built-up I-sections, 3 ft. 6 in. (1.1 m) long and 3 ft. 4 in. (1 m) deep matching with the overall depth of the floor beam including the deck plate. The details of the floor beam extensions are shown in Figure 342. The web plate was ½ in. thick matching with the web thickness of the floor beams and the flange plates were ¾ in. thick matching with the thickness of deck plate and floor beam flange. The web plate was welded to the top and bottom flange plates employing $^{5}/_{16}$ in. (8 mm) back-to-back fillet welds. The floor beam extensions were bolted spliced to the floor beams. The splice connection was designed as slip critical.

8.2.5 Cross Beam Fixtures

Wall columns (wall column A) and floor columns were used to support the cross beams, as shown in Figure 336. Both the wall column and the floor column were fabricated from W12×190 sections. The wall columns were fastened to the wall by wall anchors. The floor columns were fastened to the lab floor at its base by using floor anchor adapter and floor anchors.

8.2.6 Cross Beams

The cross beams were comprised of a pair of wide flanged sections as shown in Figure 335. W30×292 sections were used to fabricate the cross beams on the west side. W30x235 sections from the existing inventory were used for the cross beams on the east side. The cross beams were 20 ft. 6 in. (6.2 m) long and were provided with 3 in. (76 mm) long slotted holes in the bottom flange for hanging the loading beam.

8.2.7 Loading Beam

The loading beam, spanning longitudinally across the cross beams, was fabricated from W14×233 section (Figure 335). The distance between the centerlines of the east and the west cross beams were 10 ft. To increase the flexural stiffness of the loading beam and to reduce deflection under the reactions from the actuators, the moment of inertia was increased by adding a secondary beam on the top of the primary (lower) beam. The top flange of the loading beam was bolted to the bottom flange of the cross beams. The bolted holes were slotted to allow adjustments during installation of the loading at the desired position. The above-deck actuators were hung from the primary loading beam (Figure 335) at the desired position, the top clevis of the above-deck actuators were bolted to the bottom flange of the loading beam.

8.2.8 Spreader Beam

The load from each above-deck actuators was distributed to two load pads by a spreader beam (Figures 336 and 337). The spreader beams were fabricated from W12×136 sections. At the ends of the spreader beam, 1 in (25 mm) diameter semicircular rods were attached to the soffit of spreader beams aligned with the center line of the loading blocks, 6 ft (1.829 m) apart in the transverse direction. These rods were oriented transverse to the spreader beam and were welded on their flat face to the beam soffit. The spreader beams were supported on the loading blocks at the semicircular rods, creating a knife edge interface between the load blocks and spreader beam. Each loading block was restrained in position (against sliding) using four threaded rods passing through the bottom flange of the spreader beams. The loading blocks were fastened to the spreader beams by tightening the nuts on these threaded rods, only when the spreader beam and the loading blocks were lifted off the deck for balancing instruments under zero load condition. At other times, the nuts on the threaded rods were left loose to allow vertical separation between spreader beams and the loading blocks for effective knife edge interface.

8.2.9 Loading Block and Load Pads

The loading block was designed as 6 5/8 in (168 mm) high, assuming a 30° spread of load through the loading block. A pair of 5/8 in (16 mm) thick rubber pads (loading pads) was glued under the loading block to simulate a pair of rubber tires (wheels). Each loading pad was 10 in (254 mm) long and $9^1/_2$ in (241 mm) wide, and were oriented such that the longer dimension was perpendicular to the spreader beam. A transverse gap of 1 in (25 mm) was provided at the center of the loading pad, representing the separation between a pair of tires (wheels). Thus, the outer dimensions of the loading pads were 10 in (254 mm) long and 20 in (508 mm) wide, in accordance with the tire patch dimension specified in the AASHTO LRFD Bridge Design Specifications. Guide angles were secured on the deck using C-clamps that contained the loading blocks in position during fatigue testing.

8.3 Installation of Specimen and Loading Setup

The fixtures for the full-size specimen (wall columns and the support columns) were installed at ATLSS prior to the arrival of the specimen (Figure 339) as they were the primary support for the prototype specimen. The floor beam extensions were then installed. The floor beam extensions were fabricated by Haberle Steel Inc. of Souderton, Pennsylvania. Bolt holes were drilled on the floor beam extensions towards the specimen side (south side) by the fabricator. On the other side, holes were drilled on the floor beam extensions with the connection plates and angles on the wall columns as templates. A safety column was then mounted on the actuator support and connected to the lab floor thorough floor anchors. The installed fixtures in the lab are shown in Figure 339.

A discussed earlier, the prototype deck specimen was fabricated by High Steel Structures of Lancaster, Pennsylvania. The deck was fabricated in two panels, the long

panel was at the east side of the lab and the short panel at the west side of the lab. Accordingly, the long and the short panels will be referred as the east panel and the west panel respectively in subsequent texts. The fabricator of the specimen was responsible for installing the specimen. The two deck panels were spliced in the laboratory by a CJP groove weld at the deck plate and bolted splice at the ribs and the edge girder, simulating the field splice in the real bridge. This process mock up the actual deck installation in field.

The deck panels were shipped to ATLSS by the fabricator on January 27, 2014. Level measurements of the deck surface was performed on the two deck panels. A string attached two small weights placed at the two ends of the deck formed a chord. This chord was used as a reference datum from where the deck levels were measured using a measuring scale (Figure 343). Significant out-of-flatness were observed in the deck panels which exceeded the specified tolerance of ¼ in. Consequently, the deck panels were sent back to the fabrication shop for heat treatment of the deck panels. After heat straightening, the deck panels were reshipped to ATLSS on March 3, 2014. The east panel was installed first as shown in Figure 344. The north end of the floor beams were connected to the floor beam extensions by bolted splice and the bottom flange of the edge girder was bolted to support column A. The bolt holes on the floor beams and the edge girder flange were drilled with the splice plates on the floor beam extensions and the top plates on support column respectively as templates. The west panel was then installed in the similar way as the east panel and is shown in Figure 345. During assembly of the deck panels in the laboratory, significant lack of fit was noted between the panels due to the weld heat effects on asymmetric cross section of the specimen. The heat marks on the deck specimen are shown in Figure 346. The maximum out-of-flatness in the deck plate was measured to be about $^{3}/_{4}$ in, which exceeded the specified tolerance of $^{1}/_{4}$ in. At the transverse splice, a relative out-of-flatness of the deck plates exceeding $^{5}/_{8}$ in. existed before welding, which also exceeded the specified tolerance of $^{1}/_{16}$ in. between the mating deck panels (Figures Figure 347 and Figure 348). The out-of-flatness was reduced considerably to about $^{3}/_{16}$ in. (Figure 348) by jacking up the west panel (Figure 349) and tack welding the panels, which still exceed the specified tolerance. The maximum root gap at the transverse splice location was about ½ in. (Figure 350) which also exceeded the specified tolerance of $^{3}/_{8}$ in. The ribs were also mis-aligned at the transvers splice location and the maximum misalignment was about $^{3}/_{8}$ in. (Figure 351) which also exceeded the specified tolerance of $^{1}/_{16}$ in.

The ribs and the edge girder were bolted spliced using slip critical bolted connections. Access holes were provide at the soffit of the ribs at the spliced sections for tightening the bolts. The ribs were hermitically sealed by provided full depth 3/8 in. (9.5 mm) sealing plates on both sides of the access hole. The edge girder was also spliced by slip critical bolted connection. At the junction with the floor beam, it was continuous. Copes were provided in the floor beams for running the edge girder-to-deck plate weld uninterrupted. After completion of the bolted splice connection for the ribs and the edge girder, the CJP weld for the deck plate splice was done on March 24, 2014. The details of the transverse deck splice is shown in Figure 352. The backing bar for the CJP weld was specified to be removed after welding, which was accomplished by a brass backing. Copes were provided in the ribs and in the edge girder for running the backing

bar uninterrupted. Initially, a root pass with Shielded Metal Arc Welding (SMAW) process was done with the backing bar in place. In addition to the root pass, total seven passes of SAW process (Figure 353) was required to perform the CJP deck splice. The backing bar was removed after 3 passes of the SAW process. Figure 354 shows the weld root at the underside of the deck after removal of the backing par. Visual inspection of the weld root showed multiple areas of LOF, and the condition of the weld root was questionable. On March 25, 2014, the welder from High Steel performed two root passes in overhead position to repair the weld root, however without any prior approval from the client or the research team. Start and stop of the repair weld were observed at each of the rib copes (provided for running the backing bar), as those areas cannot be repaired due to lack of access. The welded deck splice was ultrasonically inspected (Figure 355) on April 1, 2014 by KTA QA inspector. Rejectable indications were observed at the weld start and stop over the rib copes. In addition to this, rejectable indications were also observed at 10 other locations, where the depth of indications ranged between 0.54 in. to 0.73 in. (note that the deck plate thickness is ¾ in.). Accordingly, the weld root was repaired on April 21, 2014, by SMAW process in overhead position (Figures 356 and 357). Due to lack of access, extensive efforts were required for repairing the weld root inside the rib (Figure 357). Figure 358 shows the weld root after the repair. The weld root over the rib copes could not be repaired properly due to lack of access (Figure 359). Even after the repair, the weld condition at the transverse deck splice location was questionable. The maximum weld reinforcement at the deck splice location was about $^{1}/_{8}$ in. and it was observed at two locations of weld start and stop. The weld reinforcement was within the specified fabrication tolerance and hence was not grounded with deck plate surface. Laser measurements of the deck level was conducted after completion of specimen installation. A reference datum (red line in Figure 360) was established using a laser equipment, and deck levels were measured from that reference datum with a tape measure (Figure 360). The deck surface was plotted using the laser measurements and is shown in Figure 361. Maximum elevation difference of $^{3}/_{16}$ in. was observed at the transverse splice location.

As discussed in previous paragraphs, significant deviations from the specified fabrication tolerances was observed particularly at the transverse splice location during installation of the specimen. The quality of the CJP weld at the transverse splice was questionable and had the possibility of exhibiting fatigue cracks during the course of the fatigue test. The transverse splice location was at one of the loaded section (east above-deck actuator), which gave the opportunity of testing the splice to see the effect of these deviations on the fatigue performance of the deck.

After installation of the specimen, the under-deck actuator was installed on the actuator support and was bolted to the bottom flange of the edge girder through actuator connector. The floor columns were fastened to the laboratory floor. Crawl tests were performed first on the deck before the static and the fatigue tests. The crawl test setup is discussed in detail in section 8.6. After the completion of crawl tests, the loading setup for the static and fatigue tests were installed. The cross beams were installed at a height of 23 ft. 5 in. (Figure 336) above the lab floor and were connected to a wall column (Wall Column A in Figure 336) attached to the reaction wall at the north end, and to a floor column at the south end (Figure 336). The above-deck actuators were

bolted to the loading beam and the entire assembly was hung from the cross beams at the desired longitudinal and transverse position. The spreader beams along with the loading blocks and the loading pads were placed on the deck plate, oriented in the transverse direction symmetric with the actuators. The bottom clevises of the actuator was then fastened to the top flange of the spreader beams. Finally the guide angles were installed containing the loading blocks in position during fatigue testing. The final test setup at ATLSS center is shown in Figure 362.

8.4 Instrumentation

8.4.1 Overview

The prototype deck was extensively instrumented to determine its global response and to measure the local stresses at the fatigue sensitive connection details. The instrumentation plan was developed based on FEA of the full-size specimen model (refer to section 6.4 of Volume III). Stresses were measured using surface mounted, encapsulated metallic, bonded or welded electrical resistance strain gauges. In addition, vertical displacement of the ribs, the inner floor beam and the deck plate were measured using linear variable differential transformers (LVDTs). The majority of the strain gauges were installed at the Rib 1-to-inner floor connection on: the inner floor beam web and the north and south walls of Rib 1. Strain gages were also installed on the top and the bottom surfaces of the deck plate and the inner and the outer surfaces of rib wall of ribs 1, 2, 4 and 5. The strain gages on the top and the bottom surfaces of the deck plate were concentrated near the deck splice and at the rib-to-deck plate connection. These two transverse sections are identified as X-X and Z-Z, which are at 2 ft. (610 mm) west and east of inner floor beam, respectively. Sections X-X and Z-Z coincided with the west and the east above-deck actuators, respectively. Gages on the top surface of the deck plate were also installed at the centerline of inner floor beam identified as section Y-Y. The gages on the inner and the outer surfaces of the rib wall were installed at section Z-Z abutting the rib-to-deck welds on either side of the ribs. Other strain gauges were installed at: the soffit of Rib 1; the rib wall and sealing plate at the rib-to-sealing plate connection; the inner floor beam flange and the edge girder web near the edge girder-to-inner floor beam connection; the bottom flange of inner floor beam at section Y-Y; the splice plates and the stiffeners to the edge girder. The instrumentation on the full-size specimen is shown in Figure 363.

During the initial static tests, 106 uniaxial gauges of ¼ in. (6 mm) gage length, 75 uniaxial gauges of 1 mm gage length, 18 rosettes and 7 LVDTs were installed on the prototype deck, involving a total of 242 data channels. In addition, the load and the displacement outputs from the three actuator load cells were recorded in 6 data channels. During subsequent fatigue testing, the LVDTs were disconnected.

In this document, each channel associated with the instruments is identified by a number for reporting purposes. The channel number is denoted by the Arabic numeral such as “1, 2, 3, etc.”. Each element of the rosette is identified by a unique number.

8.4.2 Details of Sensors

Strain gauges of uni-axial and rosette configurations having different resistances and applicable temperatures were used. Gauges had either 1 mm or ¼ in (6 mm) gauge lengths. On the deck plate, both weldable and bondable uni-axial gages were used. The strain gages used on the inner floor beam web and the ribs were bondable and weldable uniaxial gages and rosette type. The different types of strain gauges used were:

1. Vishay Micro Measurements LWK-06-W250B-350 uni-axial weldable gauges having 350Ω resistance and ¼ in. (6 mm) gauge length;
2. Texas Measurements FLA-1-11-1L uni-axial bondable gauges having 120Ω resistance and 1 mm gauge length; and
3. Texas Measurements FRA-1-11-1L stacked rosette (also called rectangular rosette) bondable gauges having 120Ω resistance and 1 mm gauge length.

Prior to installation of strain gauges, the rust on the surface of the specimen was ground to bare steel at the strain gauge locations. The strain gauges were installed in accordance with the guidelines provided by the strain gauge manufacturers.

The LVDTs were Macro Sensors DC 750-1000, having a nominal displacement range of ±1 in. (±25 mm).

8.4.3 Instrumentation on Deck Plate

45 weldable uni-axial gages of ¼ in. gauge length and 8 bondable uni-axial gauges of 1 mm gauge length were installed on the top and bottom surfaces of the deck plate (channels 163 to 215).

The strain gauges on the deck plate were installed primarily at the rib-to-deck plate connection, at section Z-Z (channels 163 to 180 and 191 to 207). The strain gages were provided at ribs 1, 2, 4 and 5, both at the north and the south intersection of the rib walls with the deck plate, and were oriented in the transverse direction of the deck as detailed in Figure 364. The strain gages were intended to capture the local out-of-plane bending at the rib-to-deck plate connection under wheel loads. At each intersection with the rib wall, two back-to-back strain gages were provided on the top and the bottom surfaces of the deck plate adjacent to the rib-to-deck plate weld toe, outside the rib, to capture bending stress in the deck plate. Gages on the bottom of the deck plate were of 1 mm gage length to capture the peak localized strain due to steep stress gradient observed in FEA at the weld toe notch. These gages were installed at a distance 0.5t or $^{3}/_{8}$ in. (9.5 mm) from the weld toe on the deck plate, where “t” is the thickness of the deck plate. Another uniaxial gage of ¼ in. gauge length was installed on the bottom surface of the deck plate at 1.5t or 1 $^{1}/_{8}$ in. (28.6 mm) from the weld toe on the deck plate. The rationale behind having gauges at 0.5 t and 1.5 t was to extrapolate the stress values from these two measurements to the weld toe as per the AASHTO recommendations. A uniaxial strain of ¼ in. (6 mm) gage length was also provided on the top of the deck plate, within the projection of the rib, close to the root of the rib-to-deck plate weld. Due

to the limitations posed by the fabrication of the requirements of closed rib orthotropic decks, the strain gage at the bottom of the deck plate aligned with this gage on the top surface could not be installed. The layout of the gages on the deck at the intersection with a typical north wall of a rib is shown as Detail A in Figure 364. The layout of the gages on the deck plate at the intersection with the south wall of a rib is similar to Detail A but handed. The gages on the top of the deck plate were covered with mastic to protect it from getting damaged from the pounding effect of the load pads, as most of the gages at the rib-to-deck plate connection were under the load pads. At each intersection with the rib, a pair of back to back strain gauges was also installed on the rib walls, abutting the rib-to-deck plate weld toe on the rib. These gauges were provided to capture the bending of the rib wall and are discussed in section 8.4.4 along with the instrumentation on ribs.

Uniaxial gages of ¼ in. (6 mm) gauge length were installed in back-to-back configuration on the top and the bottom surfaces of deck plate on either side of the transverse CJP deck plate splice at section X-X, abutting the weld toes as shown in Figure 365 (channels 181 to 188 and 208 to 215). These gages were oriented in the longitudinal direction of the deck plate, along the centerline of the south-west and the north-west load pads and were installed in the 1 in. gap between the load pads. On each side of the splice, the gages were installed at a distance of 0.5t or $^{3}/_{8}$ in. (9.5 mm) and 1.5t or 1 $^{1}/_{8}$ in. (28.6 mm) from the weld toes on the deck plate. The rationale behind having gauges at 0.5 t and 1.5 t has already been discussed earlier. The purpose of these gages was to measure the high tensile and compressive stresses observed from FEA at the bottom and the top surfaces of the deck plate locally under the load pads due to longitudinal bending of the deck. The arrangement of the gages in back-to-back configuration also allowed to determine the membrane stresses in the deck plate if any. The gages on the top of the deck plate were covered with mastic to protect it from getting damaged from the pounding effect of the load pads

Three LVDTs were installed under the deck plate at section Z-Z, for measuring the vertical displacement of the deck (Figure 366). The LVDTs were attached to the soffit of the deck plate: between ribs 1 and 2 (channel 8); between ribs 3 and 4 (channel 10); and between ribs 4 and 5 (channel 12). Additional LVDTs were also installed at the same section on the soffit of the ribs, which are discussed in the following section along with instrumentation on ribs. The relative displacements between the LVDTs provided an assessment of deformation of deck plate with respect to the rib. Two uniaxial gages (channels 189 and 190) of ¼ in. (6 mm) gage length were installed on the top surface of the deck plate at section Y-Y, orientated along the transverse direction of the deck. These gages were intended to capture the global transverse bending stress in the deck. Aligned with these gages, uniaxial gages were installed on the bottom surface of the inner floor beam flange, which will be discussed in section 8.4.5.

8.4.4 Instrumentation on Ribs

31 uni-axial gages of ¼ in. gauge length, 34 uni-axial gages of 1 mm gauge length and 10 rosettes were installed on the rib wall (channels 68 to 162). Apart from the gages at the rib-to-floor beam and rib-to-deck plate connection, gages were also installed on the

inner surface of the rib walls at the connection with the sealing plates provided inside the ribs near the transverse deck splice.

3D FEA of the full bridge deck identified the rib 1-to-inner floor beam connection as the most fatigue critical. All the gauges on the Rib 1 wall at the junction with the inner floor beam were installed on the north and south walls symmetric with respect to the centerline of Rib 1, both to the east and the west sides of the rib (channels 68 to 137 in Figure 367). The figure shows the north wall of Rib 1. The channel numbers of the gages installed on the south wall of Rib 1 are shown in parenthesis. Fatigue cracking at the weld toe is primarily attributed to the crack growth from the micro discontinuities at the weld toe subject to the stress range normal to the weld toe. FEA results showed that the maximum stress in the Rib 1 wall normal to the rib-to-floor beam weld toe occurred at a section of the rib wall at about 50° from the centerline of the rib soffit. So the weld toe at 50° was identified as the potential zone for fatigue cracking and it was decided to install gages extensively at that location. Accordingly, a bondable rectangular rosette gauge of 1 mm gauge length was installed abutting the rib-to-floor beam weld toe on the rib wall at a distance of 0.4t or $^{1}/_{8}$ in. (3.2 mm) from the weld toe, to capture the complex stress distribution at that location and to determine the magnitude and direction of principal stresses at that location. One of the arms of the rosette was aligned normal to the weld toe. Due to the presence of steep stress gradient close to the weld toe, it was needed to capture the peak localized strains to have the correct stress distribution normal to the weld toe along the 50° radial line. Accordingly, a uniaxial gage of 1 mm gage length was installed on the rib wall next to the rosette, at t or $^{5}/_{16}$ in. from the weld toe measured normal to the weld toe on the rib. The uniaxial gage was oriented normal to the weld toe. The rationale behind having gauges at 0.4 t and t was to extrapolate the stress values from these two measurements to the weld toe. In order to get the complete distribution of stress normal to weld toe along the 50° radial line, three more uniaxial gauges of ¼ in. gauge length were installed at a distances of 1 in., 2 ½ in. and 4 in. respectively, oriented normal to the weld toe on the rib. The stress obtained from the gauge measurements at 4 in. from the weld toe was essentially the nominal stress on the rib wall due to global longitudinal bending of the rib, free from the notch effect of the weld toe. Gages were also installed in identical pattern along the 25° radial line and also at the soffit of Rib 1. Though 50° was the location of highest stresses normal to the weld toe, weld root at 25° was identified from FEA as the location of maximum principal stress. Maximum principal stress is critical for crack growth from volumetric discontinuities as was observed from the fatigue tests of small-size mockups. However, it is not possible to measure the stress at weld root with the available technology. So, gages were installed along 25° radial lines and also at the rib soffit to capture the entire stress distribution at the weld toe near the rounding of Rib 1 wall at the junction with inner floor beam.

As discussed in the previous section and shown in Figure 364, strain gages were installed on the deck plate and the rib wall at the rib-to-deck plate welds of ribs 1, 2, 4 and 5, at the transverse section Z-Z. The strain gages (channels 138 to 141 and 146 to 158) were installed on both inner and outer faces of the rib wall in back-to-back configuration and were oriented along the inclined depth of the rib wall. The inside strain gages were installed at 13/32 in. (10 mm) from the weld root. High temperature resistant

weldable strain gages of ¼ in. (6 mm) gage length were installed on the inner face of the rib wall to avoid damage to the strain gages from the high heat produced during welding of the rib to the deck plate. However, all the gages on the inner surface of the rib walls were damaged during the rib-to-deck weld fabrication. On the outer surface of the rib wall, uniaxial gages of 1 mm gage length were installed at distances of at 0.5t or 5/32 in. and 1.5t or 15/32 in. from the weld toe on the deck plate. The rationale behind having gauges at 0.5 t and 1.5 t has already been discussed earlier. The purpose of the strain gauges on the ribs walls was to measure the out-of-plane bending of the rib wall under wheel loads and the high compressive stress which was observed from FEA at the weld toe on the ribs due to localized bending of the rib-to-deck plate connection under the wheel loads.

Gages were installed on the inner surface of north and south walls of ribs 1 and 5, adjacent to the rib-to-sealing plate connection (channels 142 to 145 and 159 to 162 in Figure 368). Gages were installed only for the sealing plate towards the inner floor beam. These gages were installed at High Steel facility (Figure 369). It was observed from FEA that the stress normal to the weld toe was maximum at 60° from the rib soffit. So, uniaxial gages of 1 mm gauge length were installed at distances of 0.5t or 5/32 in. and 1.5t or 15/32 in. from the weld toes on the ribs, along 60° radial lines. These gages were oriented along the longitudinal direction of the deck.

Three LVDTs were installed on the soffit of the ribs 1, 2 and 4 at section Z-Z. The LVDTs were identified as: channel 7 on Rib 1; channel 9 on Rib 2; and channel 11 on Rib 4.

8.4.5 Instrumentation on Floor Beam

Among the three floor beams, only the inner floor beam around which the loads were positioned, was instrumented with strain gages. In total, 7 uni-axial gages of ¼ in. gauge length, 23 uni-axial gages of 1 mm gauge length and 8 rosettes were installed on inner floor beam (channels 14 to 67). Strain gauges on the inner floor beam were primarily installed at the connection with Rib 1, symmetrically on the north and south sides of the rib as shown in Figure 370. The strain gages were installed in back-to-back configuration on the east and the west faces of the floor beam web to measure the in-plane membrane and out-of-plane bending stress components. Figure 370 shows the east face of the floor beam, and the channel numbers of the gages installed on the west face are shown in parenthesis. Additional strain gauges were installed on the top and bottom faces of the inner floor beam bottom flange at the connection with edge girder and on the bottom face of the bottom flange at section Y-Y.

FEA of the full bridge deck showed that a diagonal tension field developed from the bottom flange of the of the floor beam to the top corner formed by the floor beam web and the edge girder. As the stress field deviated around the cutout in the floor beam web, high stress concentration was observed at the rib 1-to-inner floor beam weld toe, which was further elevated by the weld toe notch. As such, the rib 1-to-inner floor beam weld toe around the rib rounding was identified as the most critical for fatigue cracking. Fatigue cracking at the weld toe is primarily attributed to the crack growth from the

micro discontinuities at the weld toe subject to the stress range normal to the weld toe. Similar to Rib 1, FEA results showed that the maximum stresses in the inner floor beam web normal to the rib-to-floor beam weld toe on the floor beam web occurred at a section at about 50° from the centerline of the rib soffit. So, the weld toe at 50° was identified as the potential zone for fatigue cracking and it was decided to install gauges extensively at that location. A bondable rosette gage of 1 mm gage length was installed abutting the rib-to-floor beam weld toe on the floor beam web at a distance of 0.4t or $^1/_5$ in. (5 mm) from the weld toe, to capture the complex stress distribution at that location and to determine the magnitude and direction of principal stress at that location. One of the arms of the rosette was aligned normal to the weld toe. Due to the presence of steep stress gradient close to the weld toe, it was needed to capture the peak localized strains to have the correct stress distribution normal to the weld toe along the 50° radial line. So a uniaxial gage of 1 mm gauge length was installed on the floor beam web next to the rosette, at t or 1/2 in. from the weld toe measured normal to the weld toe on the floor beam, where “t” is the thickness of the floor beam web. The uniaxial gage was oriented normal to the weld toe. The rationale behind having gauges at 0.4 t and t was to extrapolate the stress values from these two measurements to the weld toe. In order to get the complete distribution of stress normal to weld toe along the 50° radial line, another uniaxial gauge of 1 mm gauge length was installed at a distance of 1.5t or ¾ in. (19mm) from the weld toe, oriented normal to the weld toe on the floor beam. Gages were also installed in the identical pattern along the 25° radial line. Though 50° was the location of highest stresses normal to weld toe at the rib 1-to-inner floor beam connection, weld root at 25° was identified from FEA as the location of maximum principal stress. Maximum principal stress is critical for crack growth from volumetric discontinuities as was observed in the fatigue tests of small-size mockups. However, it is not possible to measure the stress at weld root with the available technology. Accordingly, gages were installed along the 25° radial lines to capture the entire stress distribution on the floor beam web along the rounding of Rib 1-to-inner floor beam connection. Uniaxial gage of 1 mm gage length was installed on the east and west faces of the floor beam web at the rib soffit, oriented along the tangent to the weld toe at a distance of 0.4t or 1/5 in. (5 mm) from the weld toe. The stress normal to the weld toe was almost zero at the soffit of the rib as observed from FEA, so gage was oriented along tangent to measure the circumferential stress at that location.

Uniaxial gages were also installed on the inner floor beam flange at the connection with the edge girder web and are shown in Figures 372 and 373 (channels 56 to 65). Gages were installed on the top and the bottom surfaces of the floor beam flange. On the top surface, gages were installed at two sections, 1 in. (25.4 mm) on either side of the centerline of the inner floor beam web. Gages on the bottom surface were installed at three sections, one section at the centerline of the inner floor beam web and other two sections at 1 in. on either side of the centerline of the inner floor beam web. Gages were oriented along the transverse direction of the deck. At all the sections, a uniaxial gage of 1 mm gauge length was installed at a distance of 0.5t or 3/8 in. (9.5 mm) from the weld toe on the flange, where “t” is the thickness of the inner floor beam flange. Another uniaxial gage of ¼ in. (6 mm) gauge length was installed next to the 1 mm gauge at a distance of 1.5t or 1 $^1/_8$ in. from the weld toe on the flange.

Additional uniaxial gages of ¼ in. gauge length were installed on the bottom flange of the inner floor beam at section Y-Y. The gauges are shown in Figure 371 (channels 66 and 67). The gages were oriented along the transverse direction of the deck and were installed at two sections, one section centrally between ribs 1 and 2 and the other section centrally between ribs 4 and 5. These gages were aligned with gages on the top of the deck plate. The purpose of these two gages was to measure the bending stress in the floor beam flange due to global transverse bending of the deck. A LVDT (channel 13) was also installed at the bottom of the floor beam flange aligned with the centerline of Rib 3, to measure the vertical displacement of the inner floor beam.

8.4.6 Instrumentation on Edge Girder

Two uniaxial gauges of ¼ in. (6 mm) gage length were installed on the north face of edge girder web aligned with the centerline of the inner floor beam. The gages shown in Figure 373 (channels 230 and 231) were oriented along the depth of the web. High stress concentration was observed in FEA at the weld toe on the edge girder web at the edge girder web-to-edge girder bottom flange connection due to the applied upward displacement by the under-deck actuator. Accordingly, gages were installed at distances of 0.5t or $^{9}/_{32}$ in. (7 mm) and 1.5t or $^{27}/_{32}$ in. (21 mm) from the weld toe on the web, so that the stress at the weld toe can be obtained by extrapolating from these two measurements following AASHTO recommendations.

8.4.7 Other Instrumentation

Instrumentation on Splice Plates

Uniaxial gages of ¼ in. (6 mm) gage length were installed on the north and the south side splice plates of ribs 1, 2 and 4 at section X-X and are shown in Figure 374 (channels 216 to 221). The gages were oriented along the longitudinal direction of the deck.

Uniaxial gages of ¼ in. (6 mm) gage length were also installed on the north and south side web splice plates of the edge girder web at section X-X (channels 232 to 235 in Figure 374). The figure shows the south side splice plate, and the channel numbers of the gages installed on the north side splice plate are shown in parenthesis. Another uniaxial gage of ¼ in. (6 mm) gauge length was also installed at the surface of the bottom splice plate of the edge girder flange at section X-X (channel 236 in Figure 374). The gages were oriented along the longitudinal direction of the deck

The purpose of these gages was to capture the pure bending stress at the transverse splice section due to the longitudinal bending of the deck.

Instrumentation on Sealing Plates

As discussed in section 8.4.4, the maximum stress normal to the weld toe of the rib-to-sealing plate connection was observed at 60° from the rib soffit and on the sealing plate towards the inner floor beam. So, a uniaxial gage of 1 mm gage length was installed on the surface of the sealing plate towards the splice at ribs 1 and 5 at a distance of 0.5t or

$^{3}/_{16}$ in. (5 mm) from the weld toe both at the north and the south walls of the ribs. Another uniaxial gage of ¼ in. (6 mm) gage length was installed next to the 1 mm gage at a distance of 1.5t or $^{9}/_{16}$ in. (14 mm). The rationale of having gages at 0.5t and 1.5t has already been discussed earlier. All these gages were oriented along the 60°radial line normal to the weld toe on the sealing plate. The gages are shown in Figure 368 (channels 222 to 229). These gauges were installed at High Steel facility.

Instrumentation on Transverse Stiffener to the Edge Girder

Uniaxial gages were installed on the east and the west faces of the transverse stiffener provided at the south face of the edge girder web at the edge girder-to-inner floor beam connection. The gages are shown in Figure 373 (channels 237 to 242). These gages were installed near the longitudinal stiffener-to-transverse stiffener weld toe and the transverse stiffener-to-edge girder flange weld toe on the transverse stiffener. The gages were oriented along the depth of edge girder web. At each weld toe, a uniaxial gage of 1 mm gage length was installed at 0.5t or $^{5}/_{16}$ in. (8 mm) from the weld toes, where “t” is the thickness of the transverse stiffener. Another uniaxial gauge of ¼ in. gauge length was installed next to the 1 mm gauge at 1.5t or $^{15}/_{16}$ in. (24 mm) from the weld toes. The reason behind having gauges at 0.5 t and 1.5 t has already been explained earlier.

8.5 Data Acquisition

Data were collected using programmable digital data loggers manufactured by Campbell Scientific Inc. (CSI). The data loggers were provided with analog input cards (CR 9050 and CR 9051), which processed the output signal from the instruments. The processed signals were then stored in a removable memory card and could be downloaded to a permanent storage. Each analog card could accommodate 126 data channels, where each data channel was a quarter Wheatstone Bridge circuit. For the crawl tests and the initial static tests, two model CR9000 data loggers (identified as NJ_DAQ_1 and NJ_DAQ_2), and one model CR5000 data logger (identified as NJ_DAQ_3) were used. For the subsequent static and fatigue tests, only two CR9000 data loggers (NJ_DAQ_1 and NJ_DAQ_2) were retained, as the LVDTs connected to NJ_DAQ_3 were disconnected. A model CR1000 data logger was also used during the fatigue test which recorded the load outputs from the above-deck actuator load cells and the trigger from the actuator controller (see section 8.7.4). The data output from this logger was used to send automated email to the research team in case the load level in the above-deck actuators was below 3 kip or the trigger voltage was below 2.5 mV.

The inline load cells of the actuators (see section 8.7.3) were also connected to the data logger. These were the six channels of NJ_DAQ_1 after the first channel which was recording the trigger from the actuator controller to the data loggers. For the crawl tests and the initial static tests, the strain gages were connected to the data loggers as: strain gage channels 56 to 67, 138 to 154, 159 to 203 and 208 to 248 to NJ_DAQ_1; strain gage channels 14 to55, 68 to 137, 155 to 158 and 204 to 207 to NJ_DAQ_2; and the LVDT channels 7 to 13 to NJ_DAQ_3. For the fatigue test, NJ_DAQ_3 was discarded.

For the crawl tests and the static tests, data was sampled at a frequency of 10 Hz and averaged over one second (i.e. 10 samples) before recording on the memory card. For the fatigue test, the data was collected at a frequency of 10 Hz without averaging. The analog cards did not have any real time filtering capabilities. To reduce noise and spurious signal in collected data, the settling time was set at 100 µsecs and the integration time was set at 670 µsecs. The settling time is the time taken for the input channel to settle to its new value when switched between the channels and a change in signal occurs. The integration time is the time over which the input signal is averaged to reduce the noise caused due to random fluctuations in the signal.

8.6 Crawl Tests

Three types of tests were performed on the prototype deck: crawl tests, static tests and fatigue test. The crawl tests involved rolling a bogie (test truck) representing the AASHTO tandem axle, as shown in Figure 375, across the deck at a very slow speed to determine the response of the deck elements under moving load. The crawl tests were conducted for three transverse positions to assess the response of the deck under different disposition of the wheel loads. The first set of crawl tests were performed on July 22, 2014. During the subsequent static tests, however, it was realized that the west support column was not fully fastened to the laboratory floor, and the resulting flexibility affected the global deformation of the specimen and invalidated the crawl test results. Since, the overhead loading fixtures were already installed for the static and the fatigue tests, repeating the crawl tests would have required disassembling the overhead loading fixtures for providing access for the crawl truck. To avoid any further delay to the project, it was decided to proceed with the static and fatigue testing as per the work plan. The crawl tests were repeated after the completion of fatigue tests on March 18, 2015.

8.6.1 Test Truck

The test truck (Figure 375) represented the rear axles of a tractor-trailer in tandem configuration according to the fatigue loading for orthotropic decks provided in the AASHTO LRFD Bridge Design Specifications, 6th edition. The truck consisted of two axles attached to a 12 ft (4.4 m) long and 3 ft 5 in. (1.0 m) wide steel frame made of beam sections for supporting steel billets (weight). In the longitudinal or the rolling direction, the axles were spaced at 4 ft. (1.2 m.) A pair of wheels was attached at each end of each axle. In the transverse direction, the center-to-center distance between the wheel pairs at the ends of each axle was 6 ft. (1.8 m.) Each wheel was fitted with retreaded truck tires pressurized to about 90 psi (620.5 kPa). The truck was loaded with four steel billets. The combined weight of the truck and the four billets was 53.7 kip (238.9 kN), which was about 2.2 times the rear axle load of 24 kip (106.8 kN) for the AASHTO notional fatigue truck. For verification of infinite life, however, the fatigue testing of the deck was performed under a gross tandem axle weight of 82.8 kip (368.3 kN), which was 3.45 times the AASHTO notional fatigue truck. Thus, the crawl test loading was about 65% of the fatigue limit state loading.

8.6.2 Test Positions

The crawl tests were conducted for three transverse positions as shown in Figures 376 to 378. As a result, the deck and the ribs, whose responses are driven by local effects of individual wheels, were subjected to several different load dispositions, where the simulated tire contacts with the deck plate were over the ribs, and partially or fully in between the ribs. These load dispositions encompassed the possible critical stress distributions in the deck plate, the rib walls and rib-to-deck connections. The rib-to-floor beam connection which sees one stress cycle for the passage of rear tandem axle, was subjected to different longitudinal disposition of the tandem axle for the three transverse positions. The different transverse positions are further discussed in the following.

1. Transverse Load Position 28 (Figure 376): The south pair of wheels was placed centrally over the north wall of Rib 1. This position was intended to investigate the response of rib-to-deck plate weld under symmetrical bending. In this position, the north wheel pair straddled Rib 4 and the deck plate between ribs 3 and 4. Both Rib 4 and the deck plate between ribs 3 and 4 were eccentrically loaded
2. Transverse Load Position 29 (Figure 377): The south pair of wheels pair was placed centrally between ribs 1 and 2. Consequently, the wheels were located on the north wall of Rib 1 and south wall of Rib 2. This position was intended to investigate the effect of wheel load on two adjacent ribs taking into account the effect of box girder support to the deck plate and the relative distortion of the deck plate. In this position, the north wheel pair was over Rib 4.
3. Transverse Load Position 30 (Figure 378): The south pair of wheels was placed centrally over the south wall of Rib 2. This position was intended to investigate the response of rib-to-deck plate weld under symmetrical bending, when the loading moves away from the edge girder. In this position, the north wheel pair straddled Rib 4 and the deck plate between ribs 4 and 5. Both Rib 4 and the deck plate between ribs 4 and 5 were eccentrically loaded

8.6.3 Test Procedure

The test truck was pulled by a manually operated hydraulic winch and cable system that was reacted against the deck. A guide truss (Figure 379) along the length of the deck was used underneath the test truck to guide the truck in a straight line on a transverse position. The top and bottom chords of this guide truss employed 6x6x$^{3}/_{4}$ angles and the diagonal members used 2x2x$^{3}/_{8}$ angles. Brackets were provided at the ends of the guide truss, which were used to clamp the truss to the deck and also to support the hydraulic winch on the west end and a pulley on the east end (Figure 379). The test truck was rolled in the east to west (i.e. forward) and west to east (i.e. reverse) directions for each position. For the forward roll, the cable was connected to the truck and hydraulic winch via the pulley. For the reverse roll the cable was directly connected to the truck and hydraulic winch.

The following procedure was adopted for crawl tests in each transverse position. The guide truss was positioned on the deck at the desired position. The south end of the

inner floor beam was displaced upward by 0.045 in. (1 mm) by using the under-deck actuator. This value of displacement was determined from FEA of global model and submodel. The test truck was lifted on the deck using the overhead crane and aligned with the guide truss at the east end of the deck. The steel billets were lifted and placed on the truck one at a time in the sequence as shown in Figure 375. The steel rope from the winch was pulled along the truss and through the pulley on the north end and hooked onto the underside of the truck. The truck was pulled across the deck for a fixed distance of 18 ft. 9 in. (5.7 m), which was the maximum available distance for the truck to roll. The roll distance was not equal on either side of the inner floor beam due to space restrictions for accommodating the truck at the ends of the deck. The roll distances were 10 ft. 9 in. (3.3 m) and 8 ft. (2.4 m) to the east and the west of inner floor beam respectively. During the roll of the truck, the displacement given by the under-deck actuator was varied along the length of the roll. The displacements for different positions of the truck was determined from the FEA of the global model and the submodel. The displacement profile was identical for all the transverse positions and is shown in Figure 380. The time taken by the truck to cover the distance was noted using a stop watch. The steel rope was hooked to the truck directly for the reverse roll. The truck was reverse rolled the same distance and the time taken for the reverse roll was measured using the stop watch. The average speed maintained for the crawl test in every transverse position was about 0.08 mph (1.2 km/h). Once the reverse roll was completed, the truck was disconnected from the winch, the billets were unloaded one by one, and the truck was taken off the deck. The under deck actuators were returned to zero position, and the procedure was repeated for the next transverse position.

As explained in section 8.5, the crawl test data was sampled at a frequency of 10 Hz and averaged over one second (i.e. 10 samples) before recording on the memory card. For each transverse position, the strain gauges and the LVDTs were zeroed before placing the truck and billets on the truss and giving initial displacement. The sensors were zeroed to remove any offsets caused due to the electrical characteristics of the system. Data collection was started as soon as the sensors were zeroed. The collection of the data was stopped after the crawl test was completed, the truck was lifted off the deck, and the under deck actuator was returned to zero position.

8.7 Static and Fatigue Tests

8.7.1 Loading

As explained earlier, the deck design needed to be verified for infinite fatigue life or Fatigue I Limit State according to AASHTO LRFD Bridge Design Specifications, 6th edition. Thus the above-deck actuators, each representing one axle of the tandem rear axle, was cycled between a minimum of 5 kip (22.2 kN) and maximum of 46.4 kip (206.4 kN), resulting in a load range of 41.4 (184.2 kN) or a total load of 82.4 kip (368.4 kN) at the two actuators. The under-deck actuator was displaced upward synchronously with the above-deck actuators, between 0.0121 in. (0.3 mm) and 0.1121 in. (2.8 mm) corresponding to the minimum and the maximum loads respectively, resulting in a displacement range of 0.1 in. (2.5 mm). The minimum load was maintained to simulate

dead load effects and to avoid loss of contact between the loading pads and the deck during tests.

8.7.2 Loading Arrangement

The above-decks actuators were installed on the deck to simulate the most critical disposition of the tandem axle as determined from the FEA of the global model. The two above-deck actuators were placed symmetrically 2 ft. on either side of the inner FB (Figure 335) to simulate the symmetric load position, resulting in a 4 ft. spacing between the two actuators following the AASHTO specifications. As discussed earlier, the load from each actuator was distributed through a spreader beam into two rectangular load pads (simulating the wheel contact with the deck plate) 10 in long and 20 in wide, spaced 6 ft. apart in transverse direction (according to AASHTO LRFD Bridge Design Specifications). In the transverse direction, the south side load pads were placed centrally between ribs 1 and 2 adjacent to the edge girder to simulate the most critical transverse disposition of the tandem axle.

The under-deck actuator, which was used to simulate the global displacement boundary condition, was floor mounted and aligned with the centerline of the inner floor beam at the south end of the deck.

8.7.3 Hydraulic Actuator

Three hydraulic actuators were used for testing the deck (Figure 335). Two above-deck actuators were used to simulate the tandem axle load on the prototype deck and one under-deck actuator was used to simulate the global displacement boundary condition. Arrangement of the above-deck actuators in the test setup is shown in Figure 381. The above-deck actuators were Hannon 5110 with a maximum load rating of 110 kip. These actuators were double acting fatigue rated and had a total stroke of 10 in.

The under-deck actuator was Lynair H-B1003, which had a maximum load rating of 220 kip. The actuator had 10 in. diameter rod with a 6 in. stroke

Hannon 5110 actuators had inbuilt LVDTs with a measuring range of ± 10 in (254 mm) and for Lynair H-B1003 actuator, external LVDT with a measuring range of ±3 in. (76 mm) was used to measure the displacement of the actuator.

The load applied by the above-deck actuators were measured using Lebow 3129-112 load cells whose maximum load rating is 150 kip and they were designed specifically to resist fatigue failure. The load feedback in the under-deck actuator was measured by Lebow 3129-112 load cell whose maximum load rating is 220 kip.

All the actuators were fitted with Vickers SM-440 valve, which regulate the flow of hydraulic oil in and out of the actuator. To regulate the flow between the pump and the actuators two hydraulic service manifolds (HSM) were used. The above-deck actuators were assigned to one HSM and the under-deck actuator was assigned to the second HSM.

8.7.4 Actuator Controller

The actuators were controlled by a MTS Flextest 100 digital controller. The controller had a capability of controlling nine actuators (channels) and two hydraulic service manifolds (HSM) simultaneously. The above-deck actuators were operated under load control. The displacements of these actuators were monitored. A haversine wave-form was used as command for all actuators. The under-deck actuator was operated under displacement control.

8.7.5 Loading Protocol

The objective of the loading protocol was to impart the maximum in-plane stress in the inner floor beam. Single load step was defined in the loading protocol for each cycle. In load step 0 of the loading protocol, the two above-deck actuators applied a uniform load of 5 kip (22.2 kN). In load step 1, the above-deck actuators were loaded to 46.4 kip (206.4 kN). Load step 1 was followed by load step 0, when the above-deck actuators were unloaded to 5 kip (22.2 kN).

In each loading step, the under-deck actuator applied a displacement corresponding to the global vertical displacement boundary condition. In load step 0, the under-deck actuator was displaced upward by 0.0121 in. (0.3 mm) and in load step 1 it was displaced upward by 0.1121 in. (2.8 mm).

8.7.6 Test Procedure

Static tests were performed prior to initiating the fatigue test and intermittently during the fatigue test. These so called “static tests” followed the same sequence as the fatigue test, but was conducted at a slow (or almost static) loading rate. The loading and displacement protocols for static tests is shown in Figures 382 and 383 respectively for the above-deck and the under-deck actuators. During the static tests the load at each actuator was changed between the minimum and the maximum value in 5 seconds and the loads were held at load step 1 for 10 seconds. The first static test was conducted prior to initiating the fatigue test to determine the base sate of the structure. Subsequent static tests were conducted at regular time interval to determine the change in state of the deck in terms of the measured stresses at the strain gauges. The static test results are discussed in detail in Chapter 9.

The fatigue testing of the prototype deck was performed by repeated application of the loading sequence as discussed under the loading protocol. The loading and displacement protocols for the fatigue test is shown in Figures 384 and 385 respectively for the above-deck and the under-deck actuators. Initially, the fatigue test was run at 1 Hz frequency for about 400,000 cycles till September 18, 2014. Subsequently the test frequency was increased to 2 Hz, when stability of the test could be ensured. The test was conducted uninterrupted 24 hours a day and seven days a week, except for interruptions due to routine checks, maintenance or significant events. To verify infinite life fatigue performance, the prototype deck was tested for 8 million load cycles without any fatigue cracking. The fatigue test results are discussed in Chapter 9.

8.7.7 Inspection Regimen

The specimen was inspected for possible fatigue cracking regularly at an interval of 4 hour with the exception during night time when the last inspection for a day was at 10:30 PM while the first inspection for the next day was at 7:00 A.M. The inspections were aided with 10X magnifying glass. The inspection plan is shown in Figure 386. The critical areas of the deck: rib 1-to-inner floor beam connection; rib-to-deck welds at the loaded section; CJP deck splice at the loaded section and the edge girder-to-inner floor beam weld were inspected at every four hour interval. The complete prototype deck was inspected once every day during fatigue testing. After 5 million cycles, the guide truss for the load pads was removed, the area on the deck plate in the loaded area was cleaned, and the deck plate underneath the load pads was inspected for any fatigue cracking. Subsequent to this inspection, deck plate underneath the load pads was inspected at every 1 million cycle till the termination of the test at 8 million cycles.

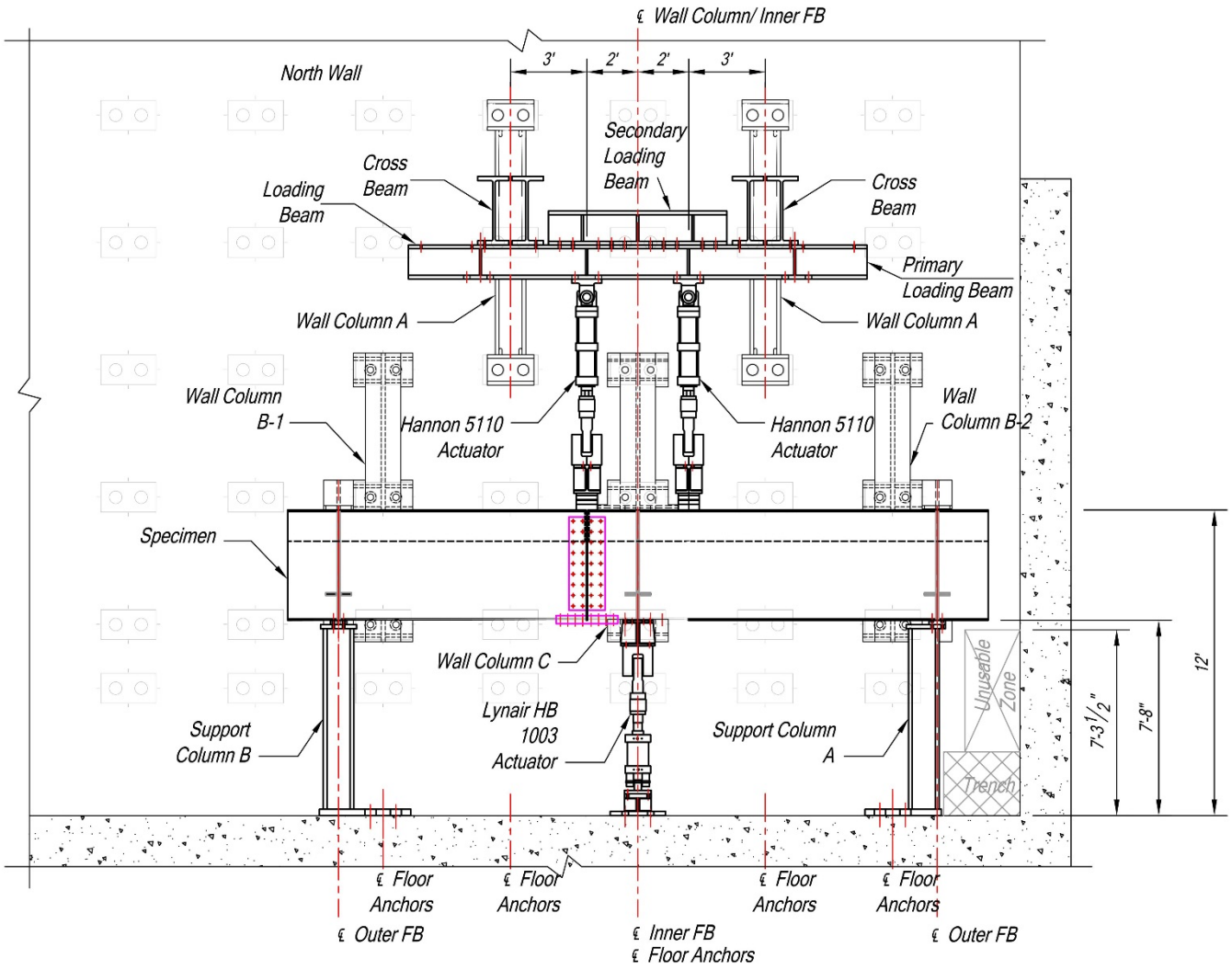

Figure 335. North elevation of the test setup

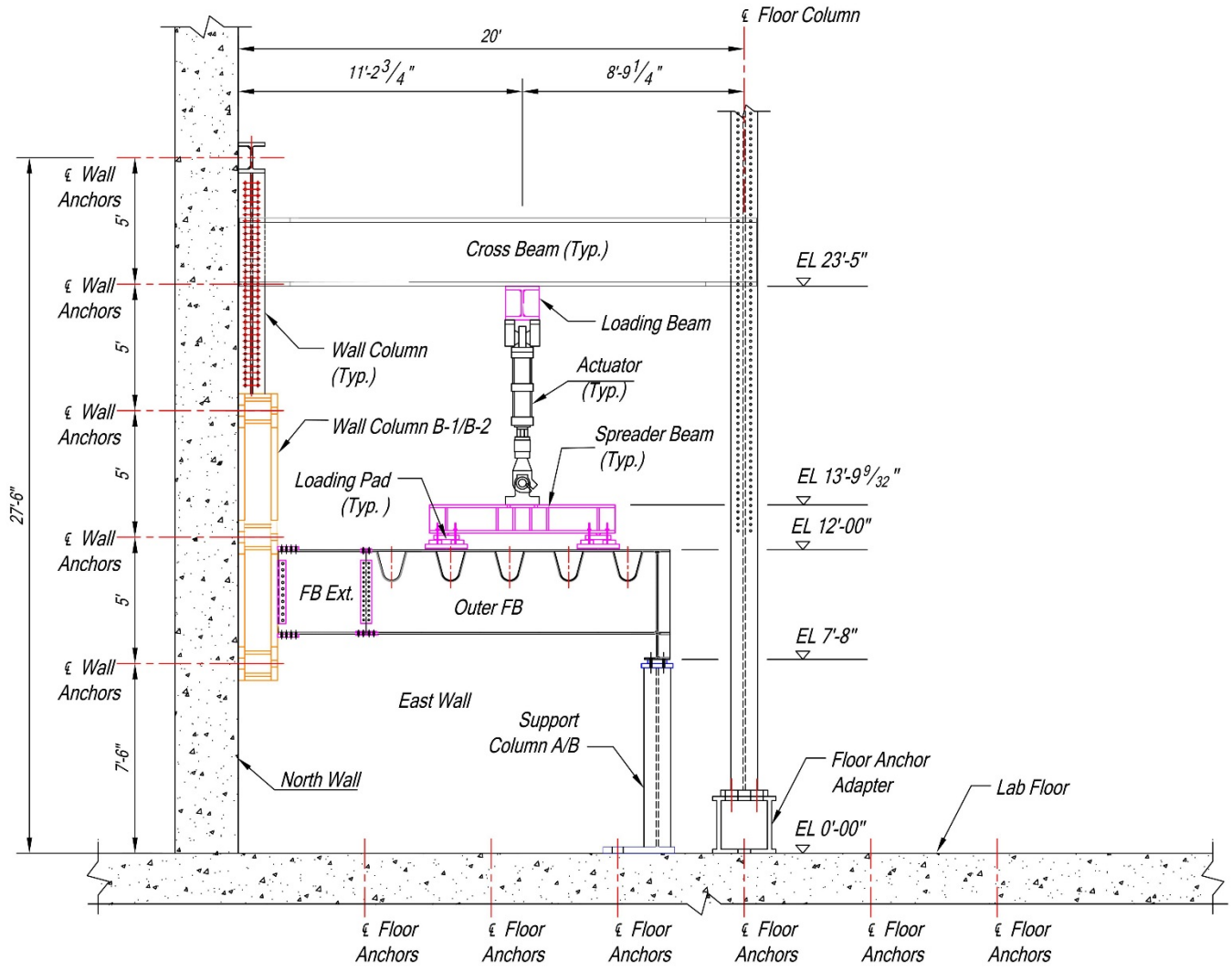

Figure 336. Side elevation of the test setup (looking east)

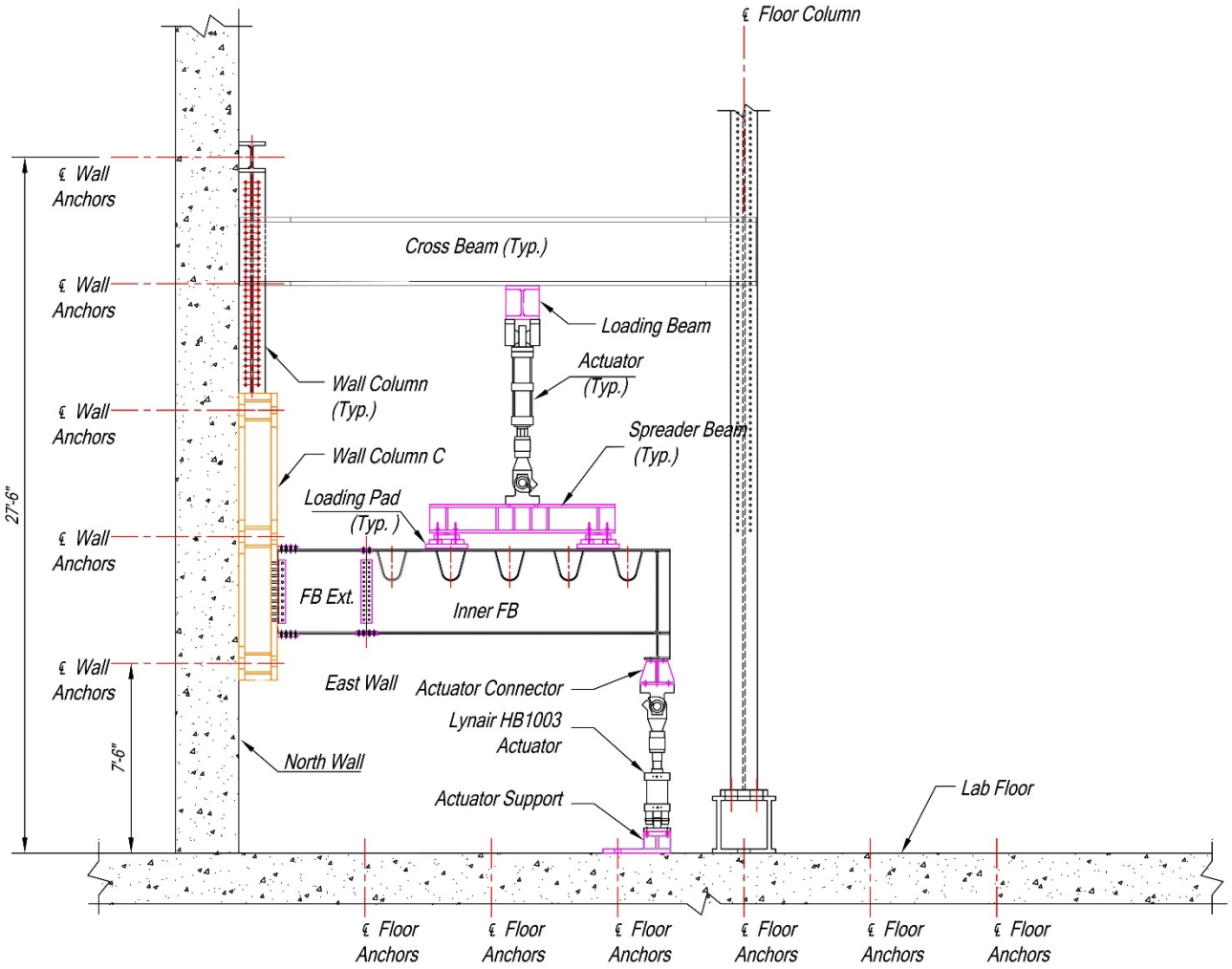

Figure 337. Sectional elevation of the test setup at the inner floor beam (looking east)

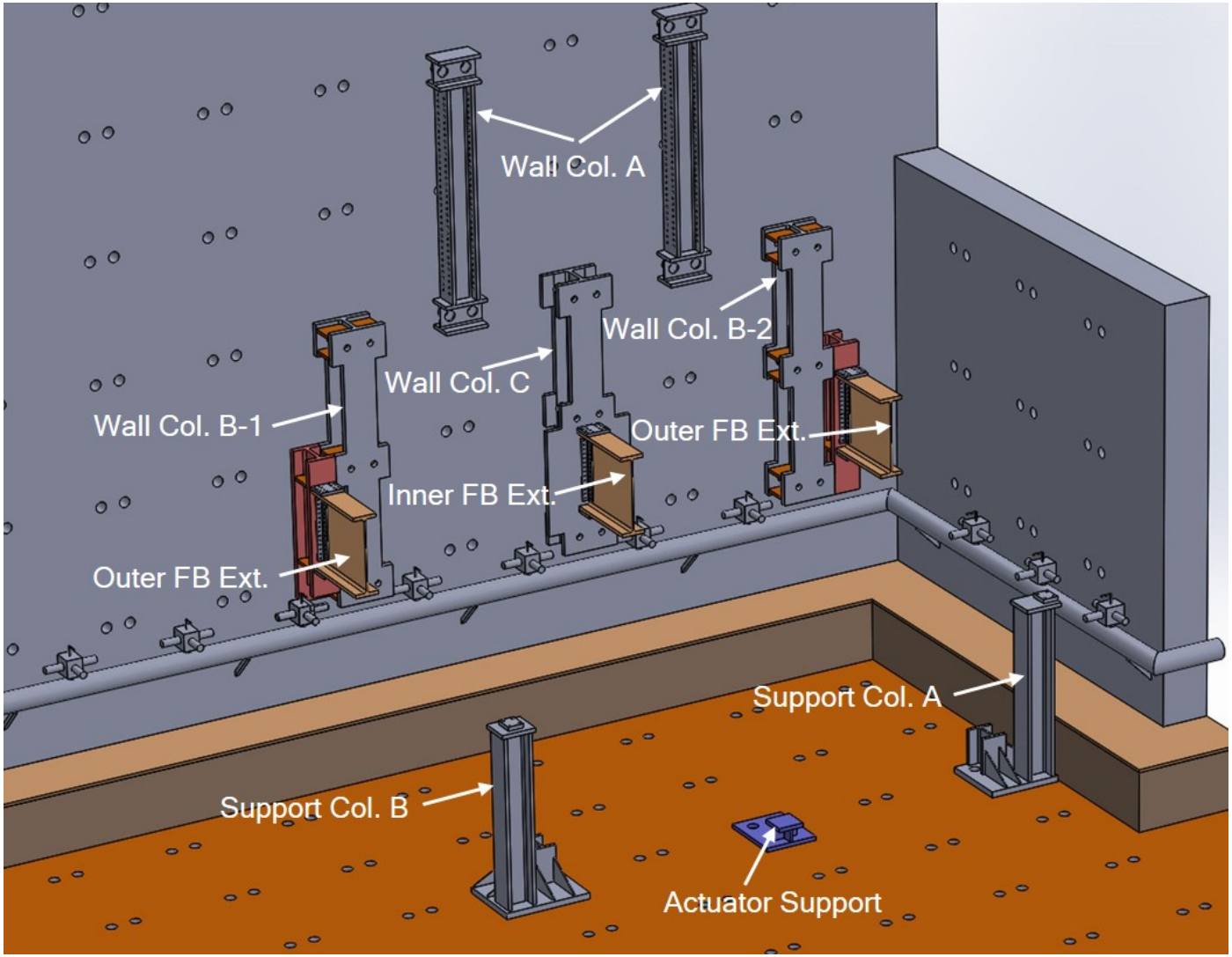

Figure 338. Fixtures for the prototype deck specimen

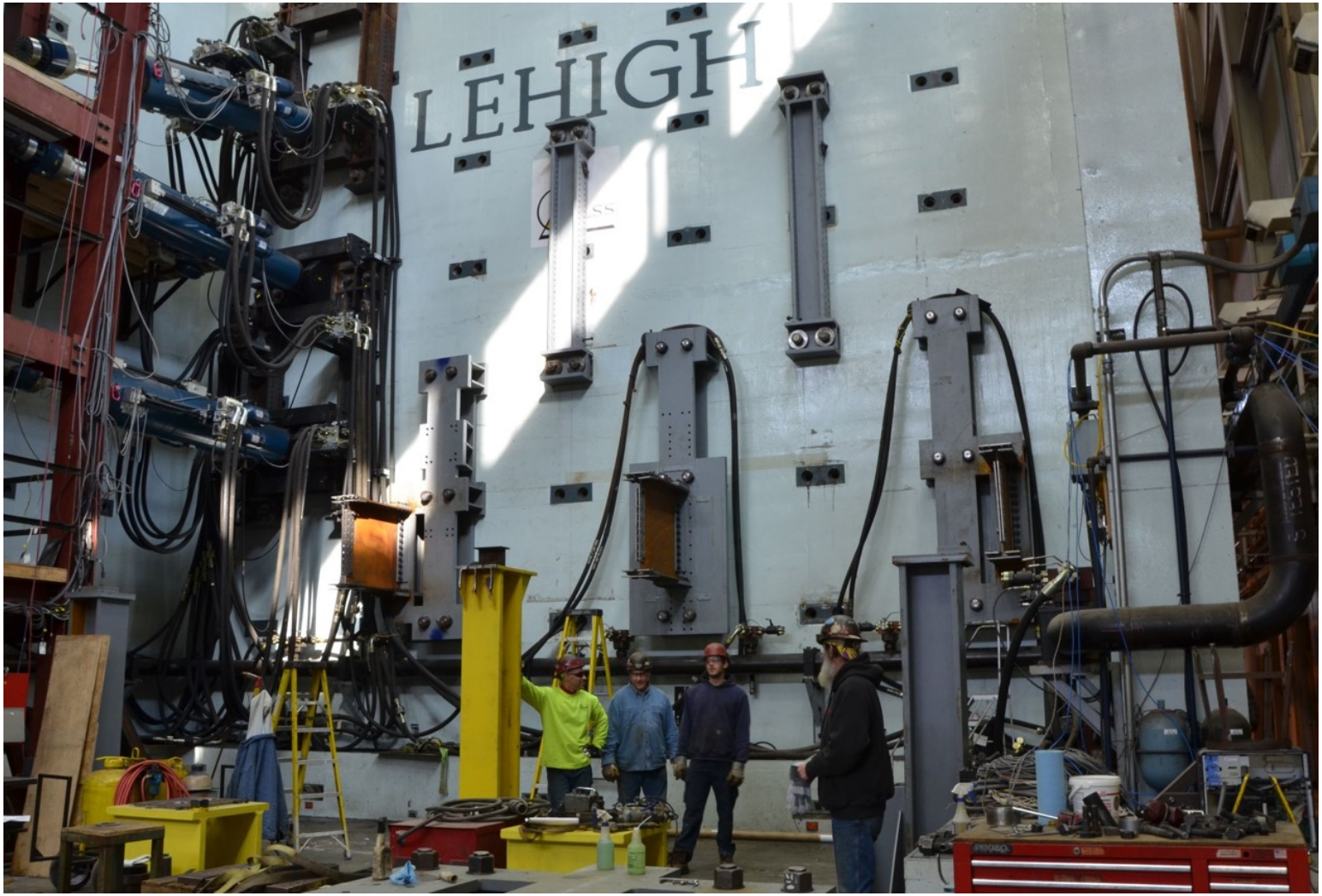

Figure 339. Fixtures for the prototype deck specimen

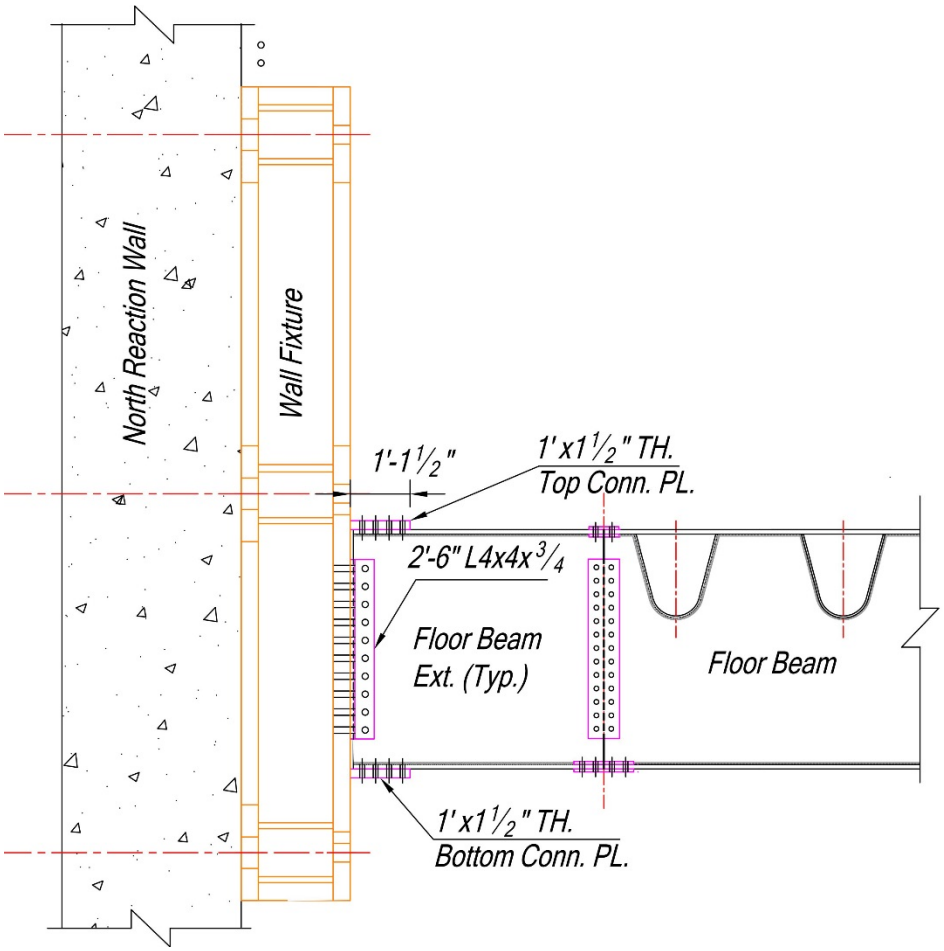

Figure 340. Floor beam wall fixture

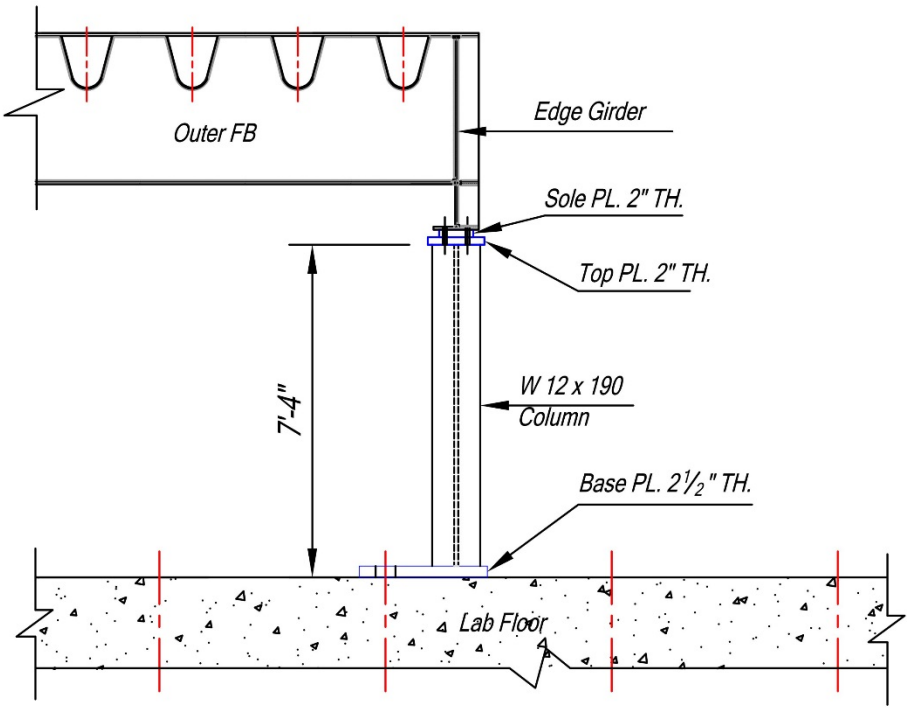

Figure 341. Support columns

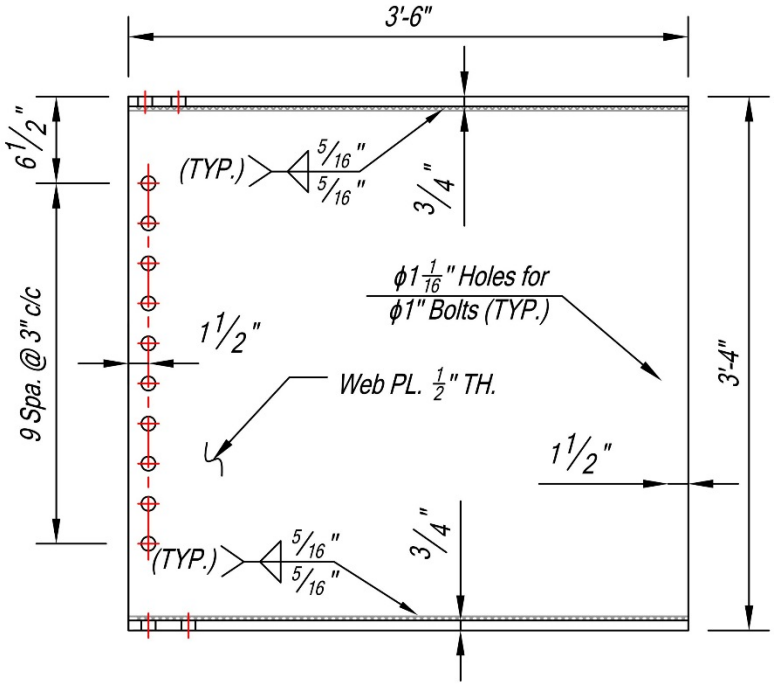

Figure 342. Floor beam extension

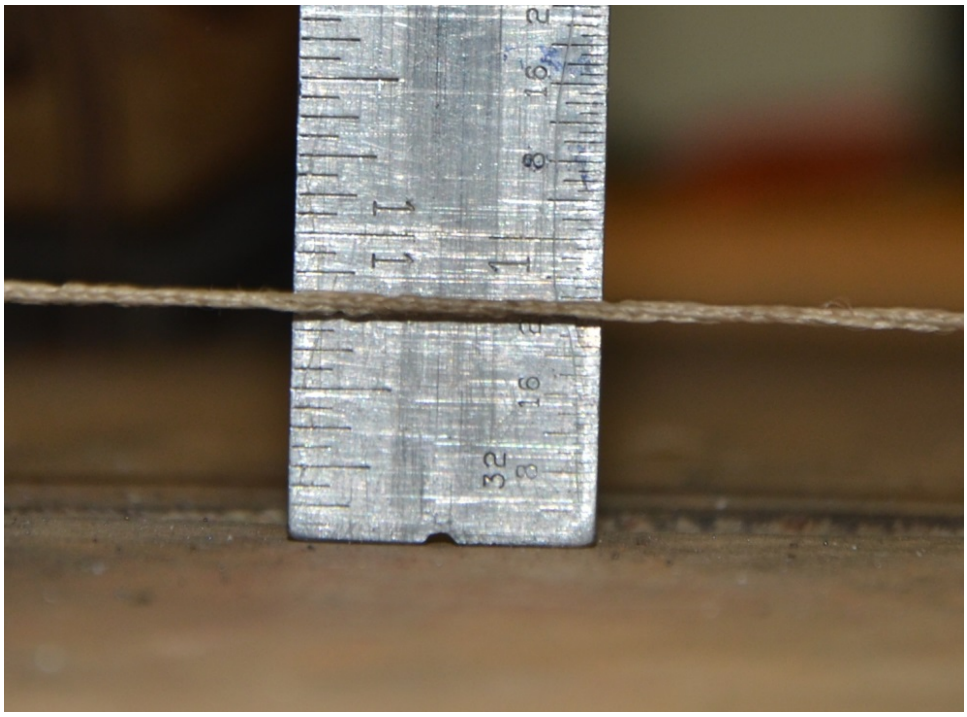

Figure 343. Measurement of deck level

Figure 344. Installation of the east panel

Figure 345. Installation of the west panel

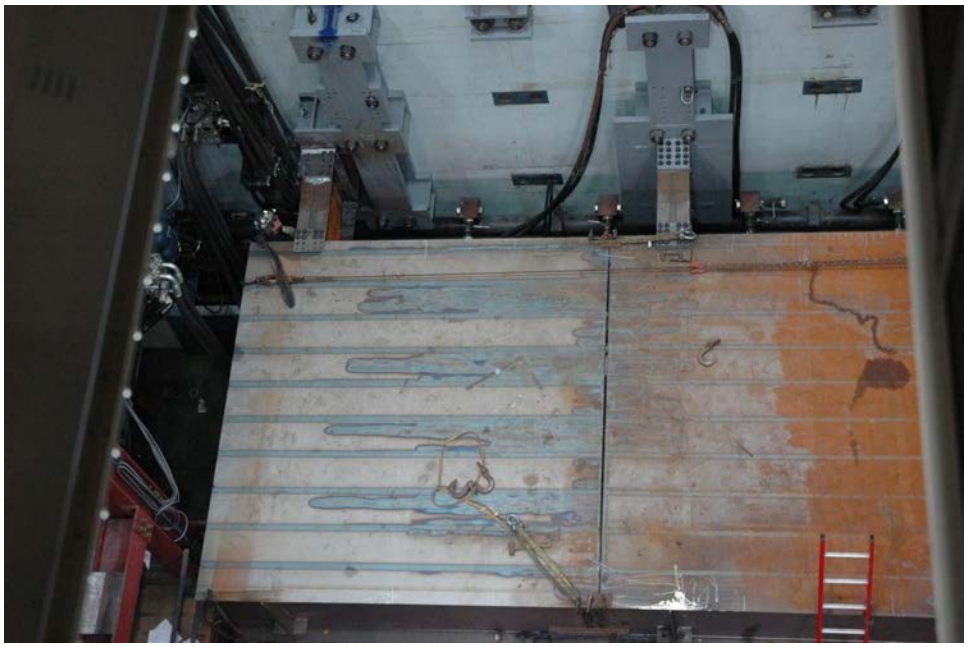

Figure 346. Heat marks on the deck after heat treatment

Figure 347. Elevation difference at splice location before tacking

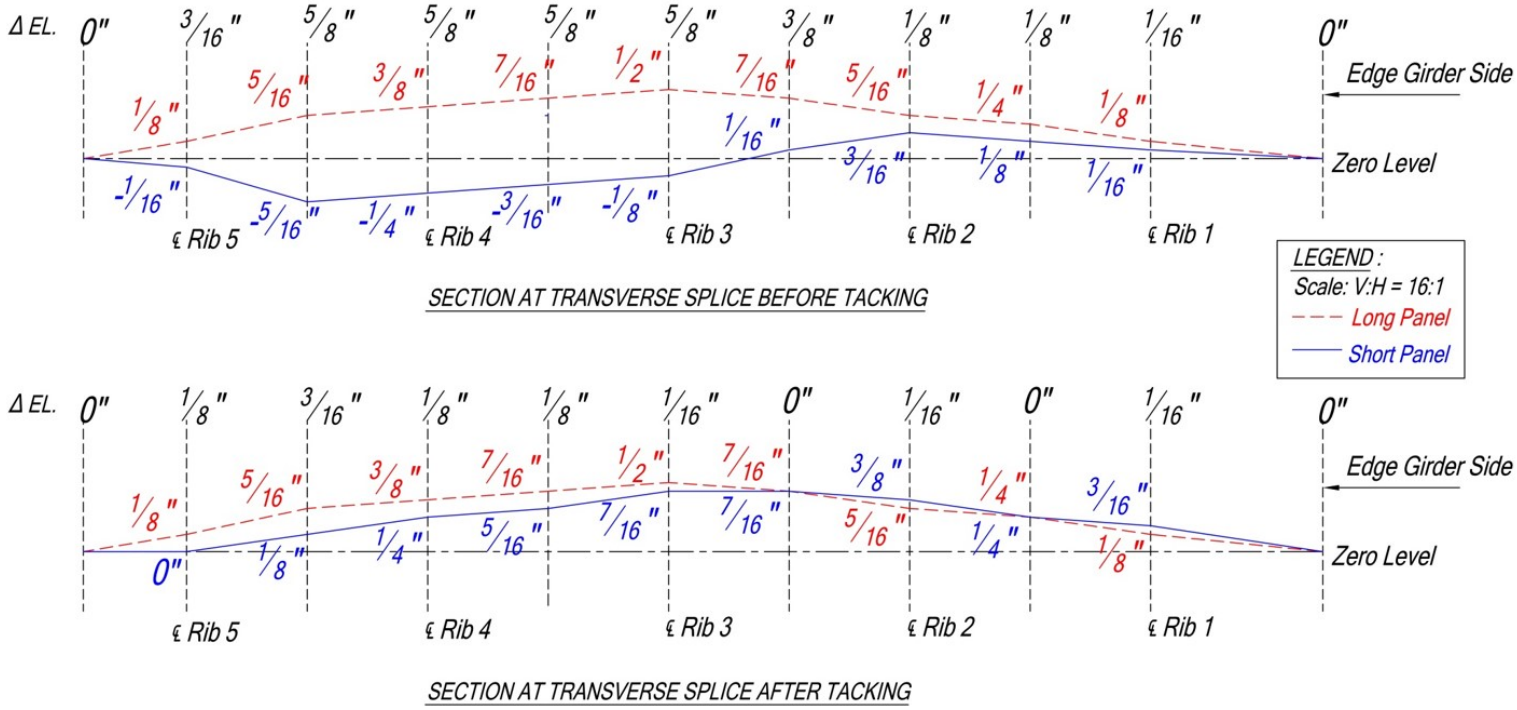

Figure 348. Comparison of elevation difference at transverse splice location before and after tacking

Figure 349. Jacking of west panel

Figure 350. Maximum root gap of ½ in.

Figure 351. Lack of alignment of the ribs

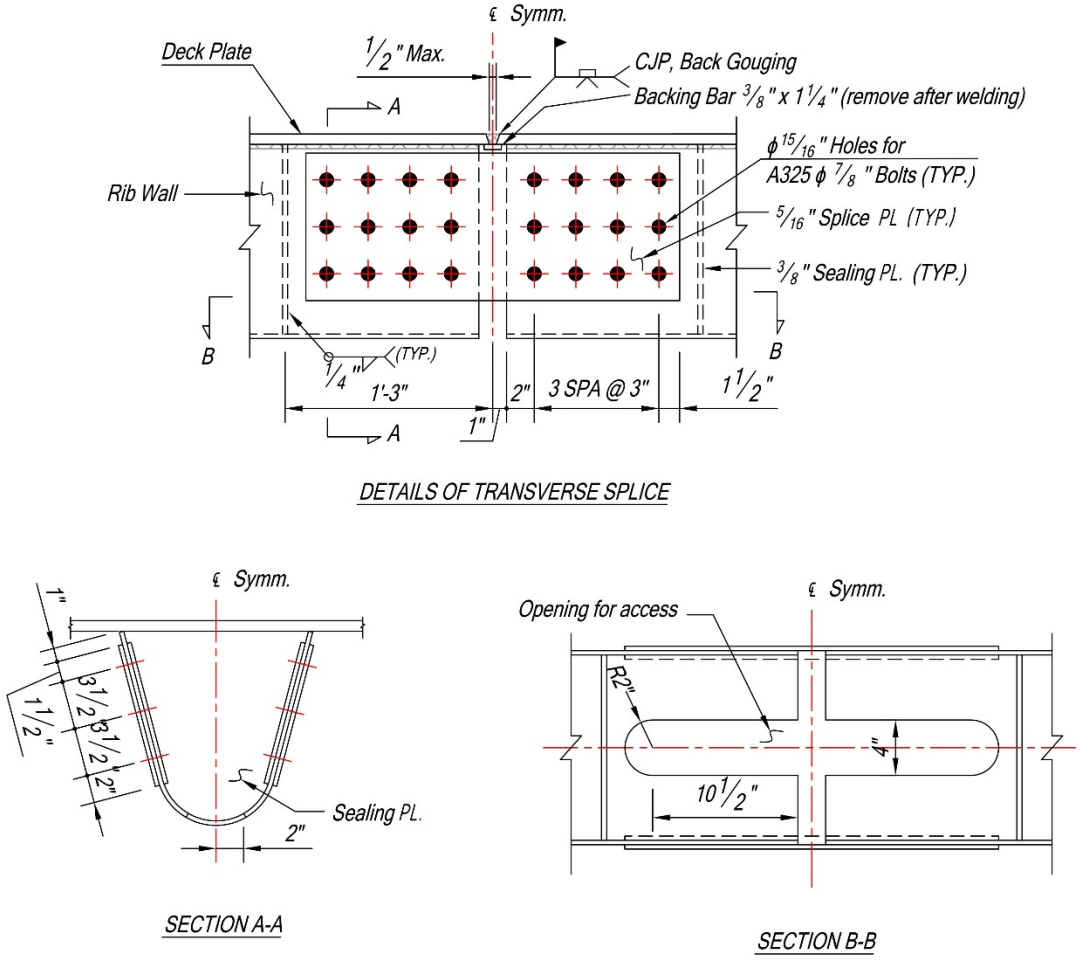

Figure 352. Details of transverse splice

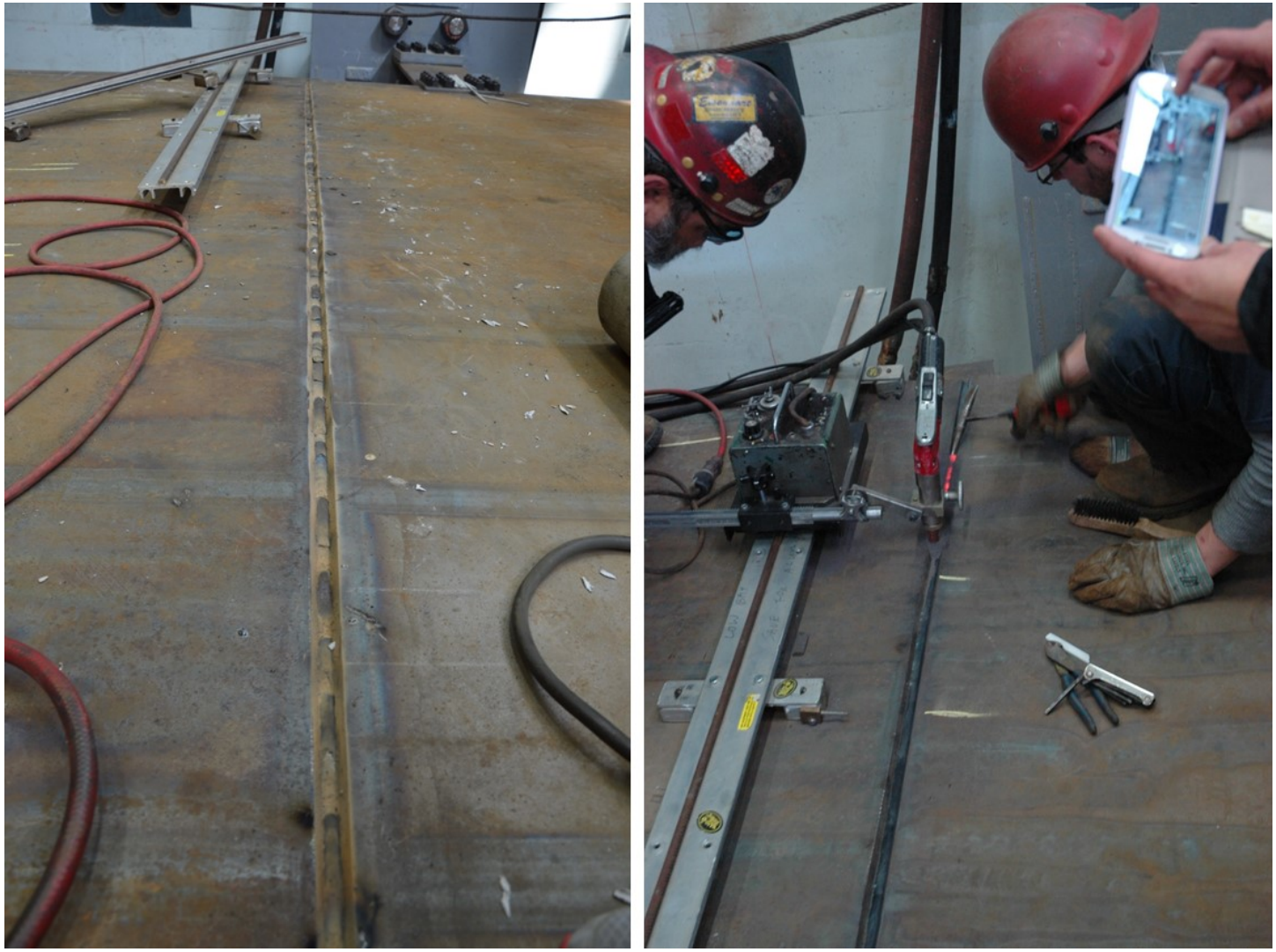

Figure 353. Root pass and fill pass for the CJP weld at the transverse deck splice at deck plate

Figure 354. Weld root after removing of backing bar

Figure 355. UT of CJP Deck Splice

Figure 356. Back gouge and re-welding in between the ribs

Figure 357. Extensive efforts for back gouge and re-welding inside the rib

Figure 358. Weld root after re-welding

Figure 359. Lack of access over the rib wall for re-welding

Figure 360. Deck level measurements using laser

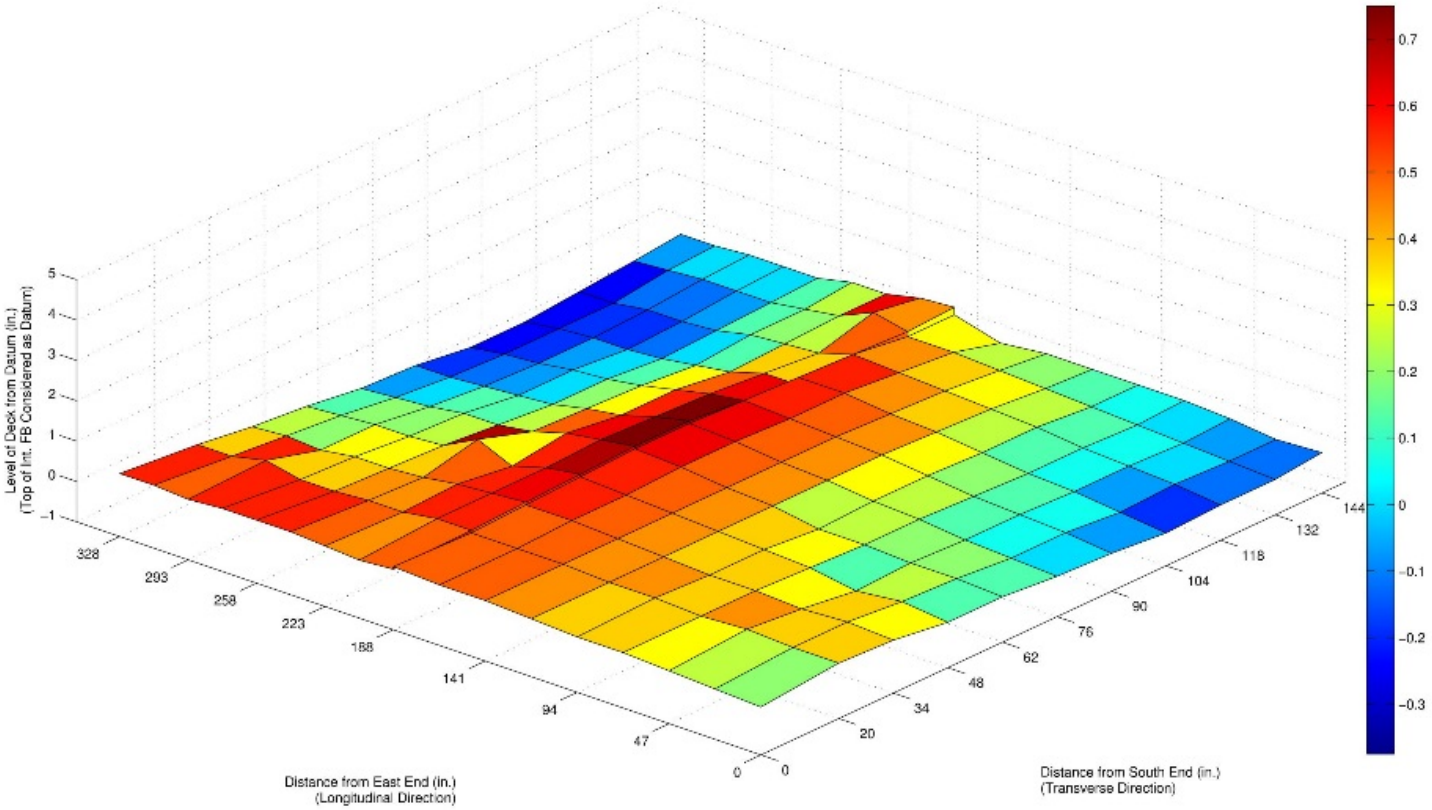

Figure 361. Laser measurements of deck level after installation

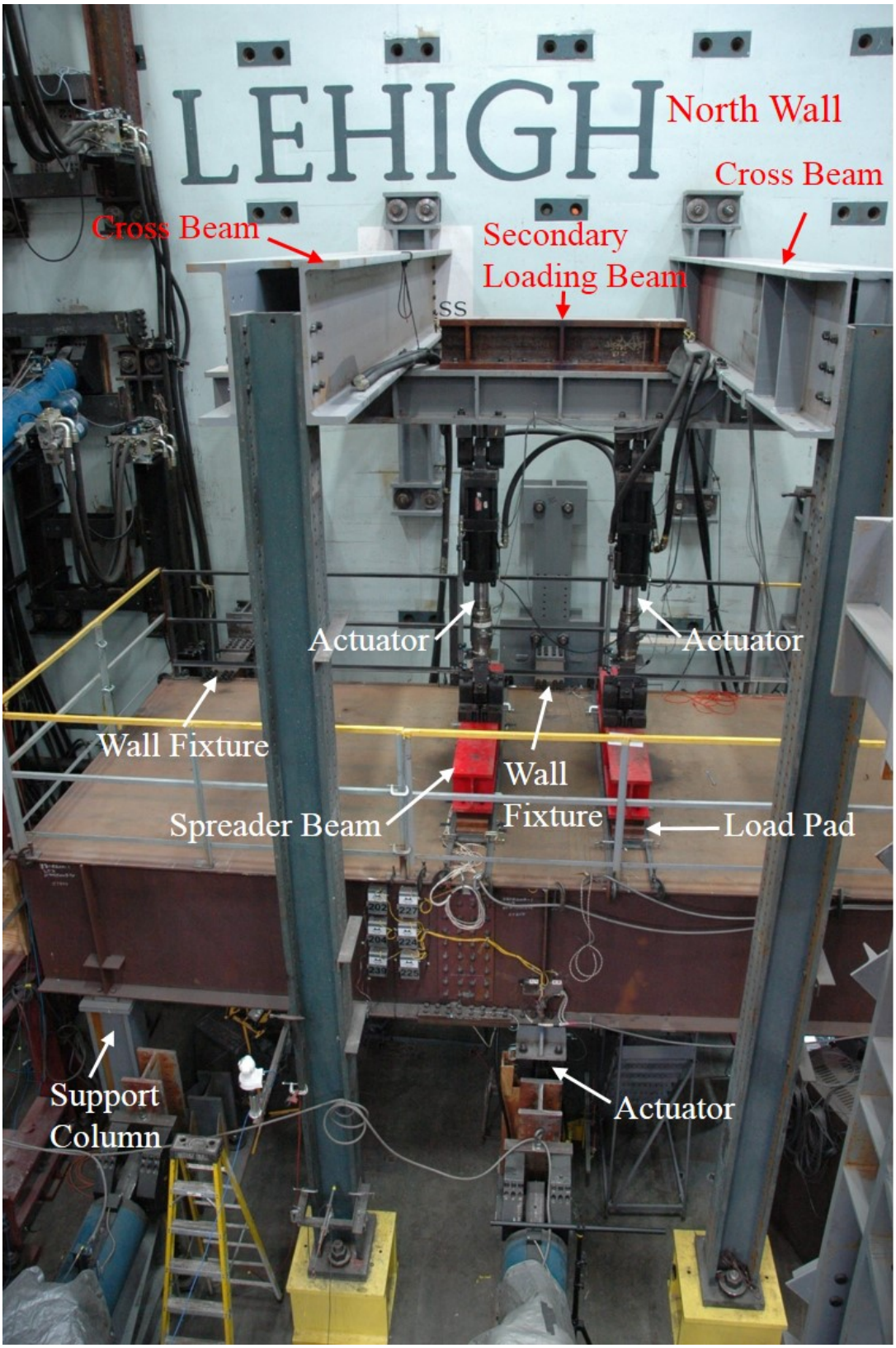

Figure 362. Test setup

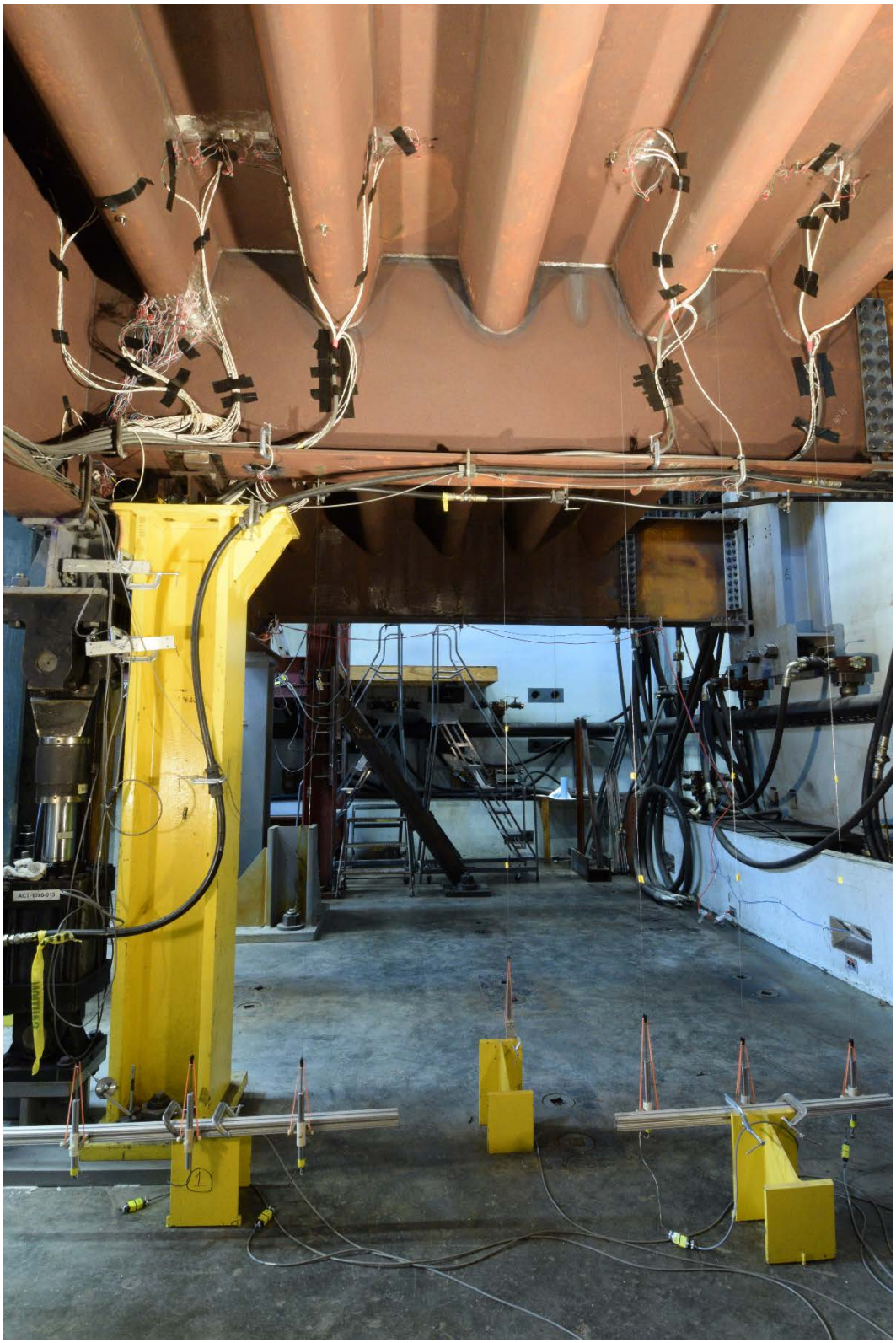

Figure 363. Instrumentation on the specimen

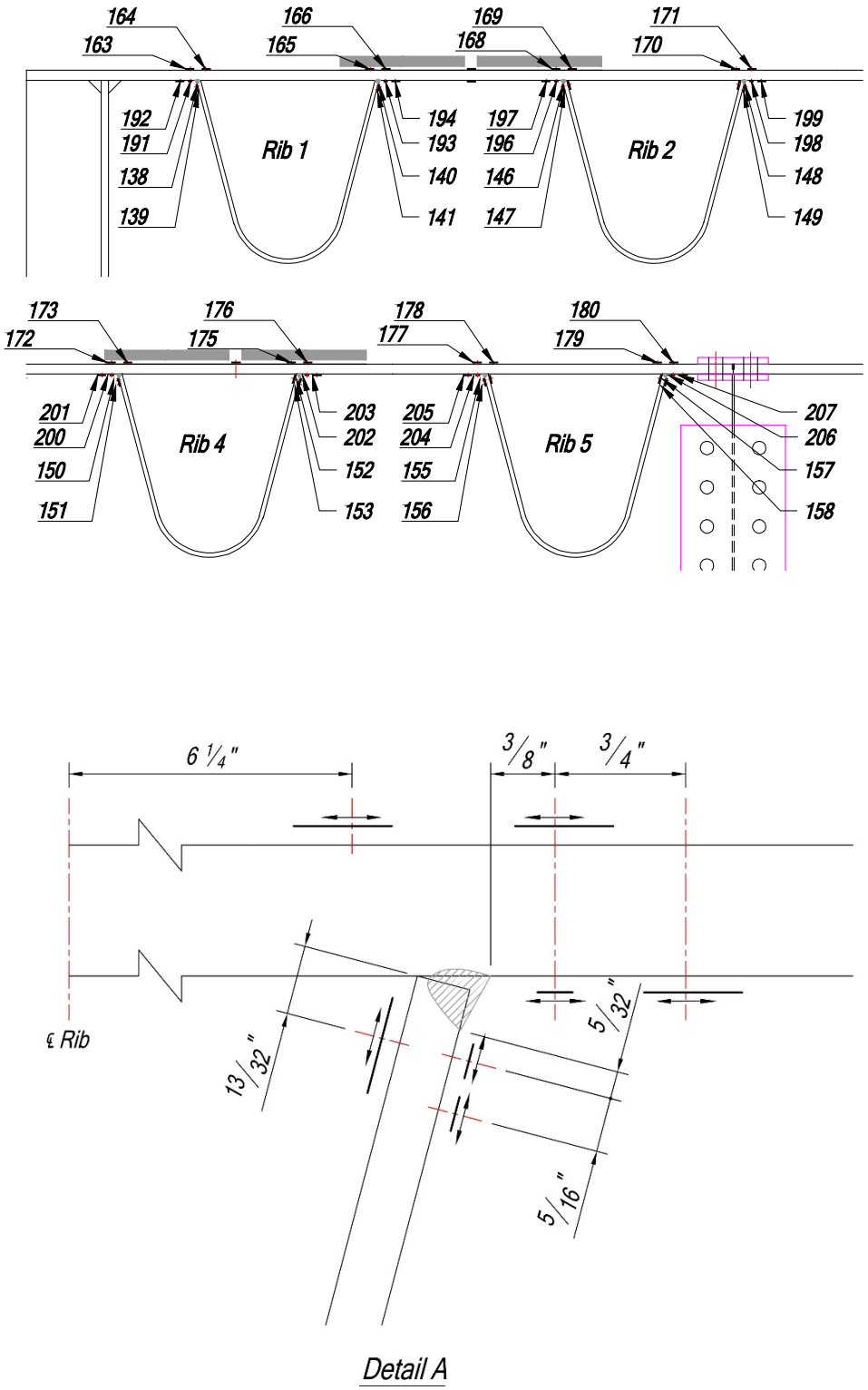

Figure 364. Gauges on deck plate at section Z-Z (Detail B is similar to Detail A but handed)

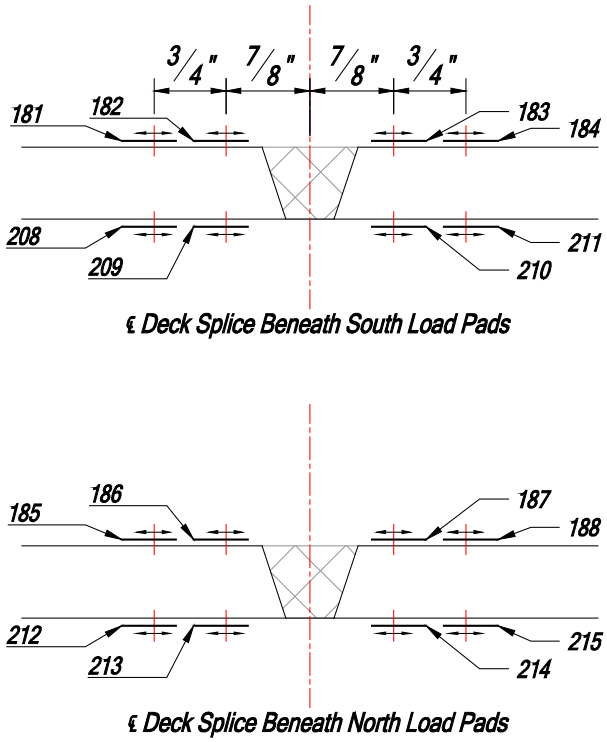

Figure 365. Gauges on deck plate around deck splice at section X-X

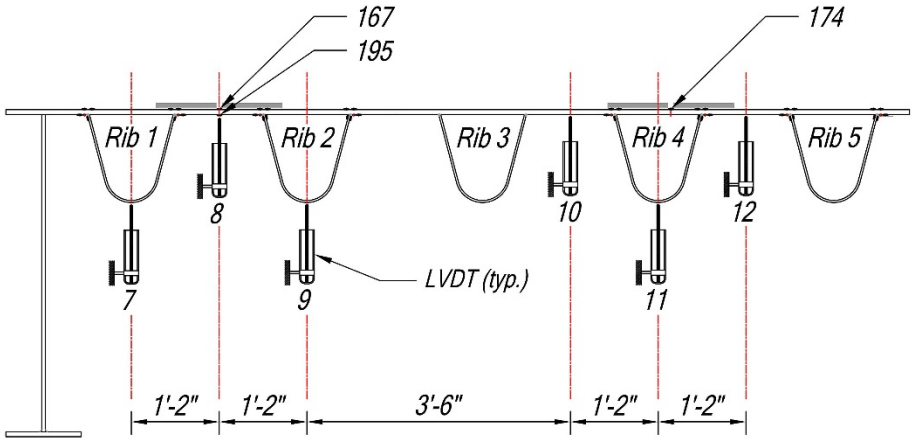

Figure 366. LVDTs at section Z-Z

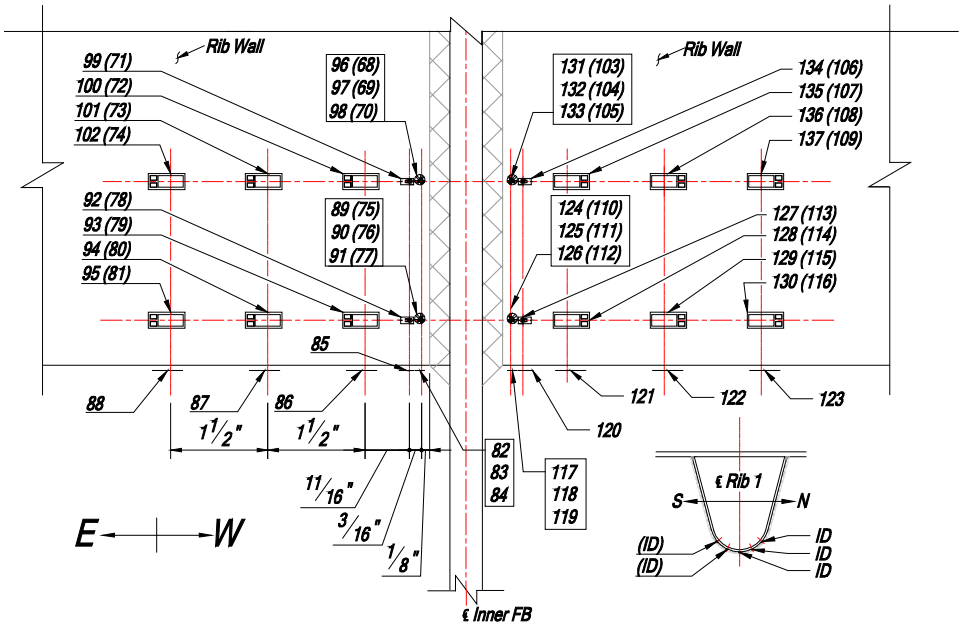

Figure 367. Gauges on north wall of Rib 1 wall at inner FB (gauges on south wall are shown in parenthesis)

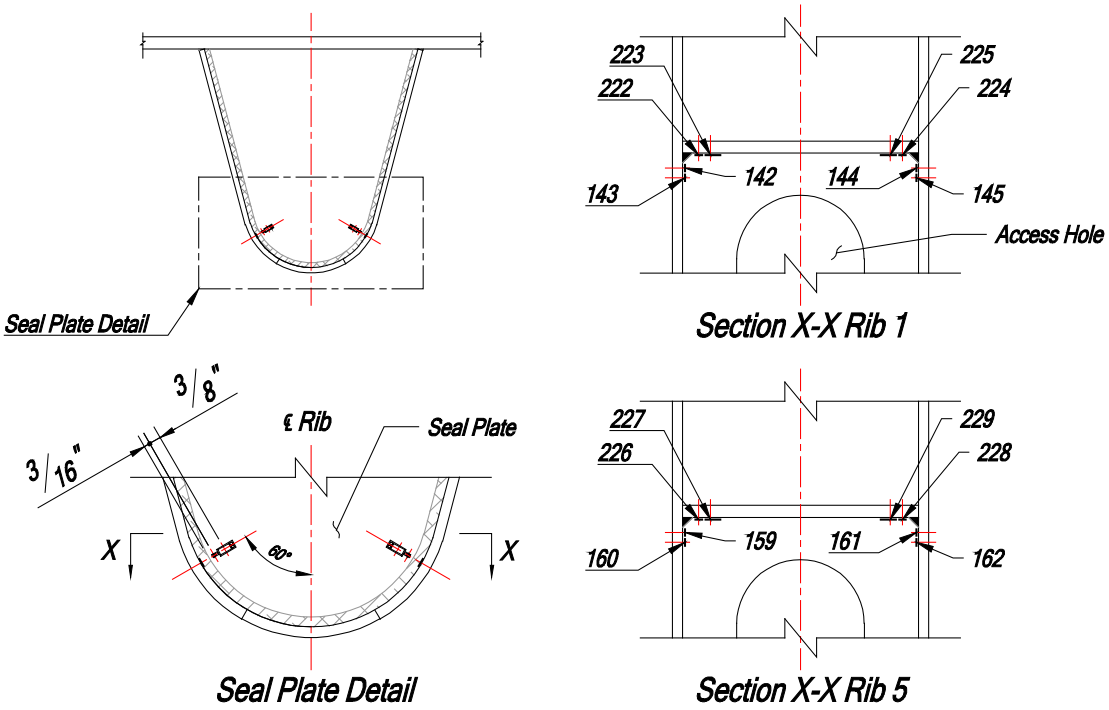

Figure 368. Gauges at rib-to-sealing plate connection

Figure 369. Installation of gauges on rib wall and sealing plate at rib-to-sealing plate connection at HIS facility

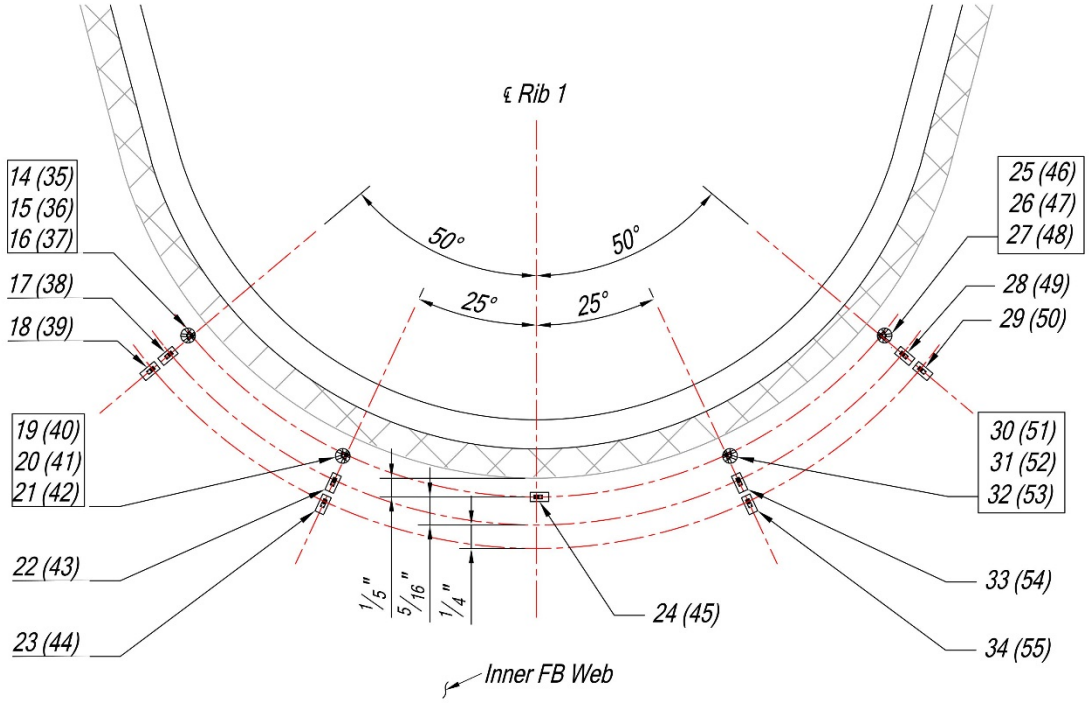

Figure 370. Gauges on east face of inner floor beam web at Rib 1 (gauges on the west face are shown in parenthesis)

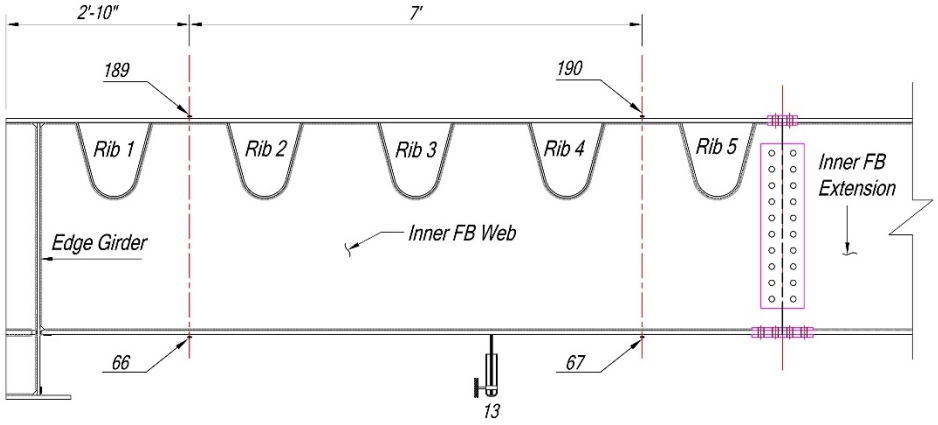

Figure 371. Gauges on inner floor beam at section Y-Y

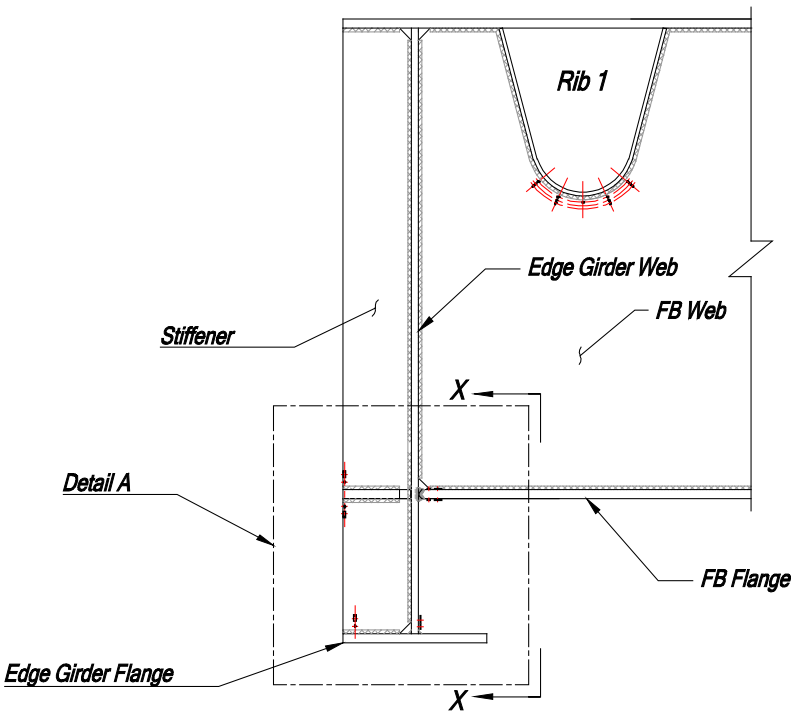

Figure 372. Gauges at inner floor beam-to-edge girder connection

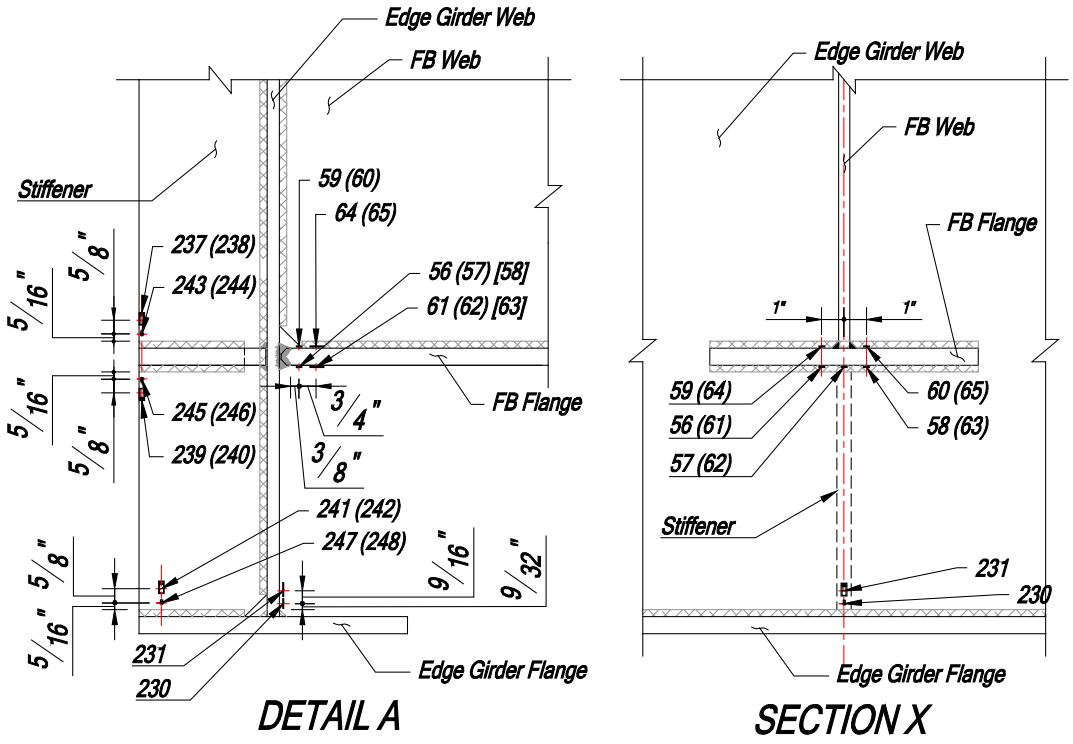

Figure 373. Gauges at inner floor beam-to-edge girder connection (refer Figure 372 for detail and section markings)

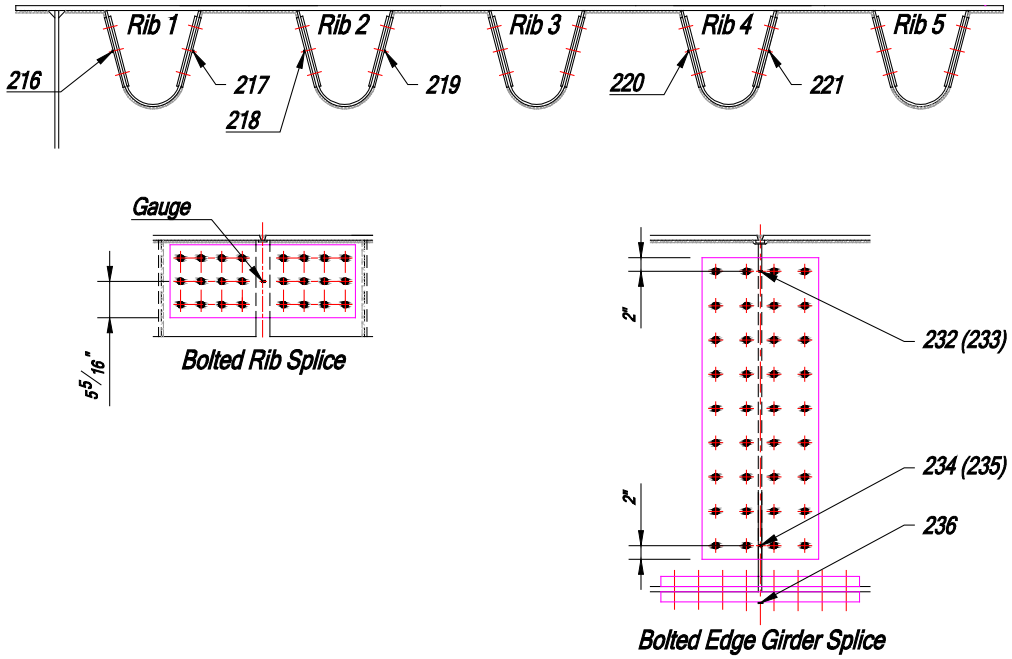

Figure 374. Gauges on the splice plates

Figure 375. Crawl truck

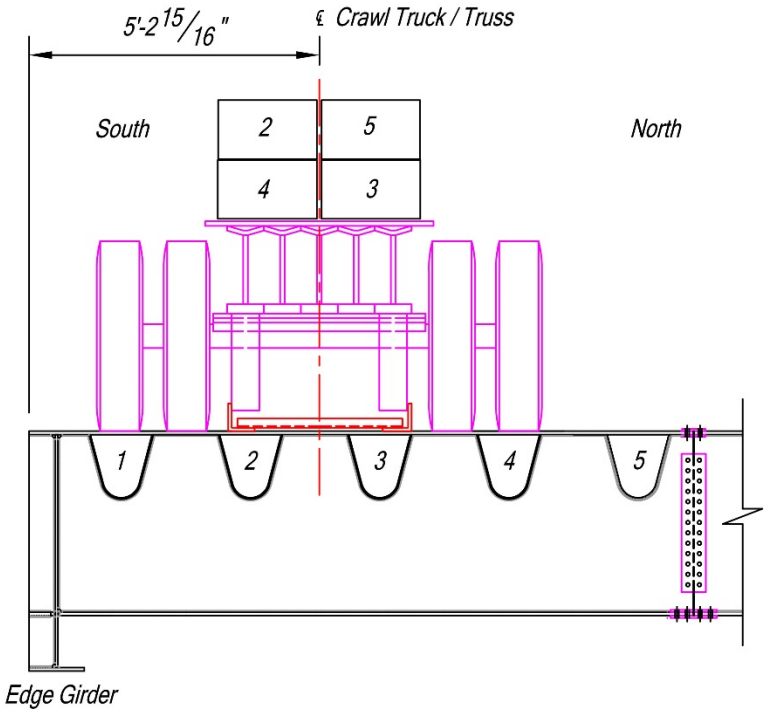

Figure 376. Crawl test position 28

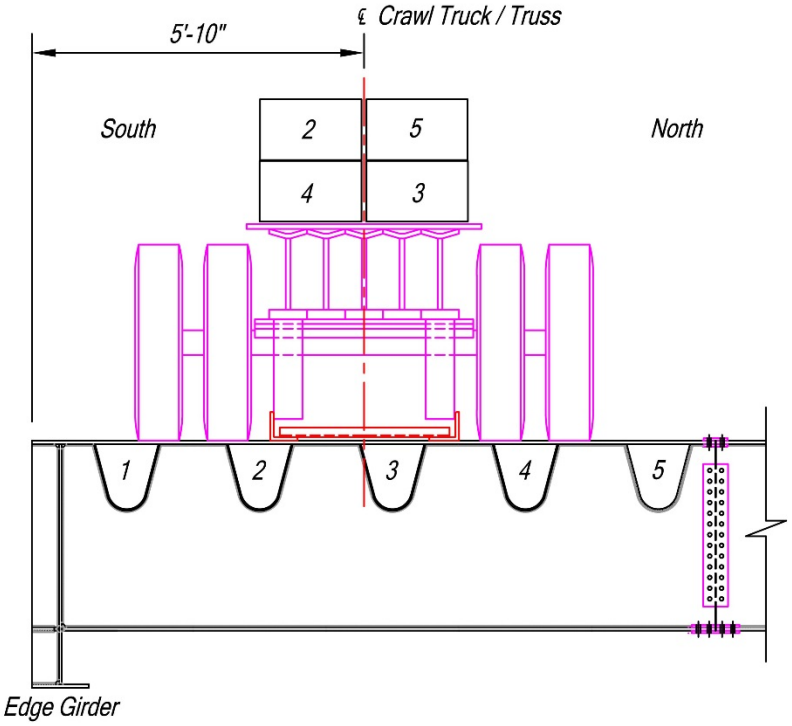

Figure 377. Crawl test position 29

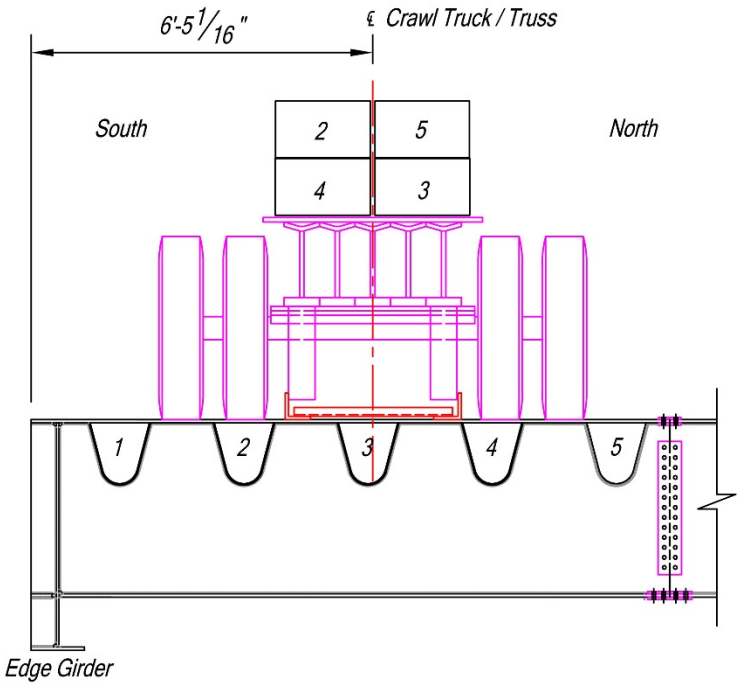

Figure 378. Crawl test position 30

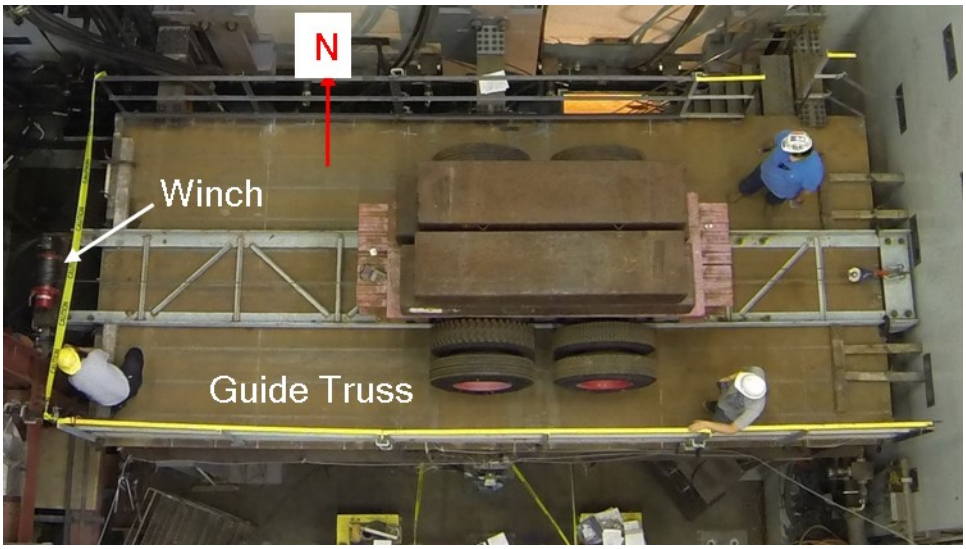

Figure 379. Crawl test setup

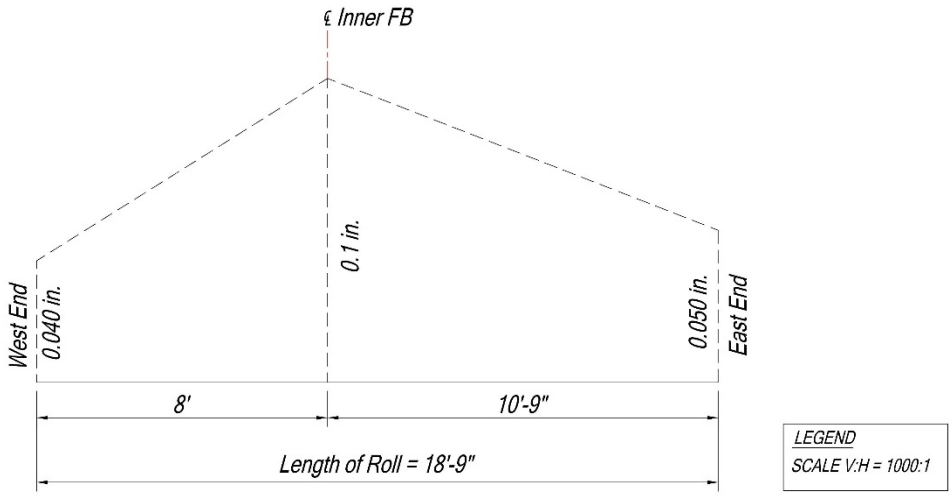

Figure 380. Displacement profile for crawl test

Figure 381. Arrangement of above-deck actuators

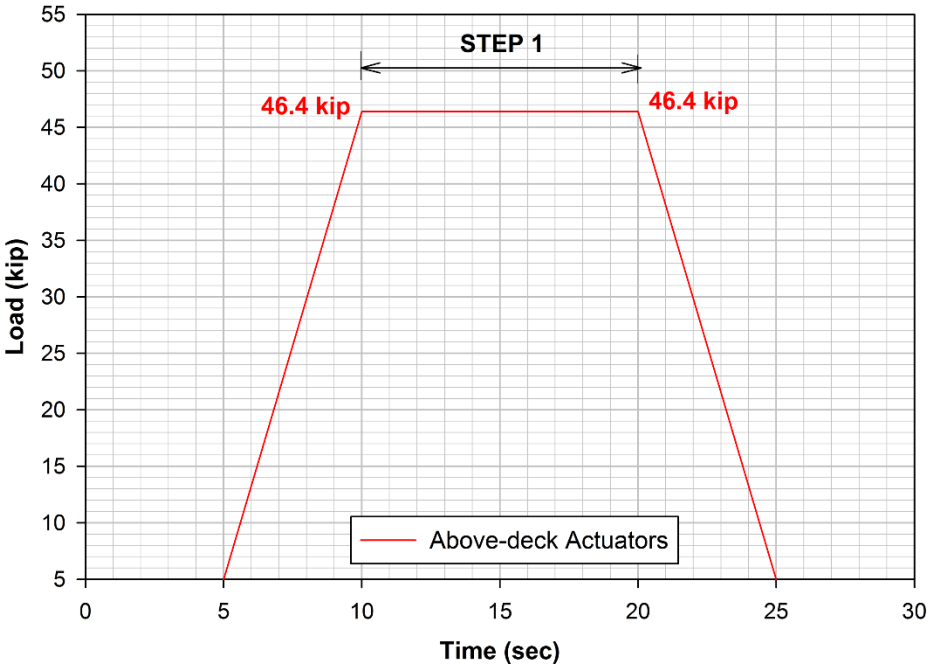

Figure 382. Loading profile for static test

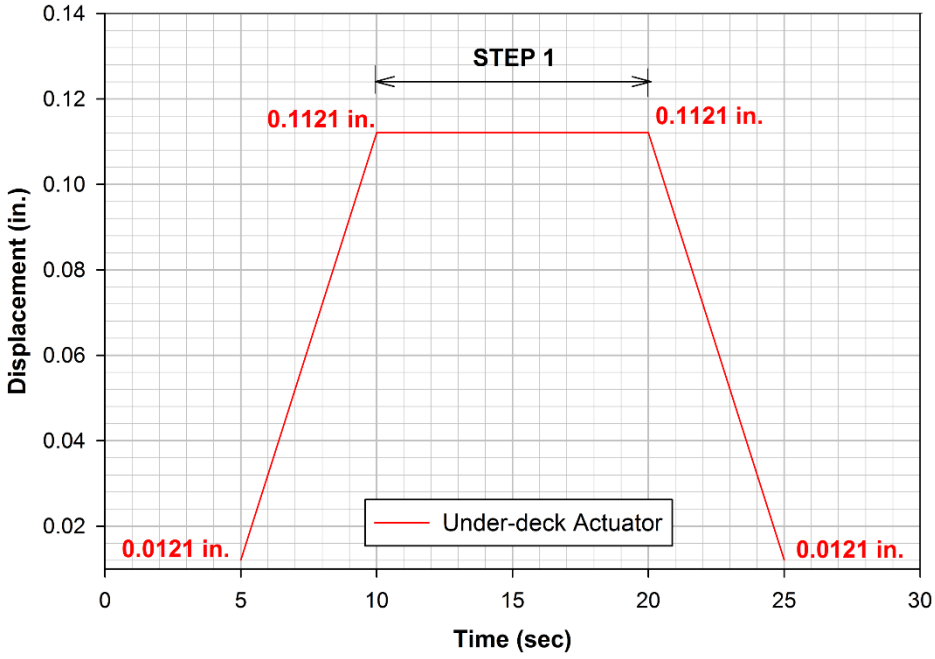

Figure 383. Displacement profile for static test

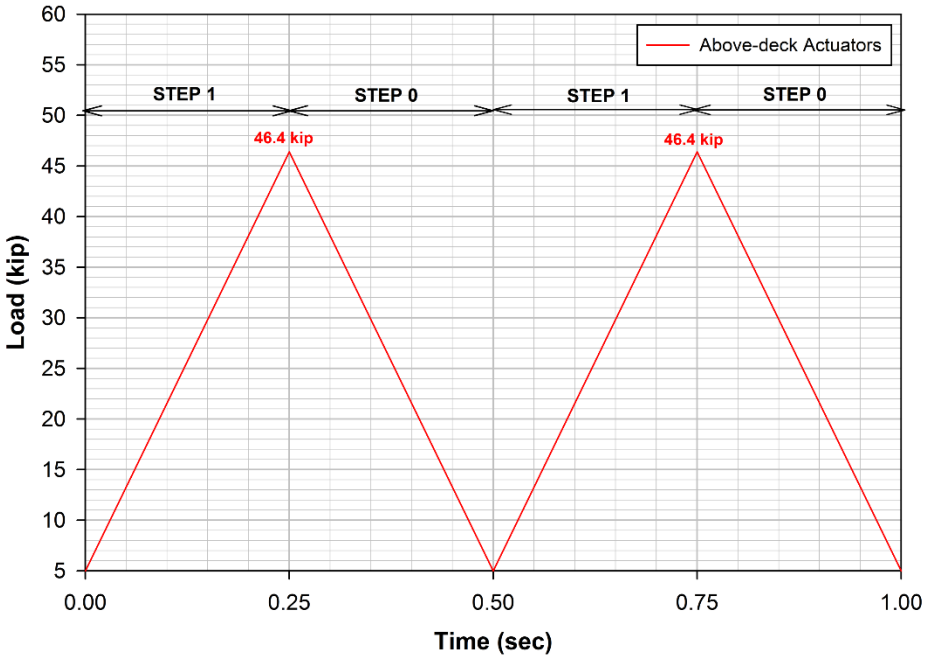

Figure 384. Loading profile for the fatigue test

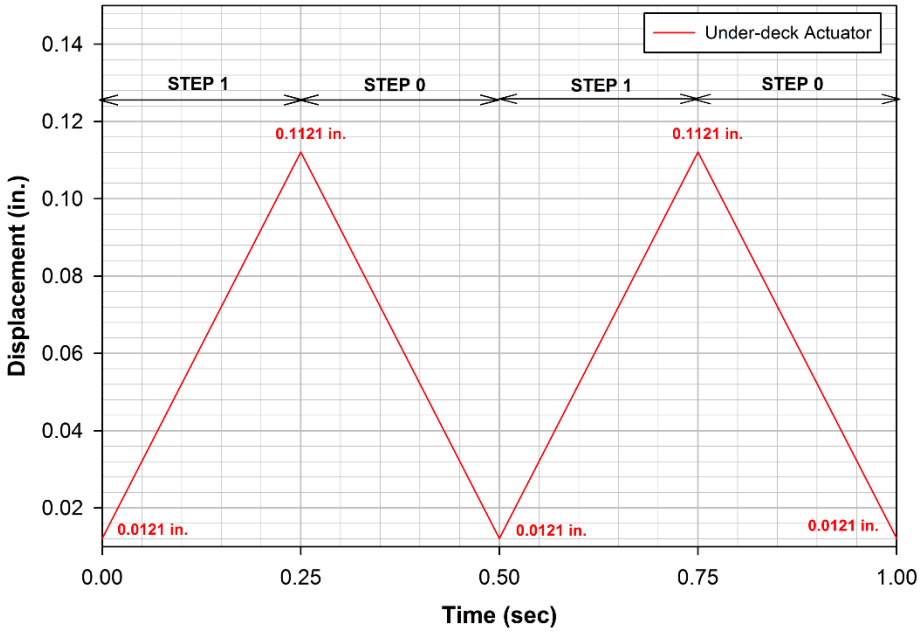

Figure 385. Displacement profile for the fatigue test

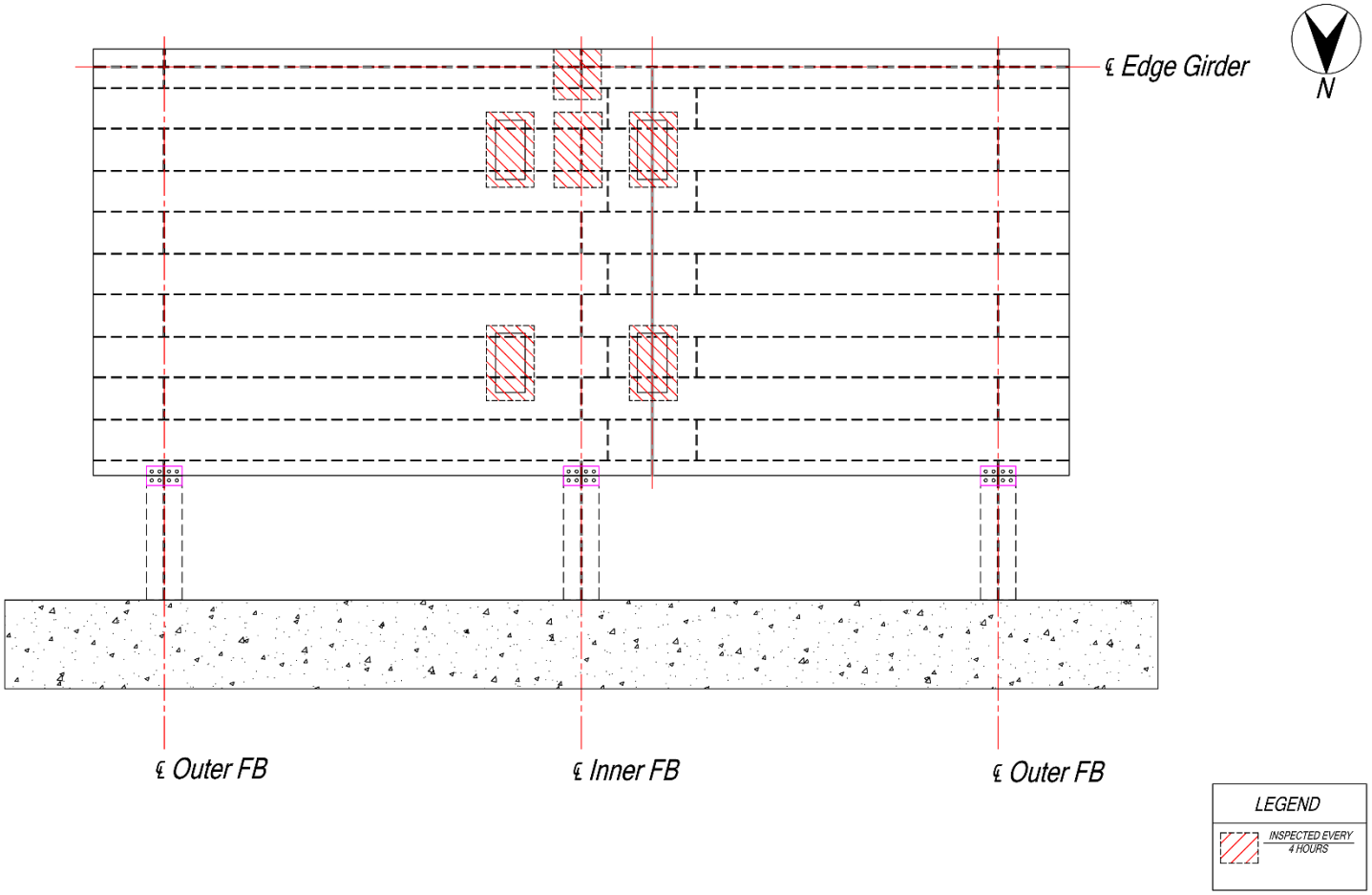

Figure 386. Inspection plan for fatigue testing

9. EVALUATION OF FULL-SIZE TEST RESULTS

The activities undertaken in Task 10 of the research project related to evaluation of test results, excluding the post-test destructive evaluation of the full-size specimen, are reported in this chapter. The results of the post-test destructive evaluation is discussed in Chapter 10.

9.1 Static Test Results

9.1.1 Introduction

At the onset of testing, a static test was performed on September 12, 2014 before initiating fatigue testing on the deck specimen. Three static trials were conducted for the shakedown of residual stresses and to determine the repeatability of the test results. The results of only the final trial are presented. These static tests were conducted with a minimum load of 5 kip (22.2 kN) at each of the two above-deck actuators and 0.0121 in. (0.3 mm) displacement at the under-deck actuator, to simulate the effect of dead load and to avoid loss of contact of the load pads with the deck plate surface.

During fatigue testing, intermittent static tests were performed at about every million load cycles, or following any significant event, to evaluate the change in state of the structure. Subsequent to the fracturing of bolts, connecting the edge girder to the east support column on September 21, 2014, static tests were conducted on September 22, 2014 before restarting the fatigue test at 0.73×10^6 cycles.

During the initial static tests, 106 uniaxial gages of ¼ in. (6 mm) length, 75 uniaxial gages of 1 mm length, 18 rosette gages of 1 mm length and 7 LVDTs were installed on the prototype deck, involving a total of 242 data channels. In addition, the load and displacement outputs from the three actuators were recorded in six other data channels. During subsequent static tests conducted intermittently during the course of the fatigue testing, the LVDTs were disconnected from the data logger. All measurements were conducted within the nominal elastic range of the material. The strains measured at the uniaxial gauges were converted to stresses by multiplying with the universally accepted modulus of elasticity for steel of 29,000 ksi (2×10^5 MPa). For the rosettes, the strains measured at the rosette arms were used to determine the principal and the directional stresses at the rosette locations. The static test results are provided as Appendix M.

9.1.2 Global Response of Prototype Deck

The global response of the prototype deck is discussed in this section in terms of the measurements at the sensors on the deck at sections Y-Y and Z-Z. Uniaxial strain gages, oriented along the transvers direction of the deck, were installed on the top surface of deck plate and at the bottom of inner FB at section Y-Y. A LVDT was also installed at the soffit of the inner floor beam at section Y-Y. At section Z-Z, LVDTs were installed on the soffit of the ribs and at the underside of the deck plate in between the ribs. Uniaxial strain gauges, oriented along the transverse direction of the deck were also installed on the top and the bottom surfaces of the deck plate at section Z-Z.

The static test results are presented as plots of strain gauge and/or LVDT measurements along sections Y-Y and Z-Z, against the distance measured from the south end of the deck. The measured quantities (stresses or displacements) are presented on the Y-axis or the ordinate, and the distance from the south end along the section on the X-axis or the abscissa. Also shown on the plots are: the plan of the deck with the section identified; the increasing direction of abscissa; and the pertaining transverse section of the deck with the instrument location and critical load position shown. It may be noted that the transverse disposition of the wheel loads are indicated on the transverse section Y-Y, although the section did not cut through the load pads. The downward displacements measured at the LVDTs are presented as –ve, and the tensile stresses measured at the strain gauges are presented as +ve.

Response of Deck Plate and Ribs

Figure 387 shows the displacements recorded by the LVDTs at section Z-Z during step 1 (loading step) of the static test along with the FEA results. The LVDTs were installed at the soffit of the ribs 1, 2 and 4 and on the underside of the deck plate in between the ribs 1 and 2, ribs 3 and 4, and ribs 4 and 5. The displacement pattern indicated reverse bending of the deck plate associated with the distortion of the rib cross section across the transverse section. The south wheel load was spread across parts of ribs 1 and 2 and the deck plate in between the ribs, which caused relatively larger local displacements of Rib 2 and the deck plate between ribs 1 and 2. The displacement of Rib 1, however, was less due to its proximity to edge girder which was displaced upward by the under-deck actuator. The larger displacements of Rib 4 and the deck plate between ribs 4 and 5 were due to the global transverse deformation of the deck under wheel loads. In fact, the maximum displacement over the transverse section was recorded at the soffit of the deck plate between ribs 4 and 5. The decrease in vertical displacement of the deck between ribs 2 and 4 (channel 9) indicated hogging flexural deformation of the deck in the transverse direction in between ribs 2 and 4. The displacements recorded by the LVDTs matched with the FEA results, verifying the accuracy of the FE model.

Figure 388 shows the stress ranges measured at the uniaxial gauges installed on the top and bottom surfaces of the deck plate at section Z-Z. FEA results are also shown in the figure. It can be seen that the deck deformed as a continuous beam in the transverse direction supported by the ribs, with the stresses peaking under the load pads and gradually decreasing away from it. The deck deformed in a sagging curvature under the load pads between ribs 1 and 2 and over Rib 4, and in hogging curvature over the rib-to-deck plate connections. As a result stresses on the top of the deck plate were compressive, and on the bottom of the deck plate were tensile in between the ribs or rib walls. Opposite trend was observed over the rib-to-deck plate connections with tensile stress on the top of the deck plate and compressive stress on the bottom of the deck plate. The measurements at the gauges matched very well with the FEA results, further verifying the accuracy of the FE model. The stresses were almost of equal magnitude on the top and the bottom surfaces of the deck plate indicating pure bending of the deck plate with insignificant membrane stresses. The distribution of transverse stresses on the deck plate were symmetrical with respect to the centerline of the simulated tandem

axle, with similar stresses at the south-east and north-east load pads. The maximum measured compressive and tensile stress ranges were about 10 ksi (69 MPa).

Response of Inner Floor Beam

Uniaxial strain gauges of ¼ in. (6 mm) gage length were installed on the soffit (underside of the bottom flange) of the inner floor beam at section Y-Y, centrally between ribs 1 and 2 and ribs 4 and 5. These strain gauges (channels 66 and 67) were oriented transversely, and was aligned with similar strain gauges on the top of the deck plate (channels 189 and 190). A LVDT (channel 13) was also installed on the soffit of the inner floor beam at section Y-Y, aligned with the centerline of Rib 3.

The measurements at these gages are shown in Figure 389 along with the FEA results. The measurements matched well with the FEA results, verifying the accuracy of the FE model. The measured stress ranges at channels 66 and 67 were 2.94 ksi (203 MPa) and 4.59 ksi (31.7 MPa) respectively. The measured stress ranges at channels 189 and 190 were -0.32 ksi (2.2 MPa) and -0.53 ksi (3.7 MPa) respectively. As expected, the inner floor beam and the deck plate experienced global compressive and tensile stresses at the top of deck plate and bottom of inner FB due to flexural deformation of the deck in the transverse direction. Because of the composite action with the deck plate, the compressive stresses were significantly smaller than the tensile stresses. Tensile stress at bottom flange was more at channel 67 (between ribs 4 and 5), which was expected as the recorded displacement (Figure 387) was maximum at the LVDT there (channel 12 between ribs 4 and 5). Since the load pads were significantly away from the gages on the deck plate under the static test load configuration, the gages did not experience any local deformation. The maximum displacement measured by the LVDT was 0.016 in. (0.4 mm).

9.1.3 Response of Rib-to-Deck Plate Connection

Response of the rib-to-deck plate connection is presented in terms of stresses measured at the uniaxial gauges installed in back-to-back configuration on the deck plate and rib walls at section Z-Z coinciding with the east above-deck actuator (Figure 364). On the deck plate, the strain gauges were installed on the top and the bottom surfaces, oriented in the transverse direction, normal to the rib-to-deck plate weld. On the rib walls, strain gauges were installed on both surfaces, oriented along the rib, normal to the rib-to-deck weld. However, the gauges on the inner face of the rib walls got damaged while welding the ribs to the deck plate. The results are presented for the ribs under the load pads i.e. north wall of Rib 1 and south wall of Rib 2 under south-east load pads and walls of Rib 4 under north-east load pads

Measured stress ranges at the rib-to-deck plate connections under the south-east load pads are shown in Figure 390. The stresses on the bottom surface of the deck plate and on the outer surface of rib wall was compressive near the rib-to-deck plate connection as the connection underwent local out-of-plane deformation under the wheel loads. However, presence of high tensile residual stress at the weld toe could create localized tensile field and could cause fatigue cracking of the connection. The maximum

compressive stress ranges were measured at the rib-to-deck plate connection for north wall of Rib 1 (channels 140 and 193) and were about 12.5 ksi (86.3 MPa) and 6 ksi (41.4 MPa) near the weld toe on rib and deck plate respectively. The compressive stress ranges at the rib-to-deck plate connection for south wall of Rib 2 (channels 146 and 196) were lower. The compressive stress range at the gage closer to rib-to-deck weld toe was higher due to weld toe notch and the stress range decreased at the next gage. Stresses were tensile on the top surface the deck plate near the welded connection. The stresses under the load pads away from the weld were compressive and tensile on the top and bottom surfaces of the deck plate respectively (channels 167 and 195), indicating sagging flexural deformation of the deck plate under the load pads in the transverse direction.

Figures 391 and 392 compare the measurements at the rib-to-deck plate connections under the south-east load pads with the FEA results. Tensile stresses are plotted on the outer face of the rib wall and the top of deck plate. Tensile stress is considered as +ve. Figure 391 shows the stresses on the top of deck plate and the outer face of rib wall. The measurements showed similar tend as FEA. The compressive stress ranges at the gauges on the rib walls were slightly higher than the FEA results. Since the response of orthotropic decks is manifested locally under wheel loads, it is possible that a small transverse shift in the load position could cause a significant change in the bending stress and rapidly changing local stress. The stresses on the outer surface of the south wall of Rib 1 showed opposite trend of flexural deformation to that of north wall with tensile stresses at the rib-to-deck plate connection, indicating distortional deformation of Rib 1. Figure 392 shows the stresses on the bottom face of the deck plate and inner face of the rib wall. As observed from FEA, the stresses on the inner face of rib wall were tensile near the connection as opposed to compressive on the outer face of the rib wall due to large out-of-plane bending of the rib wall. However, their magnitudes were not same due to presence of axial stress in the rib wall. This phenomenon could not be verified by the measurements as the gages on the inner face of the rib wall was damaged during welding the ribs to the deck plate. The gages on the bottom surface of deck plate showed similar trend as FEA. The stresses on the bottom surface of deck plate were almost of similar magnitude to that on the top of deck plate, indicating transverse bending of deck plate with insignificant membrane stress.

Measured stress ranges at the rib-to-deck plate connections under the north-east load pads are shown in Figure 393. Similar to the rib-to-deck plate connection under the south-east load pads, the stresses on the bottom surface of the deck plate and on the outer face of rib wall was compressive near the rib-to-deck plate connection as the connection underwent local out-of-plane deformation under the wheel loads, however, the stress ranges were lower. The maximum compressive stress ranges were measured at the rib-to-deck plate connection for north wall of Rib 4 (channels 152 and 202) and were about 3 ksi (20.7 MPa) and 7 ksi (48.3 MPa) near the weld toe on rib and deck plate respectively. The compressive stress ranges at the rib-to-deck plate connection for south wall of Rib 4 (channels 150 and 200) was lower than the north wall. The compressive stress range at the gage closer to rib-to-deck weld toe was higher due to weld toe notch and the stress range decreased at the second gauge. Stresses on the top surface of the deck plate were tensile near the welded connection. The stress under

the load pads away from the weld were compressive on the top surface of the deck plate (channel 174), indicating sagging flexural deformation of the deck plate under the load pads in the transverse direction.

9.1.4 Response of Rib-to-Floor Beam Connection

The response of the rib-to-floor beam connection is presented in terms of the stresses measured at the gauges on the inner floor beam web and Rib 1 at the rib-to-floor beam connection (Figure 370). As determined from FEA of the global model, Rib 1-to-inner floor beam connection adjacent to the edge girder was the most critical and hence the connection was extensively instrumented. All the gages on the floor beam web at the Rib 1-to-inner floor beam connection were installed symmetrically on the north and south sides of the rib, and on each side the gages were installed back-to-back on the east and west faces of the floor beam web to measure the in-plane and the out of plane stress components. The gages on the Rib 1 wall were installed symmetrically on the north and the south walls as well as to the east and the west sides.

Experimental studies of Phase II identified a failure mode of the rib-to-floor beam connection by crack growth from the LOF at the weld root, subjected to the maximum principal stress field. 1 mm rosette gauges were installed in back-to-back configuration on the inner floor beam web adjacent to the weld toe to capture the complex stress distribution of stresses near the weld toe and to determine the magnitude and direction of principal stresses at those locations. The principal stresses measured from the back-to-back rosettes on the south side of Rib 1 are tabulated in Table 40 to Table 43. The layout of the rosette gauges and the direction of the principal stresses are also shown in the respective tables. Tensile stresses are defined as +ve. The direction of principal stresses is presented for the principal stress of the larger magnitude, with respect to the vertical. This angle is defined +ve in counter-clockwise direction. The floor beam web to the south of Rib 1 (towards edge girder) experienced tensile stresses. The measured maxima of principal stresses were about 9.8 ksi (67.6 MPa) on the south side of the rib and -13.7 ksi (94.5 MPa) on the north side of the rib, at 25 degree from the rib soffit. The principal stresses on the west faces were less indicating presence of some out-of-plane bending of the floor beam web and/or twisting of Rib 1. The stresses on the west face was probably low due to the presence access holes at the rib soffits on the west side of the floor beam, affecting the flexural and torsional stiffness of the ribs. However, the direction of the principal stresses on the east and west faces were comparable.

The measured maxima of principal stresses at the rosette gages on the inner floor beam web are shown in Figure 394. It should be noted that, fatigue damaged is attributed to the stress range and not maxima of stresses. Accordingly, the measured principal stress ranges at the rosette gages on the inner floor beam web are shown in Figure 395, along with the FEA results. The measured maximum principal stress ranges at the rosette gages on the floor beam web were about 9.0 ksi (62.1 MPa) on the south side of the rib and -12.5 ksi (86.3 MPa) on the north side of the rib, at 25 degree from the rib soffit. The measured stress ranges were lower than FEA results. FE model has perfect weld toe notch with zero notch radius, however finite rounding exists at the weld toe in the specimen. Hence, the principal stresses in real structure were lower than the

FEA results. The distribution of principal stress on the south side of inner FB web is presented graphically in Figure 396. It is evident that the orientation of maximum principal stress was almost tangential to the rib-to-floor beam connection, and was similar to the FEA results. The distribution of principal stresses was consistent with the transfer of simulated wheel loads from the deck plate to the edge girder by shear in the floor beam web. Shear force was developed between the distributed loads and the nearest support (in this case the edge girder). In this shear span, a diagonal tension field developed in the inner floor beam web from the bottom (tension) flange to the top corner formed by the edge girder, deck plate and floor beam. The diagonal tensile field deviated around the cutout near the rib rounding due to discontinuity in the floor beam web causing stress concentration at the rib-to-floor beam connection around the rib rounding. The diagonal tension field being tangential to the connection, the maximum principal stress was about tangential to the rib-to-floor beam connection. As stated earlier and as also seen in Figure 396, the principal stress ranges on the west face of the inner floor beam were less than that on the east face indicating presence of some out-of-plane bending of the floor beam web and/or twisting of Rib 1.

Fatigue cracking at the weld toe is primarily attributed to the crack growth from the micro discontinuities subject to the stress range normal to the weld toe. The measured principal stresses and their orientation were used to calculate the stress along the rosette arms, one of which was aligned normal to the rib-to-floor beam weld toe. Figures 397 and 398 show the measured stresses and stress ranges on the inner floor beam web normal to the weld toe as obtained from the gage measurements. The maxima of the normal stress were about 3.9 ksi (27.1 MPa) and -6.9 ksi (-47.5 MPa) on the south and the north sides of the rib respectively, at 50° from the rib soffit. The maximum stress ranges were about 3.6 ksi (24.8 MPa) and -6.3 ksi (-45.5 MPa) on the south and the north sides of the rib respectively, at 50° from the rib soffit. Among the three gages along each radial lines, the largest (magnitude) of the stress was observed at the first gage or gage closest to the weld toe (the arm of the rosette aligned normal to the weld toe). It can also be seen pictorially form Figures 399 to 406, where stress ranges measured at gages installed along radial lines on the inner floor beam web are plotted along with the FEA results. The measurements showed similar trend as of FEA. The measured stress ranges on the Rib 1 wall normal to the weld toe are shown in Figures 407 to 416 along with the FEA results. The gage measurements showed similar trend as FEA, with the largest (magnitude) of the stress at the gage closest to the weld toe. Similar to FEA, reverse bending of the rib wall was observed from the static test results at about 1 in. from the weld toe.

9.1.5 Response of CJP Deck Splice

Figure 417 shows the stress ranges measured at the uniaxial gages, installed on the top and the bottom surfaces of the deck plate around the transverse deck splice under south-west load pads. FEA results are also shown in the figure. These strain gages (channels 181 to 184, and channels 208 to 211) were oriented along the longitudinal direction of the deck. The measurements at the gages under the north-west load pads are not shown as the stresses were similar to the gages under the south-west load pads. Similar to FEA, stresses were tensile at the bottom of the deck plate due to global

longitudinal bending of the deck. The maximum stress range recorded at the bottom of deck plate was about 7 ksi (48.3 MPa). The stresses measured at the bottom of the deck plate matched well with the FEA results. Two of the gages (channels 182 and 183) on the top of the deck plate under the south-west load pads got damaged during the crawl test. Gages on the top of the deck plate under the north-west load pads also got damaged during the crawl tests. Stresses on the top of the deck plate were compressive, however their magnitude was less than the stresses on the bottom of the deck plate, indicating presence of membrane stress in the longitudinal direction of the deck. In addition, stresses recorded by the gages on the top of the deck plate deviated from the FEA results. The top deck gages were directly under the wheels during the crawl tests which could have caused their malfunctioning. In that case, the stresses recorded by these gages are questionable.

9.2 Fatigue Test Results

Fatigue testing of the full-size specimen was initiated on September 12, 2014. Static tests were conducted prior to fatigue test. The initial static tests allowed keeping record of the baseline condition of the deck. Some minor issues like loud actuator noise, shaking of the hydraulic hoses and malfunctioning of data loggers were encountered at the beginning of the fatigue test. But the issues were addressed promptly. Initially, the test was run at 1 Hz frequency for about 400,000 cycles till September 18, 2014, and then was shifted to 2 Hz frequency when the stability of the fatigue test was ensured. The test was conducted uninterrupted 24 hours a day and seven days a week, except for interruptions due to routine checks, maintenance or significant events. The specimen was inspected for possible fatigue cracking regularly at an interval of 4 hour with the exception during night time when the last inspection for a day was at 10:30 PM while the first inspection for the next day was at 7:00 A.M. The inspections were aided with 10X magnifying glass. All the data collected for each day of testing was also checked regularly for any spike or irregularity in the data. Any unusual incident was flagged and immediate course of actions were taken to sort out the problem. Intermittent static tests were carried out at about every million cycles interval, when the testing was interrupted for routine maintenance and conducting the static tests.

Fatigue testing upto 5 million loading cycles on the deck was completed on October 28, 2014. The total number of fatigue test cycles subjected to the deck specimen at that time was 5,006,859 cycles. After completion of the 5 million cycles, the deck specimen was thoroughly inspected for fatigue cracks manually using a bright light and a 10x magnifying glass. No fatigue crack was detected in the specimen. As per NJDOT's advice, fatigue testing was continued upto 8 million cycles, which is the upper bound of AASHTO Category C design curve at the CAFT. Static test was conducted on November 3, 2014 before resuming fatigue testing of the deck specimen. The fatigue test was terminated on December 9, 2014 after 8 million load cycles, without any detectable fatigue damage in the deck. The results would indicate infinite life performance, as long as the site specific overloads do not exceed the above load more than 1 in 10000 occurrences. The test results also demonstrated that the large deviation from the specified fabrication tolerances and the rejected welding procedures, which were noted during the specimen fabrication and installation, did not affect the performance of the

deck. This suggests that the specified fabrication tolerances are arbitrary at best. The number of fatigue test cycles subjected to the deck specimen was 8,002,460. A static test was performed on December 10, 2014 in order to acquire information on any changes in behavior of the specimen in comparison to the start of the testing or baseline condition. The static test measurements at the strain gauges didn't show any significant variation, implying that the deck was undamaged.

9.2.1 Evaluation of Intermittent Static Test Results

As discussed earlier, intermittent static tests were carried out at about every million cycles interval, when the testing was interrupted for routine maintenance and conducting the static tests. Theses static tests permitted collection of longer duration of data at higher sampling rate that produced stable data with reduced noise and allowed assessment of the changes in the state of the deck by comparing stresses at the critical gauges with the prior static tests. Figures 418 to 423 show the change in stresses at some of the critical gages, measured during the intermittent static tests. The abscissa of these plots (the lower horizontal axis) shows the number of stress cycles on a linear scale. The dates of the static tests are marked sequentially on the upper horizontal axis of the plots, matching with the corresponding number of fatigue stress cycles.

Figures 418 and 419 show the history of maximum tensile principal stress ranges and maximum compressive principal stress ranges measured at the 1 mm rosette gages on the inner floor beam web at the connection with Rib 1. Figure 420 shows the history of maximum tensile principal stress ranges measured at the 1 mm rosette gages on the Rib 1 south wall at the connection with inner floor beam. It can be seen from the figures, the principal stress ranges at the rosettes dropped initially, by about 0.5 ksi, but later remained stable. This can be due to the wide fluctuation of ambient temperature happening during that time of the year. However, the drop was insignificant. These stress history plots confirm that the stress ranges were stable during the fatigue test and there was no fatigue damage of the connection after 8 million cycles, which was also confirmed by regular visual inspection.

Figure 421 shows the history of stress ranges measured at the uniaxial gages on the Rib 1 north wall aligned normal to the Rib1-to-deck plate weld, and abutting the weld toe. These gages were located at the loaded section Z-Z to the east of the floor beam under the south loading pad. The stress history plot shows a drop in the stress range of about 1 ksi (6.9 MPa) after 4 million cycles, however no fatigue cracking was detected at this connection by visual inspection. Figure 422 shows the history of stress ranges measured at the uniaxial gauges on the deck plate at the same section The stress ranges observed at the back-to-back (top and bottom) gauges (channels 167 and 195) showed that the deck plate was in pure bending with negligible membrane stresses. The stress ranges at both the gauges decreased by about 1.5 ksi (10.4 MPa) after 5 million cycles and remained stable till the completion of the test. However, no cracks were observed by visual inspection. Gauges identified by channel numbers 165 and 166 were located directly under the south load pad and were damaged after 1 million and 6 million cycles of fatigue testing, respectively. The stress history plots of the undamaged gauges located at the Rib 1-to-deck plate connection suggested that the rib-to-deck

plate connection directly under the load pad was undamaged. This was also confirmed by visual inspection of the connection.

Figure 423 shows the history of stress ranges measured at uniaxial gauges, installed in back-to-back on the top and bottom of the deck plate adjacent to the transverse deck splice, and under the south-west load pad. Only two gauges are shown, as the other gages on the top of the deck got damaged during the course of testing. The stress ranges observed at the gauges showed that the deck plate was in pure bending with negligible membrane stresses. However, the stress range at the top gage decreased by about 3 ksi (20.7 MPa) after 5 million cycle, but remained stable till the completion of the test. The top gages were replaced after 5 million cycles as they got damaged while lifting the load pads for inspecting the deck splice. However, no fatigue cracking could be detected visually. The stress gradient adjacent to the load pad being very high, an insignificant shift in the location of the gauge could cause significant change in the stress value

Therefore, no significant change was noted in the stress ranges at the critical gages during the intermittent static tests, confirming that the deck specimen essentially remained undamaged after 8 million cycles of fatigue testing.

9.2.2 Assessment of Fatigue Performance

Performance of Rib-to-FB connection

The fatigue performance of rib-to-floor beam connection is evaluated against cracking from weld toe and weld root, although no cracking was observed at the connection. FEA showed high stress concentration and stress gradient at the Rib 1-to-inner floor beam connection. Consequently, this connection was identified as the most critical and was extensively instrumented. Fatigue cracking at the weld toe is primarily attributed to the crack growth from the micro discontinuities subject to the stress range normal to the weld toe. The stress range normal to the weld toe was determined by local stress approach as specified in AASHTO LRFD Bridge Design Specifications. According to AASHTO, local structural stress range at the weld toe is determined by using two reference points, at 0.5t and 1.5t from the weld toe, and extrapolating from these two points to the weld toe. However, gages were installed at 0.4t, t and 1.5t from the weld toe at the connection on the inner floor beam web. FEA showed that linearly extrapolating stress values from 0.4t and 1.5t to the weld toe caused insignificant change to the stress at the weld toe as the stress values at 0.4t, 0.5t and 1.5t were essentially along a straight line (Figure 424). Accordingly, the two reference points were taken at 0.4t and 1.5t for calculating local structural stress range at the weld toe. Calculation of the local structural stress range at the tension side of the connection at the point of maximum normal stress is shown in Figure 425. In addition, fatigue cracks initiating from the weld root and propagating normal to principal stress field was observed in the mockup specimens during Phase 2 studies. Accordingly, the fatigue performance of the connection is also evaluated against cracking from the weld root using principal stress range at weld root as obtained from FEA.

Fatigue performance of the connection against cracking from the weld toe is evaluated in Figure 426, where the local stress range normal to the weld toe versus total life is plotted along with AASHTO design S-N curve. For better accuracy, the plotted stress ranges were computed from the results of initial static tests performed at the beginning of the fatigue test. The maximum value of the local stress ranges at the tension and the compression side of the connection were about 5.2 ksi (36 MPa) and 8.8 ksi (61 MPa) respectively. As it can be seen from the figure, the calculated local stress ranges matched well with the FEA results. The fatigue resistance of this connection detail is defined by AASHTO Category C against fatigue crack growth from the weld toe, having a CAFT of 10 ksi (69 MPa). The local stress ranges were below the CAFT. Therefore, the connection detail was expected not to develop fatigue cracking i.e. exhibit infinite fatigue life. It was experimentally verified when no fatigue damage was observed at the connection after 8 million loading cycles. It can also be seen from Figures 418, 419, and 420, where no significant change in the measurements at the gages at the connection was observed during the course of the experiment.

Fatigue performance of the connection against cracking from the weld root is evaluated in Figure 427, where the local principal stress range at the weld root as determined from FEA versus total life is plotted along with AASHTO design S-N curve. The principal stress ranges at the weld root were about 11.5 ksi (79 MPa) and 12.3 ksi (85 MPa) respectively at the tension and the compression sides of the connection respectively. As it can be seen from Figure 427, the performance of this connection exceeded the lower bound or 95% confidence on 95% probability of survival life for Category B details, which is close to the upper bound or 95% confidence on the 95% probability of failure of Category B' details. The limited test data shows the performance of the connection better than AASHTO Category B'. However, due to limited test data and the expected scatter in the performance of these connections due to the inherent variability in welded connections, the test result was inadequate to evaluate this scatter and draw any statistically significant conclusion against cracking from weld root. In that respect the fatigue test results from this study should be considered as indicative.

Performance of Rib-to-Deck Plate Connection

The full-size testing was conducted for the most critical disposition of the tandem axle for creating the most critical stress state at the rib-to-floor beam connection. The rib-to-deck plate connection was not subjected to its most critical stress state for this load disposition. However, the fatigue performance of rib-to-deck plate connection is evaluated for the test stress state in Figure 428, where the local stress range normal to the weld toe versus total life is plotted along with AASHTO design S-N curve. The stress ranges are plotted for the north wall of Rib 1 as maximum stress ranges were observed at that connection. For better accuracy, the plotted stress ranges were computed from the results of initial static tests performed at the beginning of the fatigue test.

As per the latest AASHTO recommendations, the local structural stress ranges at the weld toe were determined by extrapolating from measurements at 0.5t and 1.5t ahead of the weld toe; channels 193 and 194 for weld toe on deck plate and channels 140 and 141 for weld toe on Rib 1. The extrapolated stress ranges at the weld toe were about 8

ksi (55 MPa) and 12.5 ksi (86 MPa), respectively on deck plate and rib. Stress ranges were also determined from FEA in a similar manner and they were about 8 (55 MPa) and 9.5 ksi (66 MPa), respectively at the weld toe on deck plate and the rib. The local structural stress ranges were compressive at the connection. However, the presence of tensile residual stresses at the weld toe could result in the local tensile stress range leading to fatigue cracking from the weld toe.

The fatigue resistance of this connection detail is defined as AASHTO Category C against fatigue cracking from the weld toe, having a CAFT of 10 ksi (69 MPa). The stress ranges determined from FEA were below the CAFT. Therefore, the connection detail was expected not to develop fatigue crack i.e. exhibit infinite fatigue life under the test stress state. It was experimentally verified when no fatigue damage was observed at the connection after 8 million loading cycles. It can also be seen from Figures 421 and 422, where no significant change in measurement at these gages was observed during the course of the testing. The stress range at the weld toe on the deck plate determined from measurements was below CAFT, however, the measured stress range at the weld toe on the rib was more than the CAFT. The design life of the rib-to-deck plate connection with respect to the measured stress range at the weld toe on the rib was estimated to be about 2.2 million cycles. However, the connection didn't develop any crack at the weld toe on the rib after 8 million loading cycles. It should be noted that the AASHTO fatigue design curves were developed based on fatigue test results on full scale beam specimens under constant amplitude loading and represent 95% confidence on 95% probability of survival fatigue life. Due to inherent variability, welded connections are expected to exhibit scatter in their performance. The limited test data of the subject deck was inadequate to evaluate this scatter and draw any statistically significant conclusion. In that respect the fatigue test results from this study should be considered as indicative. The significant difference between the estimated design life and the test result corresponding to the cracking mode at the weld toe could be attributed to the inherent variability.

Performance of Transverse CJP Deck Splice

The fatigue performance of the CJP deck splice is evaluated in Figure 429, where the local stress range normal to the weld toe versus total life is plotted along with AASHTO design S-N curve. Evaluating the performance of this detail was very critical as lot of deviations were observed at the deck splice from the specified fabrication tolerances during specimen installation. The stress ranges are plotted for the deck splice under the south-west load pads.

Similar to the other details, the local structural stress ranges at weld toe were determined by extrapolating from measurements at 0.5t and 1.5t ahead of the weld toe; channels 181 and 182 for weld toe on the top of the deck plate and channels 208 and 209 for weld toe on the bottom of the deck plate. The extrapolated stress ranges at the weld toe were about 7 ksi (48 MPa) and 6.7 ksi (46 MPa) on the top and bottom surfaces of the deck plate respectively. Stress ranges were also determined from FEA in a similar manner and they were about 5.5 (38 MPa) and 7.4 ksi (51 MPa), respectively on the top and bottom surfaces of the deck plate. Stress ranges on the top

of the deck plate were compressive. However, the presence of tensile residual stresses at the weld toe could result in the local tensile stress range at the weld toe on the top of the deck plate leading to fatigue cracking from the weld toe.

AASHTO specifies deck plate splice done with a groove weld as Category D detail, however it assumes that the backing bar is left in place. For the subject deck, the backing bar was removed and the weld reinforcement was not ground smooth. The detail is equivalent to a transverse butt splice between two plates done by a CJP weld, with weld reinforcement in place. The fatigue resistance of the connection detail can then be defined by AASHTO Category C against fatigue crack growth from the weld toe and then extending into the base metal, having a CAFT of 10 ksi (69 MPa). The stress ranges determined from FEA as well as the test measurements were below the CAFT. Therefore, the connection detail was expected not to develop fatigue crack i.e. exhibit infinite fatigue life. It was experimentally verified when no fatigue damage was observed at the connection after 8 million loading cycles. It can also be seen from Figure 423, where no significant change in measurement at these gages was observed during the course of the testing. The test results showed that the CJP deck splice exhibited infinite fatigue life, even with significant deviations from the fabrication tolerances. It can be concluded that the specified fabrication tolerances for orthotropic decks are too stringent and ad hoc at best, and further research is required to find out rational fabrication tolerances for economic fabrication of the deck with lesser efforts.

9.3 Crawl Test Results

Crawl tests were performed to characterize the response of the deck under moving load in different positions. As discussed earlier, the initial crawl tests were discarded due to some fixture issue. Accordingly, the crawl tests were repeated after the fatigue test was completed. The LVDTs were reconnected to the deck for the crawl test.

The crawl test results are presented as plots of strain gauge and/or LVDT measurements along with the FEA results against the travel of the test truck. Considering the symmetry of the prototype deck with respect to inner FB, the travel of the test truck is presented as the distance of the truck centerline from inner FB on the X-axis or the abscissa. The measured quantities (stresses or displacements) along with the FEA results are presented on the Y-axis or the ordinate. The start and end points of travel for the crawl test truck was 10 ft. in (3 m) to the west side and 8 ft. 9 in. (2.7 m) to the east side of the inner FB respectively. Thus, the total distance travelled by the test truck in each crawl test position was 18 ft. 9 in. (5.7 m). Identifying the centerline of inner FB as the origin, the distance of the test truck to the west of inner FB is presented as negative and the distance to the east of inner FB is presented as positive. Tensile stresses are presented as +ve. Downward displacements are presented as –ve. The plots also include the elevation of the deck with the gage section and the crawl truck distance identified.

It may be noted that the combined weight of the truck and the four billets was 53.7 kip (238.9 kN), which was about 2.2 times the rear axle load of 24 kip (106.8 kN) for the AASHTO notional fatigue truck. For verification of infinite life, however, the fatigue

testing of the deck was performed under a gross tandem axle weight of 82.8 kip (368.3 kN), which was 3.45 times the AASHTO notional fatigue truck. Thus, the crawl test loading was about 65% of the fatigue limit state loading.

9.3.1 Global Response of Prototype Deck

The global response of the prototype deck is discussed in this section in terms of the measurements at the sensors on the deck at sections Y-Y and Z-Z. Uniaxial strain gages, oriented along the transvers direction of the deck, were installed on the top surface of deck plate and at the bottom of inner FB at section Y-Y. A LVDT was also installed at the soffit of the inner floor beam at section Y-Y. At section Z-Z, LVDTs were installed on the soffit of the ribs and at the underside of the deck plate in between the ribs.

Response of Ribs and Deck Plate

Plots of vertical displacements at section Z-Z are shown in Figures 430 and 431. The plots show the variation of displacements as the test truck rolled along the deck. The section of the respective sensor is shown longitudinal section of the deck, where the displacements are plotted.

The response at a sensor changed with the longitudinal position of the test truck. The maximum response occurred when the centerline of the crawl truck was over inner FB, or in other words one of the axle was over the section of the gage. In Figure 430 the vertical displacement of the Rib 1 measured at the LVDT channel 7 is plotted and in Figure 431 the vertical displacement of the deck plate between ribs 1 and 2 measured at the LVDT channel 8 is plotted.

The displacement profiles for the LVDTs under the deck plate and the ribs generally exhibited a single peak displacement with a peak at the maxima. At the LVDTs, the maximum peak response occurred when the rear axle of the crawl truck crossed the transverse section Z-Z (for a roll from east to west, or forward roll). For the reverse roll, the maximum peak response occurred when the front axle of the crawl truck crossed the transverse section Z-Z (for a roll from west to east, or reverse roll). The crawl test results showed similar trend as of FEA. The crawl test results for the three transverse positions were similar because of the fact that same displacement profile was used for the under-deck actuator for all the three positions.

Response of Inner Floor Beam

Plots of the vertical displacement and the normal stress in transverse direction recorded at the soffit of inner FB at section Y-Y by the LVDT (channel 13) and the uni-axial strain gauge (channel 66) are shown in Figures 432 and 433 respectively. The plots show the variation of displacements and stresses as the test truck rolled along the deck. The section of the respective sensor is shown longitudinal section of the deck, where the results are plotted. The sensors exhibited a single modal response as the truck rolled along the deck, with the maximum response occurring in each transverse position when the truck centerline was around inner FB. For transverse positions T30 and T28, the

response didn't peaked exactly when the truck centerline was at inner FB. This is because of the fact that a constant roll speed could not be maintained during the crawl test. Nevertheless, the centerline was close to the centerline of the inner FB. The maximum vertical displacement occurred in transverse load position T29. The maximum vertical displacements reduced as the truck position moved away from the center of the deck. The vertical displacement recorded for the other transverse positions were also close. Similar to the response of the LVDT, the response of the strain gauge under inner FB exhibited a single modal response as the truck rolled along the deck, with the maximum response occurring in each transverse position when the truck centerline was at inner FB. The measured stresses showed similar trend as of FEA, and were tensile in nature as the floor beam deflected in sagging curvature. In addition, the response of the inner FB was maximum for the symmetric disposition of the tandem axle or longitudinal load position L1 as was determined from FEA. It may be inferred that the global response of the inner FB did not get affected much by changes in transverse load positions and it peaked when centerline of truck was at inner FB i.e. for symmetric disposition of the tandem axle in the longitudinal direction.

9.3.2 Response of Rib-to-Deck Plate Connection

Response of the rib-to-deck plate connection is presented in terms of stresses measured at the uniaxial gauges installed in back-to-back configuration on the deck plate and rib walls at section Z-Z coinciding with the east above-deck actuator. On the deck plate, the strain gauges were installed on the top and the bottom surfaces, oriented in the transverse direction, normal to the rib-to-deck plate weld. On the rib walls, strain gauges were installed on both surfaces, oriented along the rib, normal to the rib-to-deck weld. However, the gauges on the inner face of the rib walls got damaged while welding the ribs to the deck plate.

Figure 434 shows the normal stress measured at the gauge (channel 140) on the outer surface of Rib 1 north wall at the rib-to-deck plate connection. Figure 435 shows the normal stress measured at the gauge (channel 147) on the outer surface of Rib 2 south wall at the rib-to-deck plate connection. The stresses were insignificant until the test truck crossed the inner FB and approached the gauged section. Bimodal responses, manifesting the effects of each axle of the tandem, were noted when the axles were close to the gauged transverse section. This indicated that the transverse stresses and the deck response were highly localized under the wheel. The stresses measured from the gauges on the outer surface of the rib walls were compressive as connection underwent local out-of-plane deformation under the wheel loads. The stresses measured from the crawl tests were comparable with the FEA results. The maximum stresses occurred for transverse load position T29 when the south side wheel pair was placed centrally between the ribs causing out of plane bending of the rib-to-deck plate connections. However, for the transverse position T-30, the south side wheel moved away from the channel 140 (at north wall of Rib 1) and caused symmetric bending of rib-to-deck plate connection for Rib 2 south wall (channel 147). Consequently, stress peaks were reduced, further signifying the localized effect of wheel loads on the rib-to-deck plate connections.

Figure 436 shows the normal stress measured at the gauge (channel 169) on the top of deck plate to the south of Rib 2 at the rib-to-deck plate connection. Figures 437 and 438 show the normal stress measured at the gauges (channels 175 and 202) on the top and bottom surfaces of the deck plate respectively, to the north of Rib 4 at the rib-to-deck plate connection. Similar to the gauges on the rib wall, the stresses were insignificant until the test truck crossed the inner FB and approached the gauged section. Bimodal responses, manifesting the effects of each axle of the tandem, were noted when the axles were close to the gauged transverse section. The stresses were tensile on the top surface and compressive on the bottom surface as the deck plate deformed locally in hogging curvature over the rib wall at the rib-to-deck plate connection. The results were comparable to FEA. The maximum stress values for the different transverse load positions were different indicating the localized effect of wheel loads on the rib-to-deck plate connections.

It should be noted that the response of the gauges at the rib-to-deck plate connections were not exactly of the same magnitude under both the axles. This was due to non-uniform tire contact and local transverse shift in wheel positions, and the sensitivity of the deck response to the transverse position of the wheel loads.

9.3.3 Response of Rib-to-Floor Beam Connection

The response of the rib-to-floor beam connection is presented in terms of the stresses measured at the gauges on the inner floor beam web at the Rib 1-to-inner floor beam connection. As determined from FEA of the global model, Rib 1-to-inner floor beam connection adjacent to the edge girder was the most critical and hence the connection was extensively instrumented. All the gages on the floor beam web at the Rib 1-to-inner floor beam connection were installed symmetrically on the north and south sides of the rib, and on each side the gages were installed back-to-back on the east and west faces of the floor beam web to measure the in-plane and the out of plane stress components.

The principal stresses on the east face of the inner floor beam to the south of Rib 1, measured at the rosette gauges at 25° and 50° from the rib soffit, are shown in Figures 439 and 440 respectively. The section of the respective sensor is shown longitudinal section of the deck, where the results are plotted. The stresses showed similar trend of FEA with tensile stress at the south side of the connection and maximum value of principal stress occurring at the 25° location. These plots show that for a single passage of the test truck, the rib-to-floor beam connection experienced only one stress cycle due to the resultant effect of the tandem axles. The stresses were highest when the center of the truck was at or close to the centerline of inner floor beam. Figure 441 show the principal stresses on the east face of the inner floor beam to the north of Rib 1, measured at the rosette gauge at 50° from the rib soffit. The stresses showed similar trend of FEA with compressive stress at the north side of the connection, and showed only one stress cycle per passage of the test truck. Similar to the south side, the stresses were highest when the center of the truck was at or close to the centerline of inner floor beam.

The stresses normal to the weld toe on the east face of the inner floor beam to the south and the north sides of Rib 1, measured at the rosette gauges 50° from the rib soffit, are shown in Figures 442 and 443 respectively. The section of the respective sensor is shown longitudinal section of the deck, where the results are plotted. The results showed similar trend of FEA, and showed one stress cycle per passage of test truck. On the south side, the stress was maximum for T30. However, FEA results showed similar stress value for T29 and T30. Note that the FEA of the specimen model for crawl test was conducted with the same displacement value at the under-deck actuator, simulating condition similar to the crawl tests. However, FEA of GM and SM showed that the stress normal to the weld toe was maximum for T29. Results confirming to the FEA results of GM and SM were observed for the north side (Figure 443), where the stress was maximum for T29.

It should be noted that for some cases, the peak response of the connection was not observed exactly when centerline of the truck was at the centerline of the inner floor beam. This is because of the fact that a constant roll speed could not be maintained during the crawl test. Nevertheless, the centerline was close to the centerline of the inner FB.

9.3.4 Response of CJP Deck Splice

The longitudinal stresses at the gauges on the top and the bottom of the deck plate around the transverse deck splice are shown in Figures 444 to 446. The section of the respective sensor is shown longitudinal section of the deck, where the results are plotted. Figures 444 and 445 show the longitudinal stresses on the top of the deck plate under the south-west (channel 184) and the north-west (channel 185) wheel pair respectively. Bimodal responses, manifesting the effects of each axle of the tandem, were noted when the axles were close to the gauged transverse section. The stresses showed similar trend as FEA with compressive stresses on the top of the deck plate, however, the stresses were much lower than the FEA results. As discussed earlier, the gauges on the top of the deck plate around the deck plate splice was replaced after 5 million load cycles. In a location with high stress gradient, a little shift from its intended location of installation could have caused this deviation. Maximum stresses were recorded for transverse position T29, when the centerline of the wheel pairs was at the centerline of the gauges. However, the stress peaks reduced for T30, when the wheel pairs moved away from the gauges. Figure 446 shows the longitudinal stresses on the bottom of the deck plate under the south-west (channel 208) wheel pair. Similar to the top gauges, bimodal responses manifesting the effects of each axle of the tandem were noted when the axles were close to the gauged transverse section. The stresses showed similar trend as FEA with tensile stress on the bottom of the deck plate, however, the stresses were much lower than the FEA results. The CJP deck splice was inspected thoroughly for fatigue cracking, however, no crack was detected. The reason for this deviation from the FEA results for the bottom gauges cannot be ascertained. It is evident that the maximum stresses at the subject gauges were due to the global longitudinal bending of the deck.

Table 40 - Measured Maxima of Stresses in Intermediate Floor Beam Web to the South of Rib 1 at 50 degree

	Measurements		Computed Principal Stresses[a] and Directions			
Face	Channel ID	Stress (ksi[b])	Maximum σp (ksi[b])	Maximum σq (ksi[b])	Direction[c] ϕ (degrees)	Illustration[d]
East	14	7.22	8.0	3.2	63.3	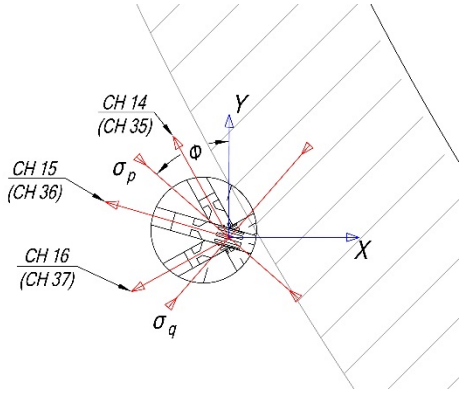
	15	3.84				
	16	3.93				
West	35	5.24	6.2	-0.9	61.5	
	36	0.26				
	37	0.09				

Notes:
[a] Tensile stresses are positive.
[b] 1 ksi = 6.91 MPa.
[c] Counter clockwise angles are positive, measured from the vertical axis (Y) passing through the center of rosette.
[d] Illustration drawn on east face. West face gauge channels are shown in parenthesis.

Table 41 - Measured Maxima of Stresses in Intermediate Floor Beam Web to the South of Rib 1 at 25 degree

	Measurements		Computed Principal Stresses[a] and Directions			
Face	Channel ID	Stress (ksi[b])	Maximum σp (ksi[b])	Maximum σq (ksi[b])	Direction[c] ϕ (degrees)	Illustration[d]
East	19	5.59	9.8	-3.7	98.7	
	20	-3.22				
	21	0.43				
West	40	5.64	8.2	-4.6	91.6	
	41	-3.31				
	42	-2.01				

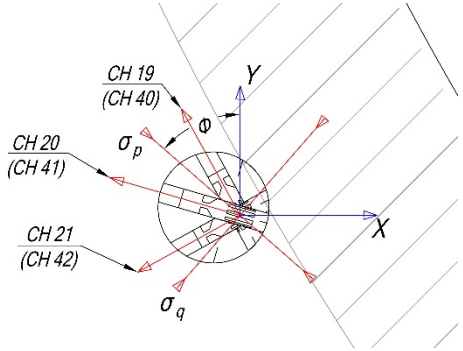

Notes:
[a] Tensile stresses are positive.
[b] 1 ksi = 6.91 MPa.
[c] Counter clockwise angles are positive, measured from the vertical axis (Y) passing through the center of rosette.
[d] Illustration drawn on east face. West face gauge channels are shown in parenthesis.

Table 42 - Measured Stress Ranges in Intermediate Floor Beam Web to the South of Rib 1 at 50 degree

	Measurements		Computed Principal Stresses[a] and Directions			
Face	Channel ID	Stress (ksi[b])	Maximum σp (ksi[b])	Maximum σq (ksi[b])	Direction[c] ϕ (degrees)	Illustration[d]
East	14	6.63	7.3	2.9	63.3	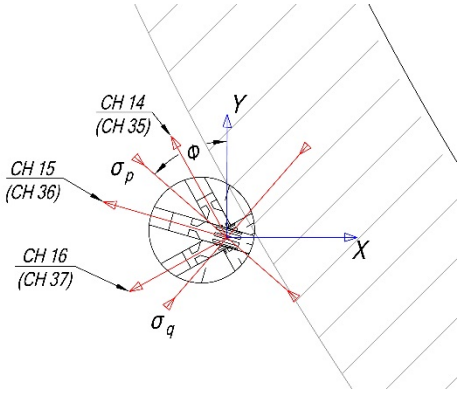
	15	3.55				
	16	3.60				
West	35	4.84	5.7	-0.7	61.5	
	36	0.29				
	37	0.13				

Notes:
[a] Tensile stresses are positive.
[b] 1 ksi = 6.91 MPa.
[c] Counter clockwise angles are positive, measured from the vertical axis (Y) passing through the center of rosette.
[d] Illustration drawn on east face. West face gauge channels are shown in parenthesis.

Table 43 - Measured Stress Ranges in Intermediate Floor Beam Web to the South of Rib 1 at 25 degree

	Measurements		Computed Principal Stresses[a] and Directions			
Face	Channel ID	Stress (ksi[b])	Maximum σp (ksi[b])	Maximum σq (ksi[b])	Direction[c] ϕ (degrees)	Illustration[d]
East	19	5.18	9.0	-3.4	98.7	
	20	-2.93				
	21	0.39				
West	40	5.21	7.6	-4.2	91.6	
	41	-3.01				
	42	-1.82				

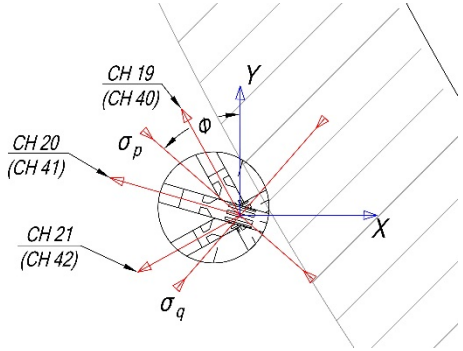

Notes:
[a] Tensile stresses are positive.
[b] 1 ksi = 6.91 MPa.
[c] Counter clockwise angles are positive, measured from the vertical axis (Y) passing through the center of rosette.
[d] Illustration drawn on east face. West face gauge channels are shown in parenthesis.

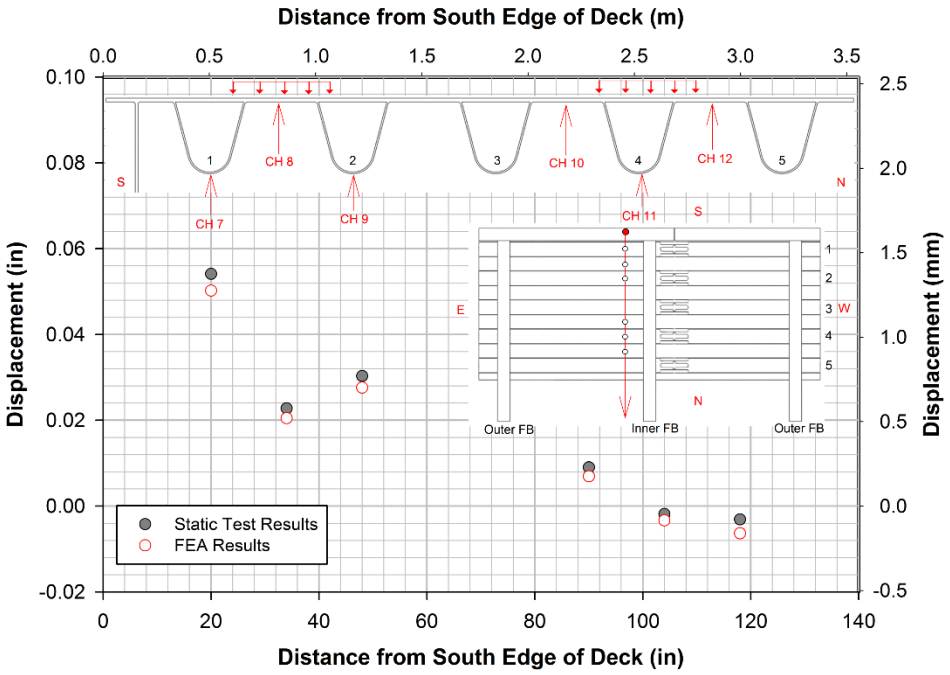

Figure 387. Comparison of vertical displacements at section Z-Z between static test and FEA

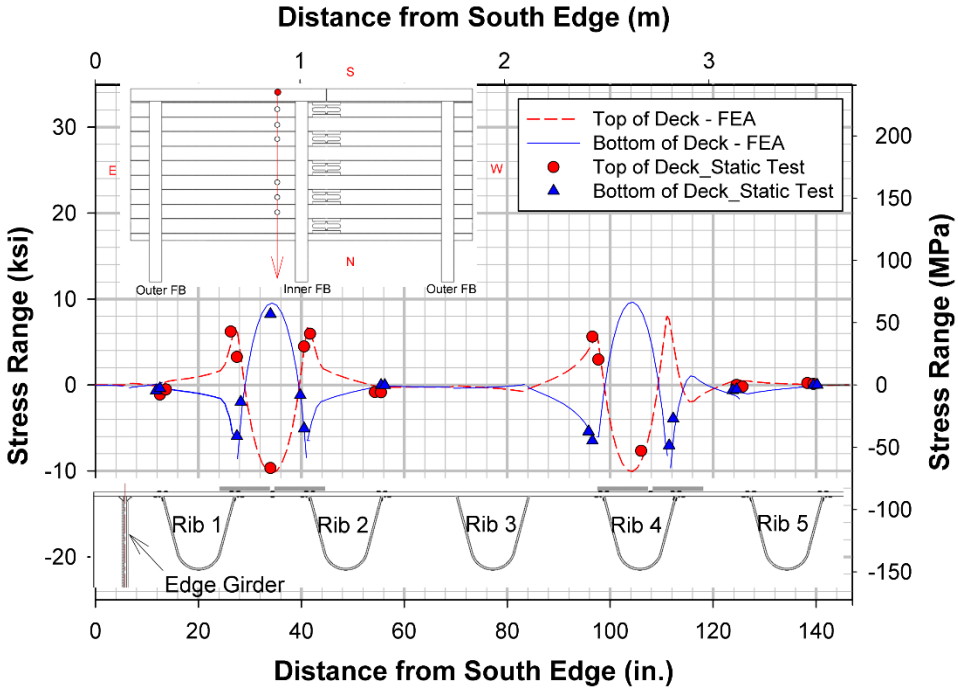

Figure 388. Comparison of transverse stress ranges at section Z-Z between static test and FEA

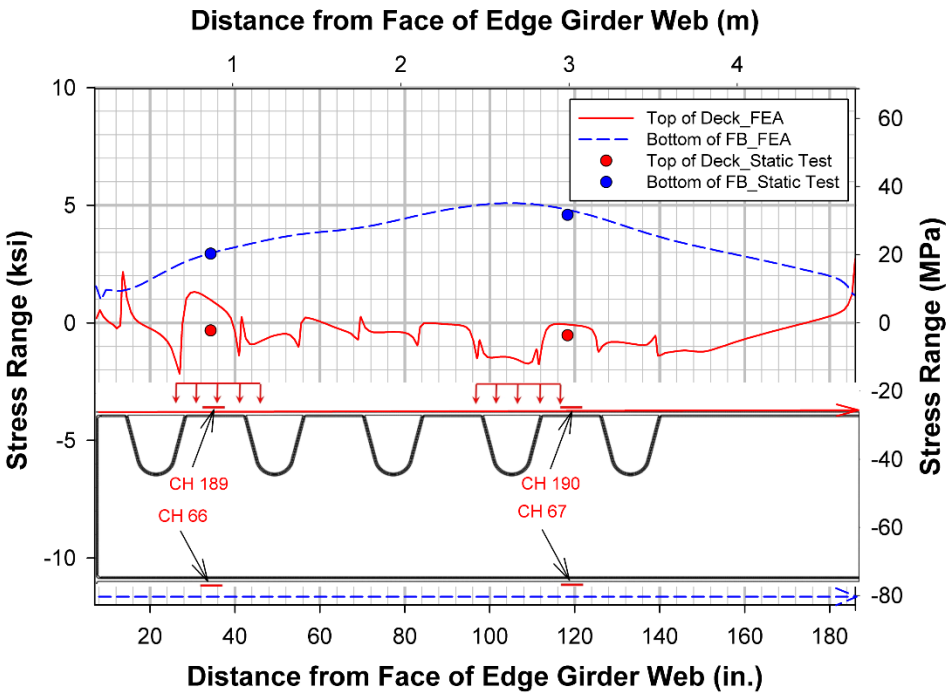

Figure 389. Comparison of transverse stress ranges at section Y-Y between static test and FEA

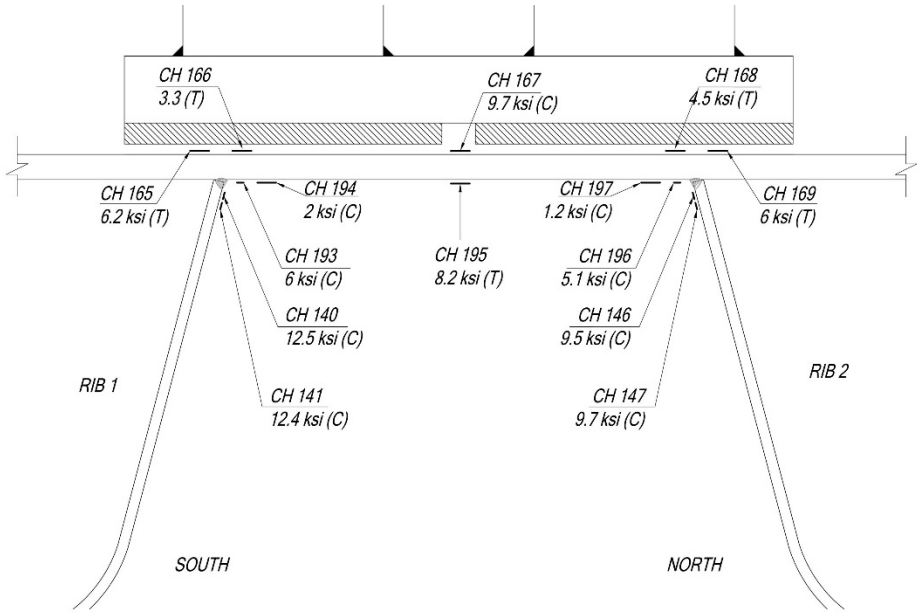

Figure 390. Measured stress ranges at the rib-to-deck plate connection at section Z-Z under south-east load pads

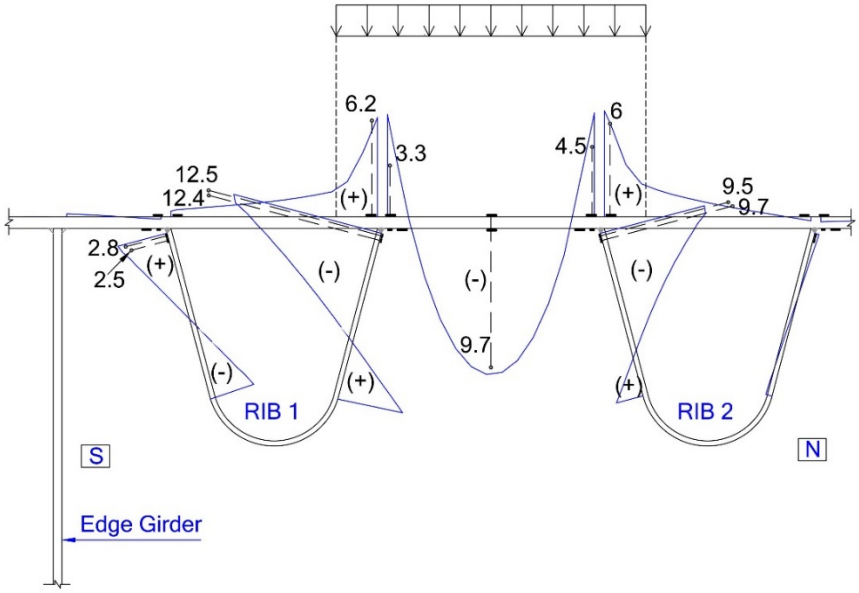

Figure 391. Transverse stresses on top of deck and outer face of rib wall from FEA at rib-to-deck plate connection at section Z-Z under south-east load pads with static test results plotted as dots

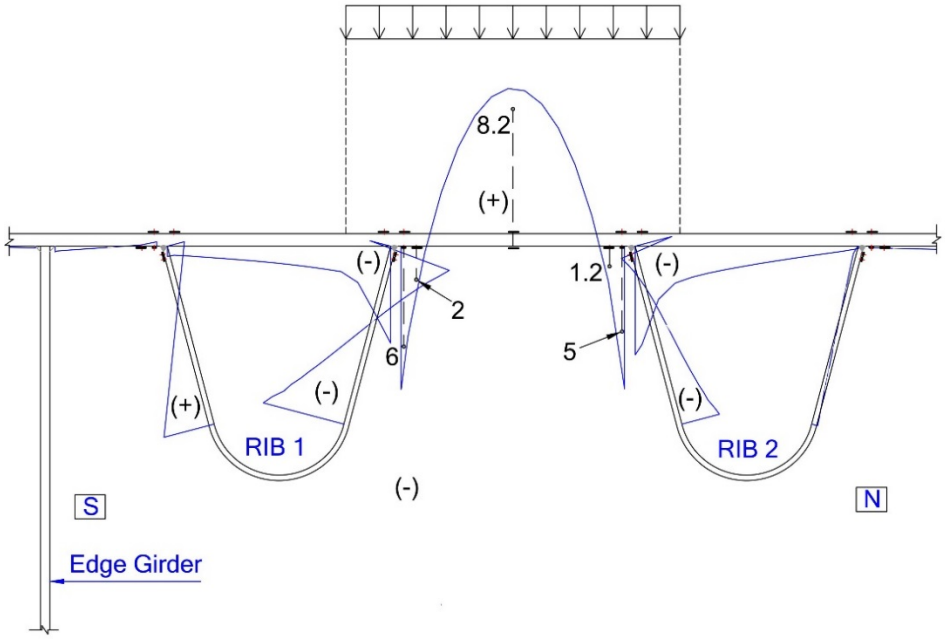

Figure 392. Transverse stresses on bottom of deck and inner face of rib wall from FEA at rib-to-deck plate connection at section Z-Z under south-east load pads with static test results plotted as dots

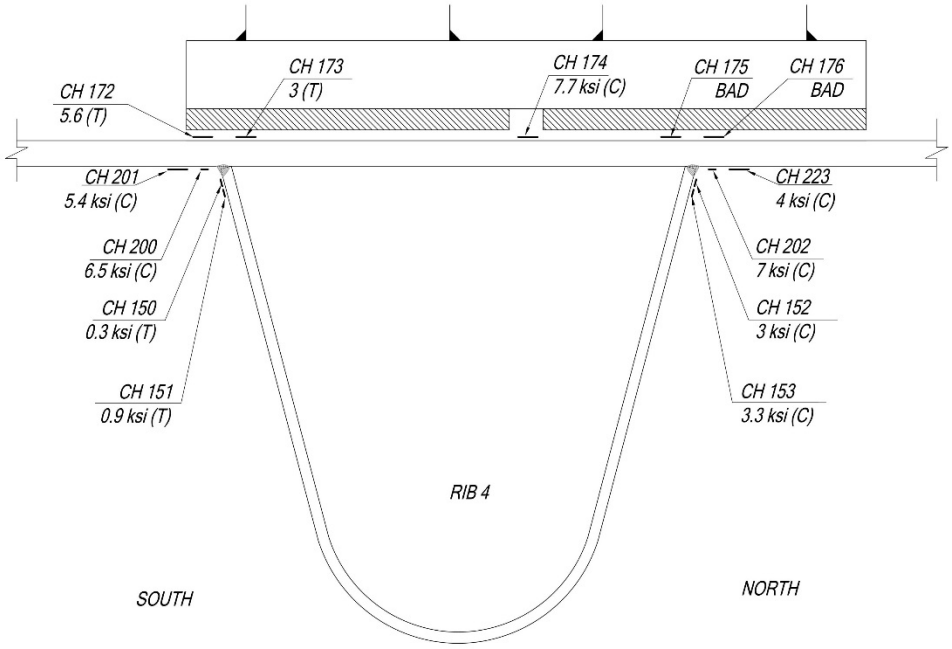

Figure 393. Measured stress ranges at the rib-to-deck plate connection at section Z-Z under north-east load pads

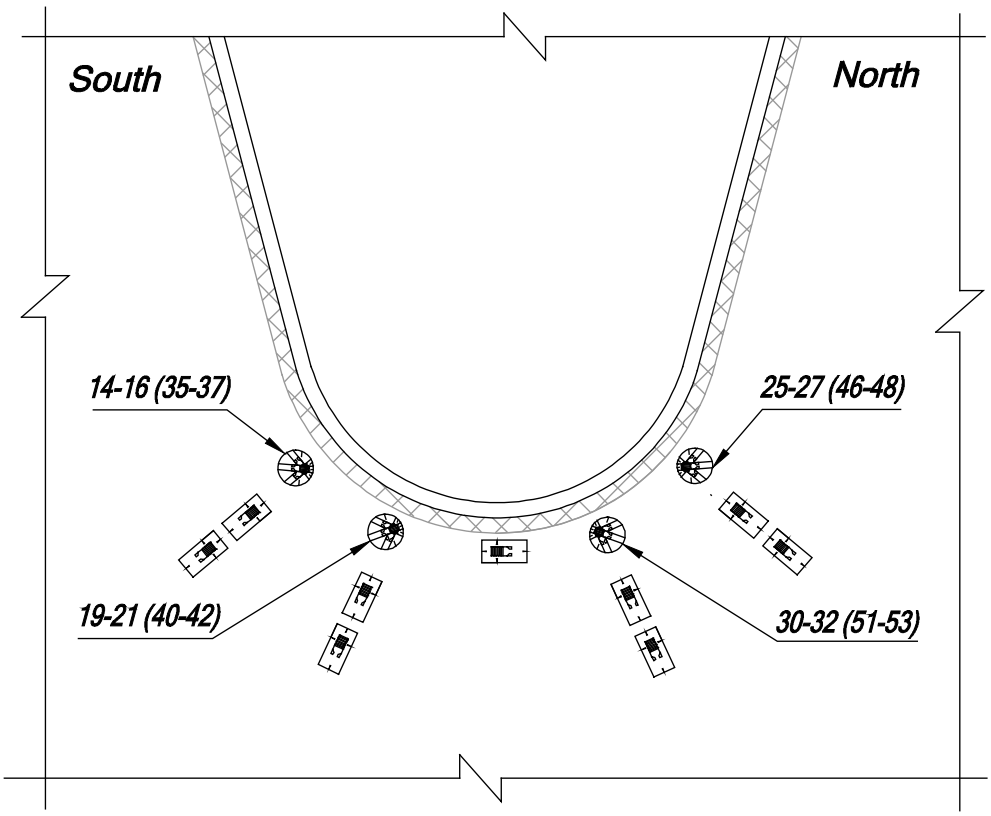

View looking west (showing east face); Gauges on the west face are identified in parenthesis

East Face		West Face	
CH	Measured Principal Stress (ksi)	CH	Measured Principal Stress (ksi)
14-16	7.96	35-37	6.18
19-21	9.76	40-42	8.21
25-27	-11.61	46-48	-10.23
30-32	-13.65	51-53	-11.09

Figure 394. Measured principal stresses at the rosette gauges on the inner FB web

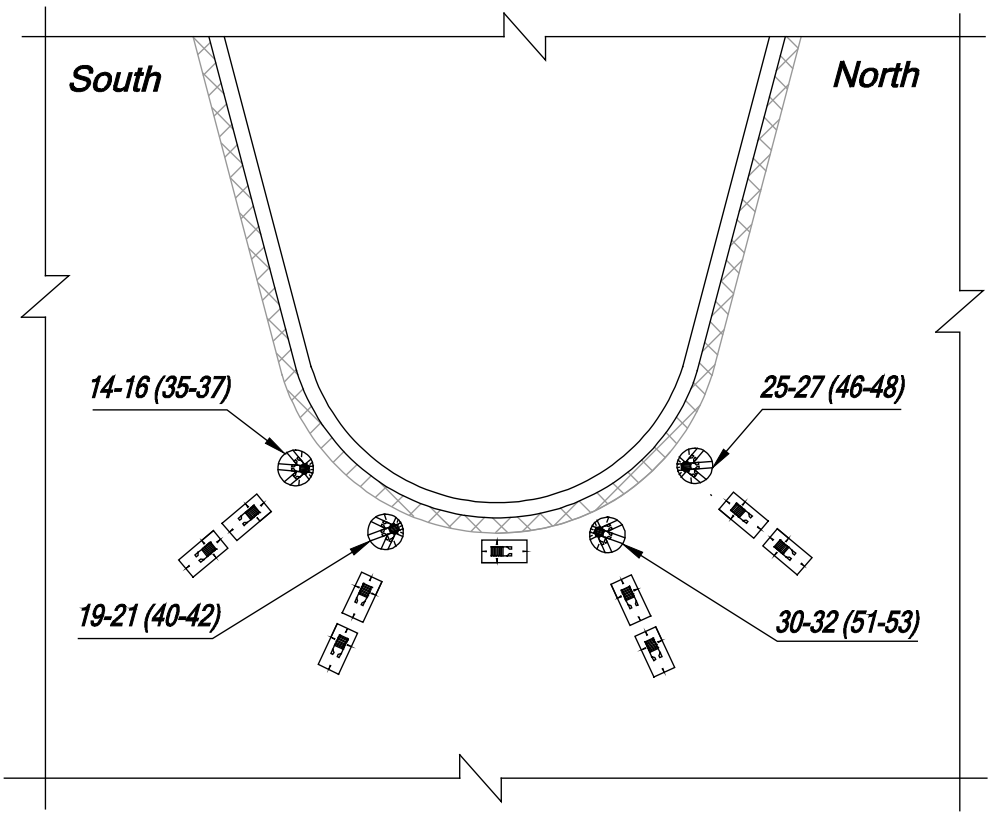

View looking west (showing east face); Gauges on the west face are identified in parenthesis

East Face			West Face		
CH	FEA Principal Stress Range (ksi)	Measured Principal Stress Range (ksi)	CH	FEA Principal Stress Range (ksi)	Measured Principal Stress Range (ksi)
14-16	8.67	7.29	35-37	6.38	5.7
19-21	10.23	8.98	40-42	8.25	7.57
25-27	-13.21	-10.67	51-53	-10.76	-9.43
30-32	-13.62	-12.51	46-48	-11.77	-10.19

Figure 395. Comparison of measured principal stress ranges at the rosette gauges on the inner FB web with the FEA results

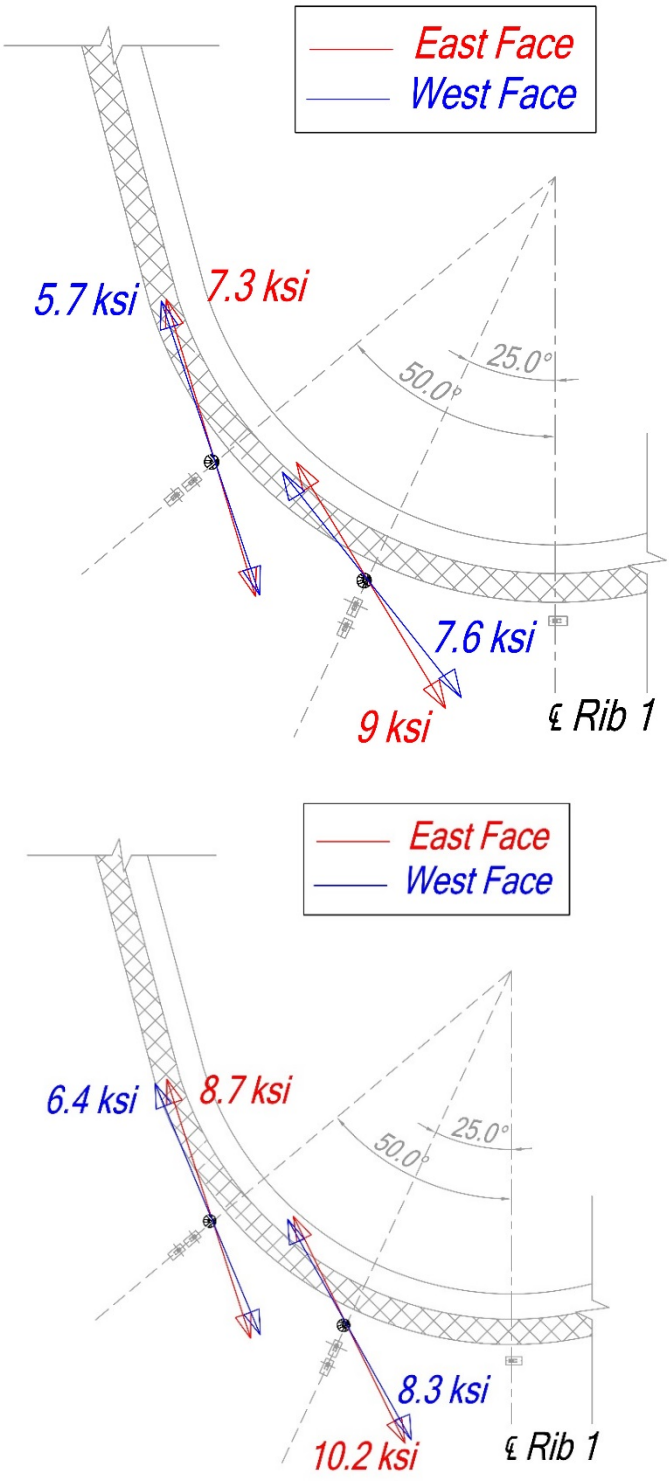

Figure 396. Comparison of the measured principal stress ranges at the rosette gauges on inner FB web to the south side of Rib 1 with FEA results (top figure is test results and bottom figure is FEA result)

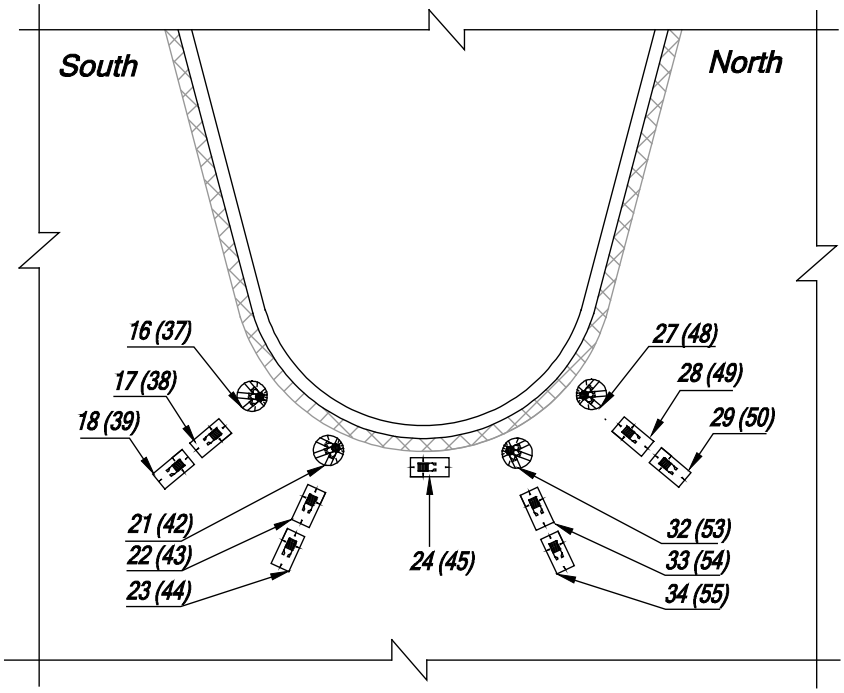

View looking west (showing east face); Gauges on the west face are identified in parenthesis

South of Rib 1			
East Face		West Face	
CH	Measured Value (ksi)	CH	Measured Value (ksi)
16	3.93	37	0.09
17	1.32	38	-1.83
18	1.37	39	-1.68
21	0.43	42	-2.01
22	-2.04	43	-3.59
23	-1.44	44	-2.38
24	0.45	45	-0.73

North of Rib 1			
East Face		West Face	
CH	Measured Value (ksi)	CH	Measured Value (ksi)
27	-6.89	48	-2.61
28	-2.75	49	-0.25
29	-2.74	50	-0.18
32	-3.28	53	0.07
33	-1.52	54	1.16
34	-2.14	55	-0.56

Figure 397. Measured stresses normal to the weld toe on the inner FB web

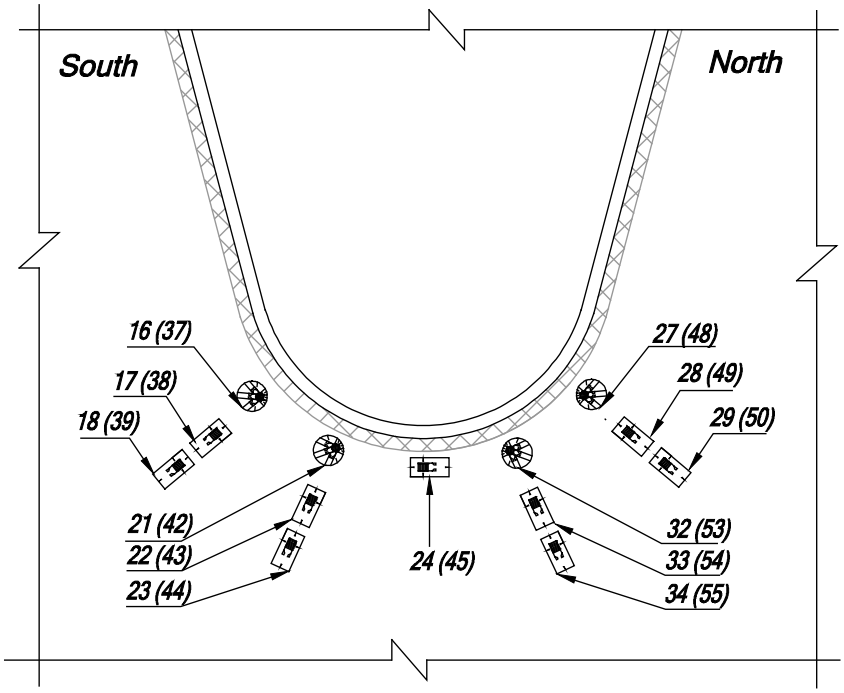

View looking west (showing east face); Gauges on the west face are identified in parenthesis

South of Rib 1			
East Face		West Face	
CH	Measured Range (ksi)	CH	Measured Value (ksi)
16	3.6	37	0.13
17	1.19	38	-1.66
18	1.13	39	-1.51
21	0.39	42	-1.82
22	-1.87	43	-3.25
23	-1.32	44	-2.17
24	0.43	45	-0.66

North of Rib 1			
East Face		West Face	
CH	Measured Value (ksi)	CH	Measured Value (ksi)
27	-6.31	48	-2.36
28	-2.52	49	-0.21
29	-2.54	50	-0.17
32	-2.95	53	0.1
33	-1.4	54	1.1
34	-1.99	55	-0.5

Figure 398. Measured stress ranges normal to the weld toe on the inner FB web

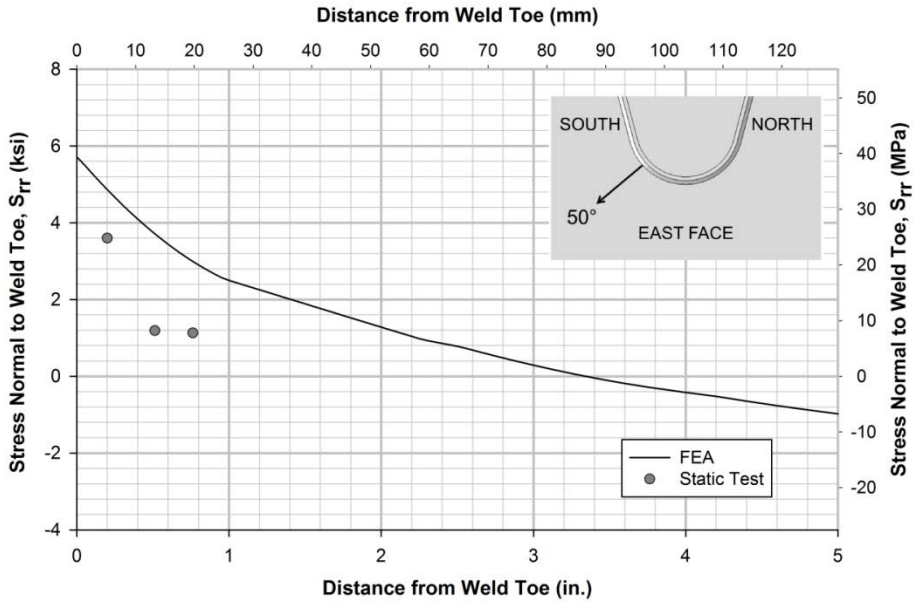

Figure 399. Radial stress range along 50 degree south path on east FB face

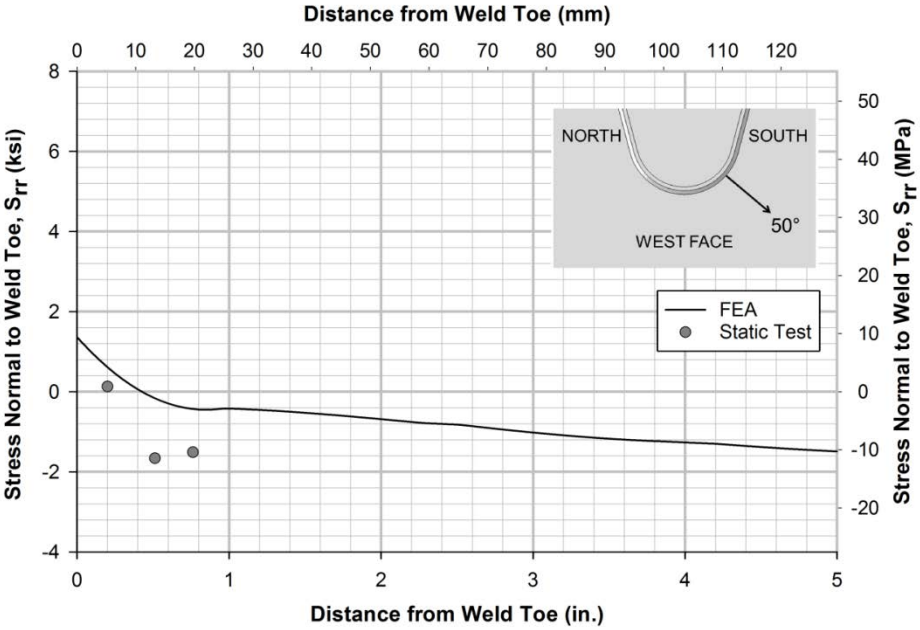

Figure 400. Radial stress range along 50 degree south path on west FB face

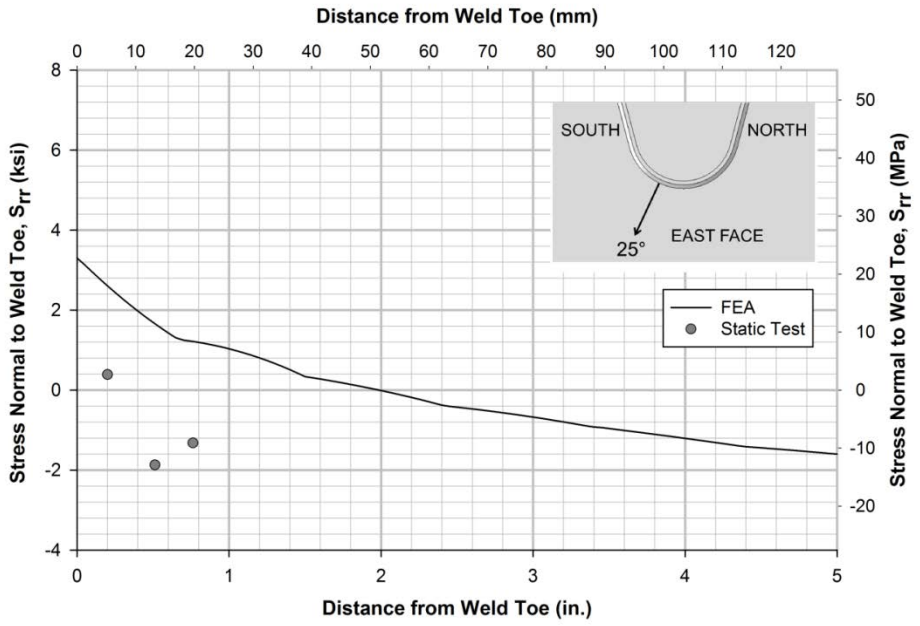

Figure 401. Radial stress range along 25 degree south path on east FB face

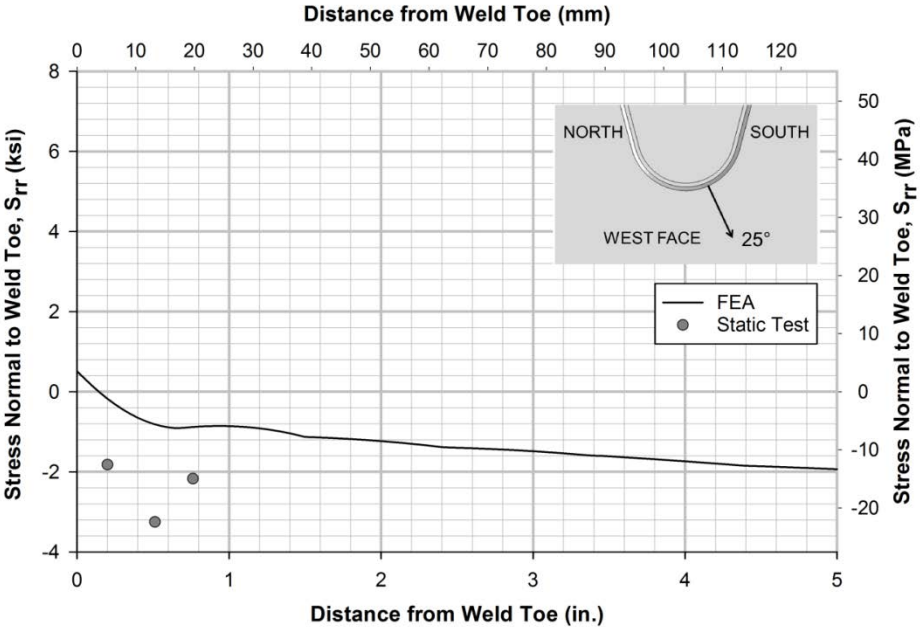

Figure 402. Radial stress range along 25 degree south path on west FB face

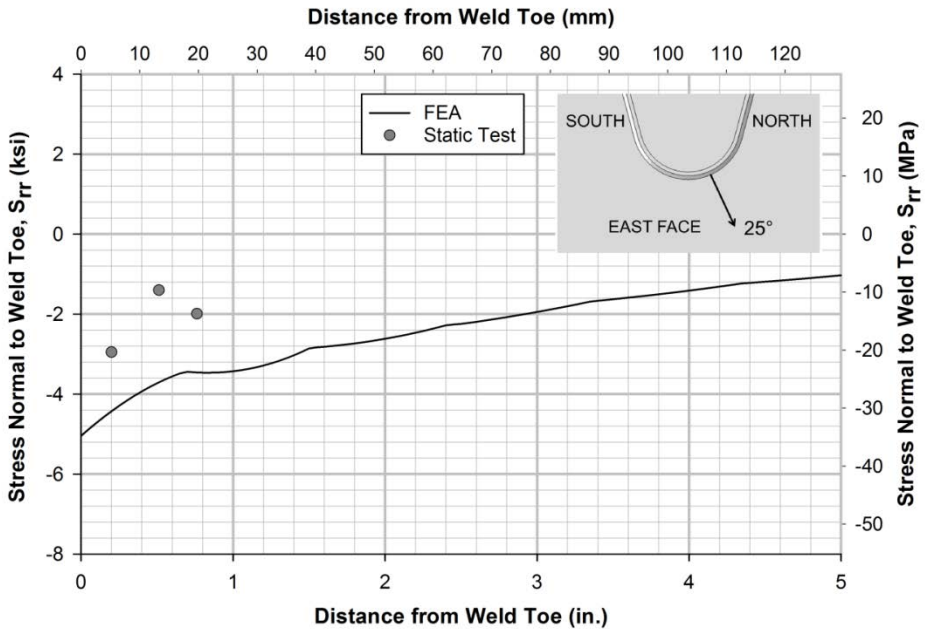

Figure 403. Radial stress range along 25 degree north path on east FB face

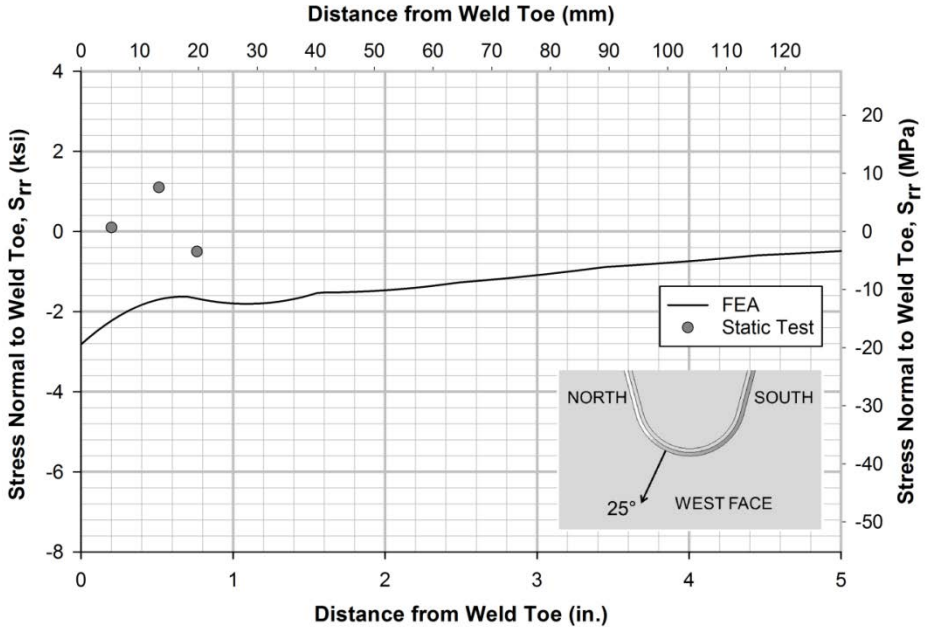

Figure 404. Radial stress range along 25 degree north path on west FB face

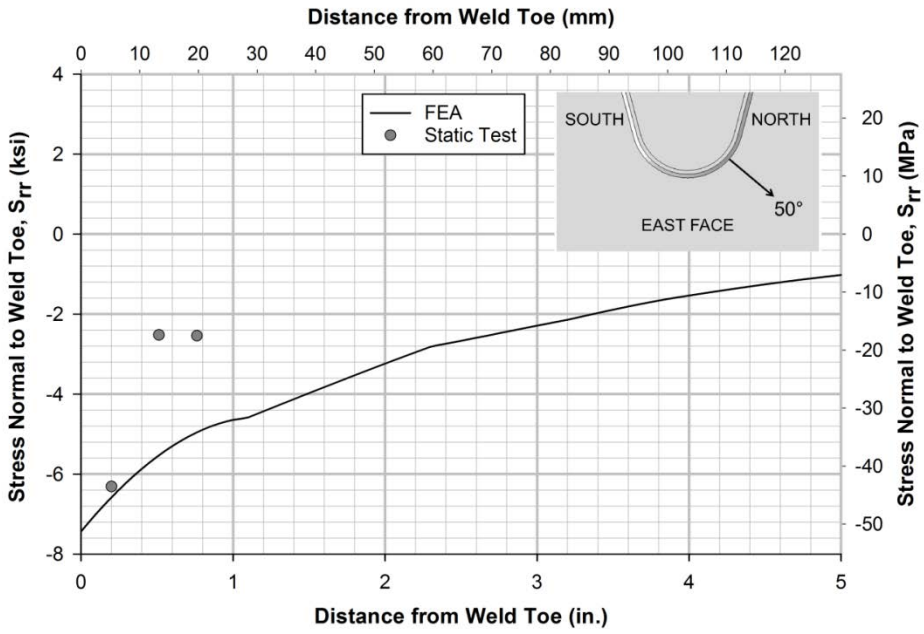

Figure 405. Radial stress range along 50 degree north path on east FB face

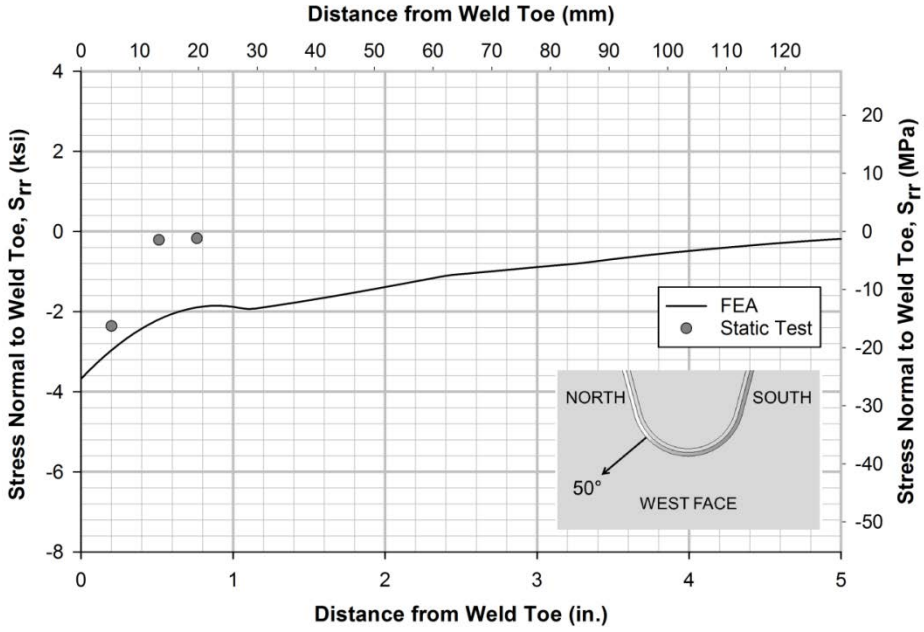

Figure 406. Radial stress range along 50 degree north path on west FB face

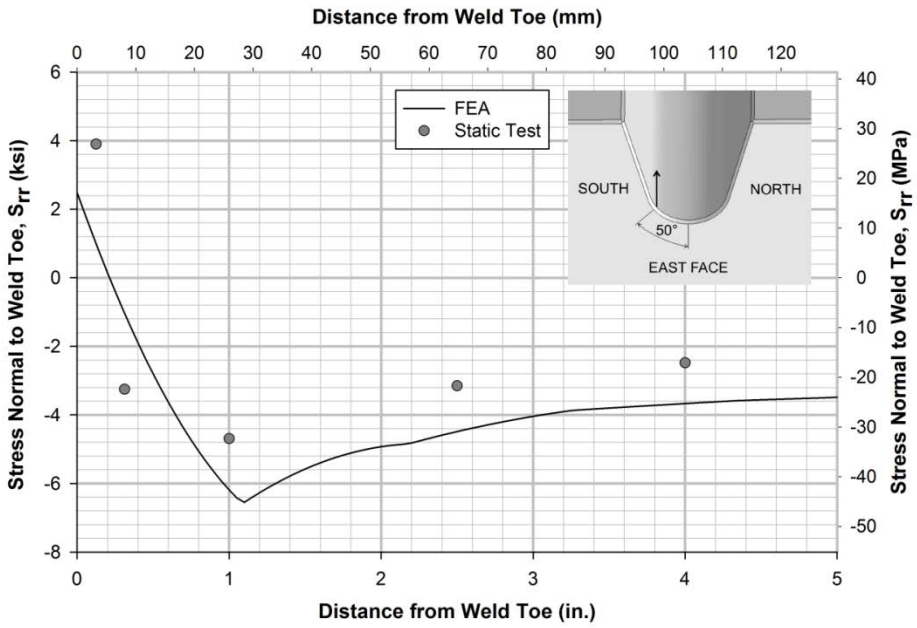

Figure 407. Radial stress range along 50 degree southeast path on rib 1

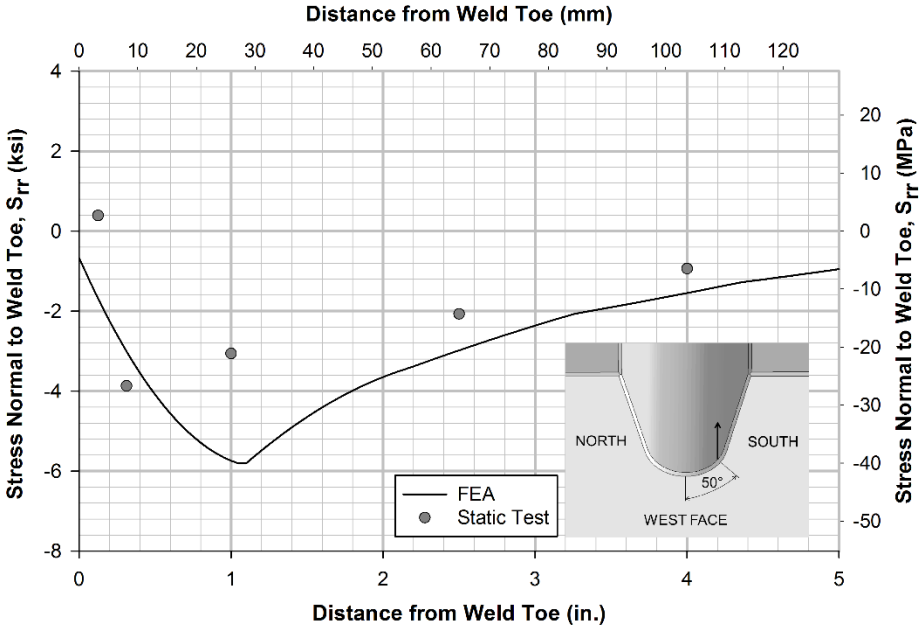

Figure 408. Radial stress range along 50 degree southwest path on rib 1

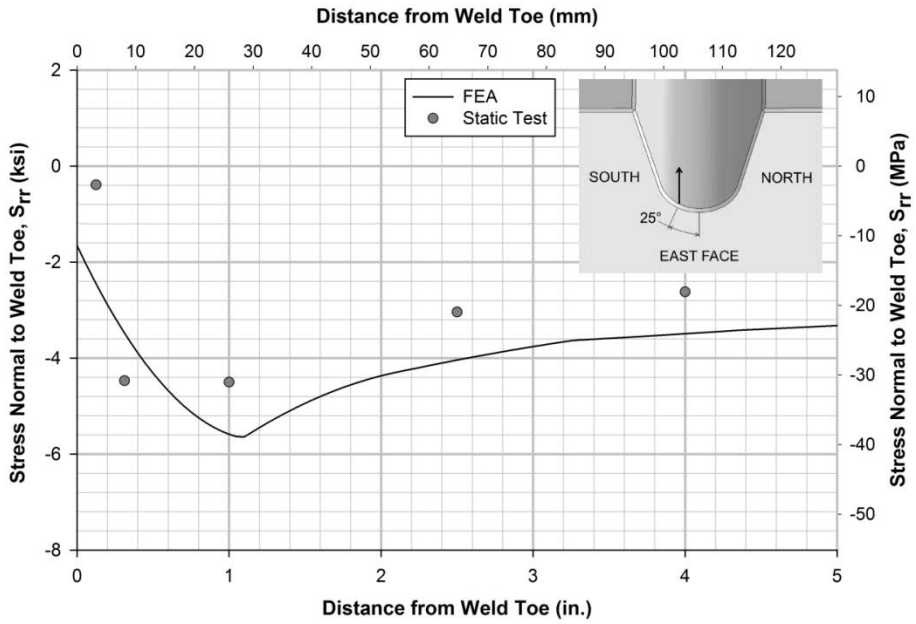

Figure 409. Radial stress range along 25 degree southeast path on rib 1

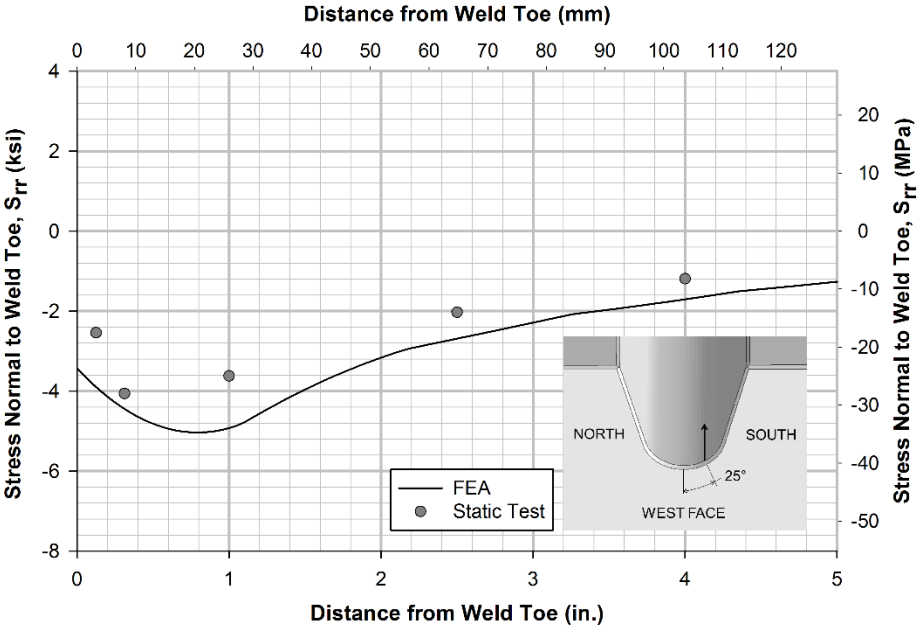

Figure 410. Radial stress range along 25 degree southwest path on rib 1

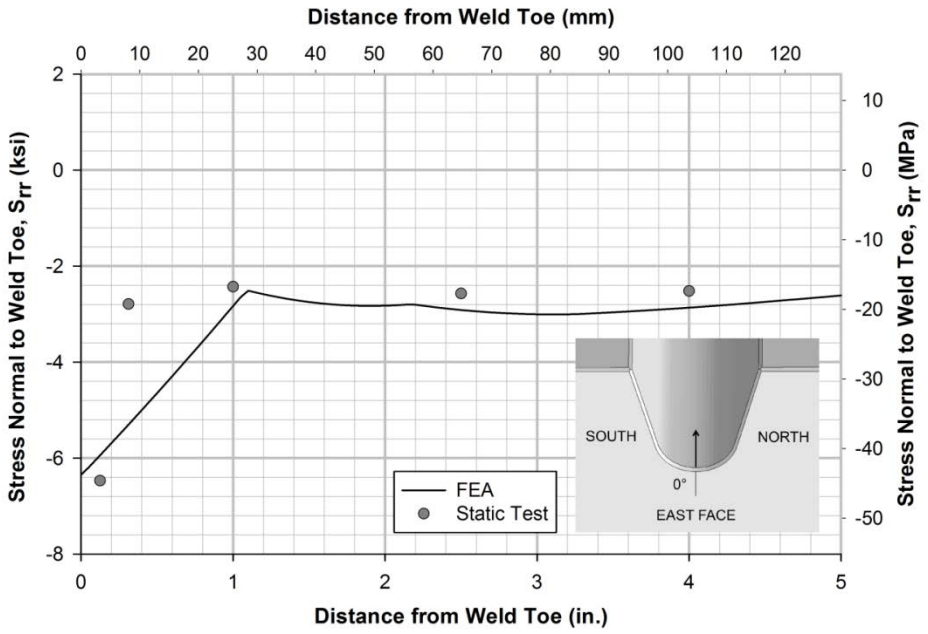

Figure 411. Radial stress range along 0 degree east path on rib 1

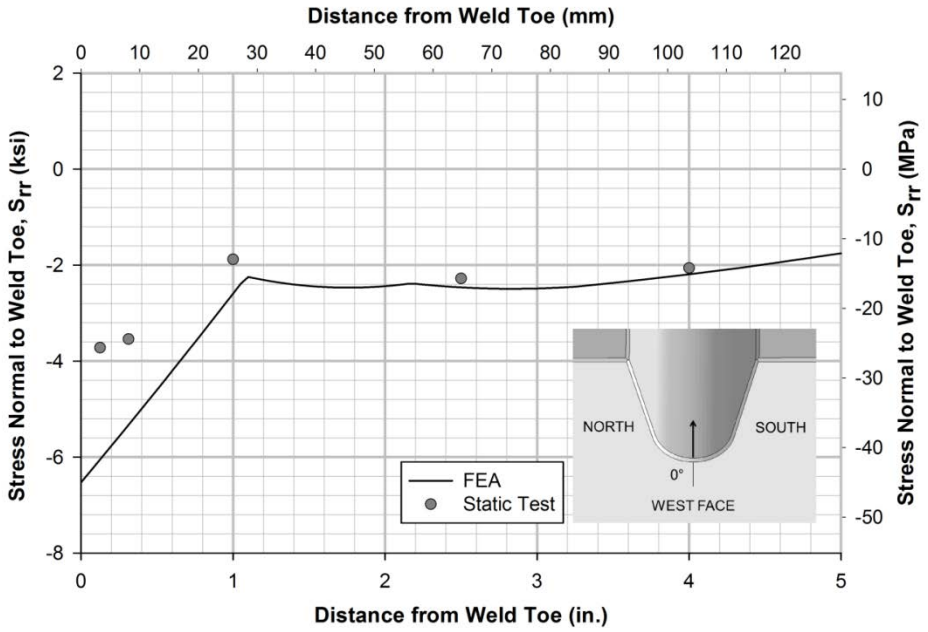

Figure 412. Radial stress range along 0 degree west path on rib 1

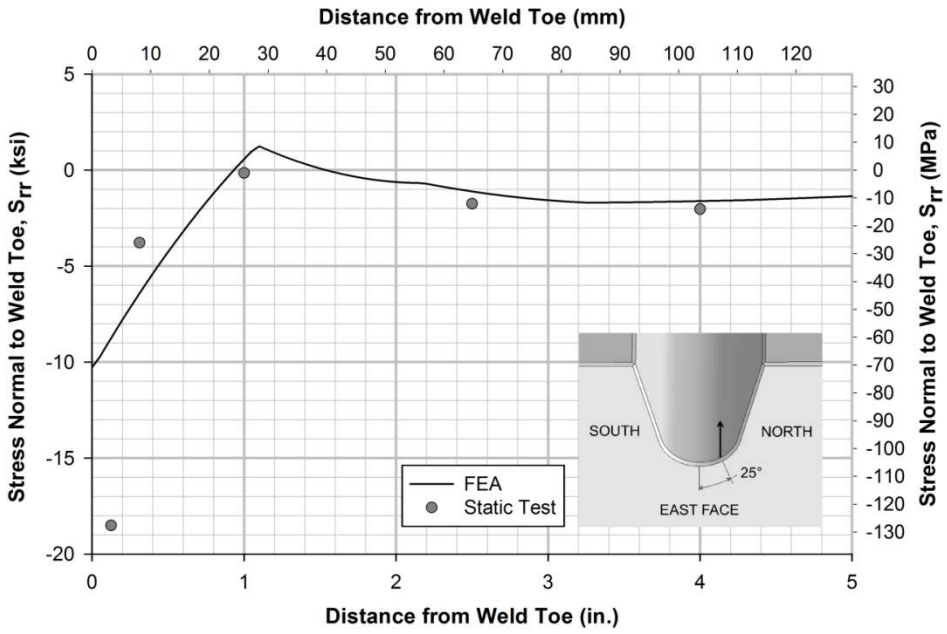

Figure 413. Radial stress range along 25 degree northeast path on rib 1

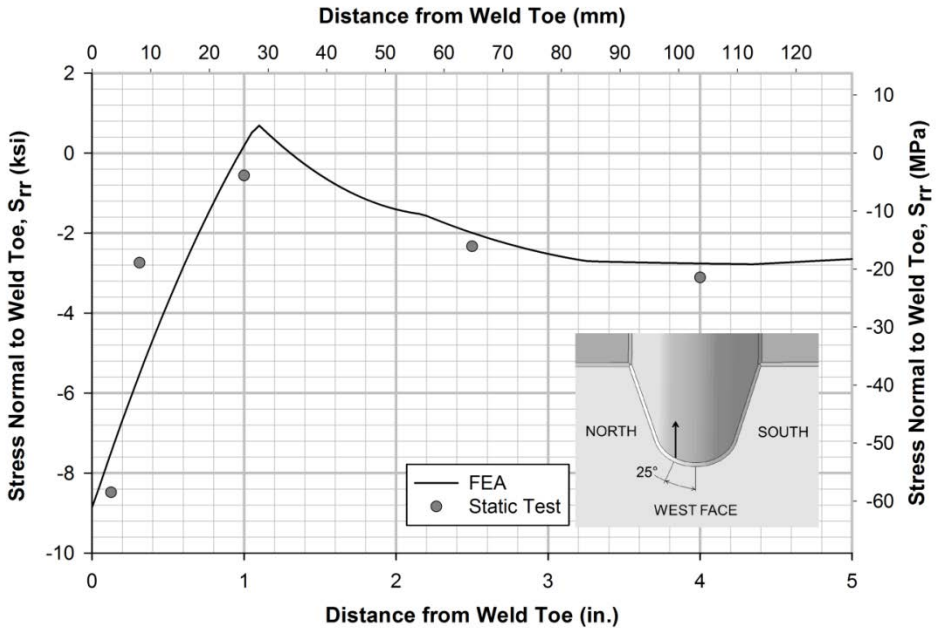

Figure 414. Radial stress range along 25 degree northwest path on rib 1

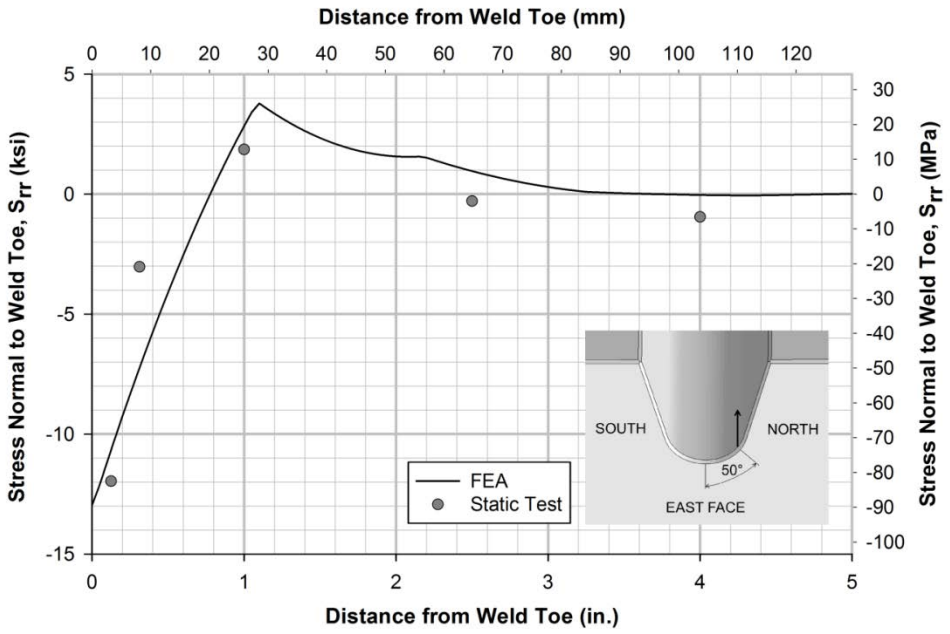

Figure 415. Radial stress range along 50 degree northeast path on rib 1

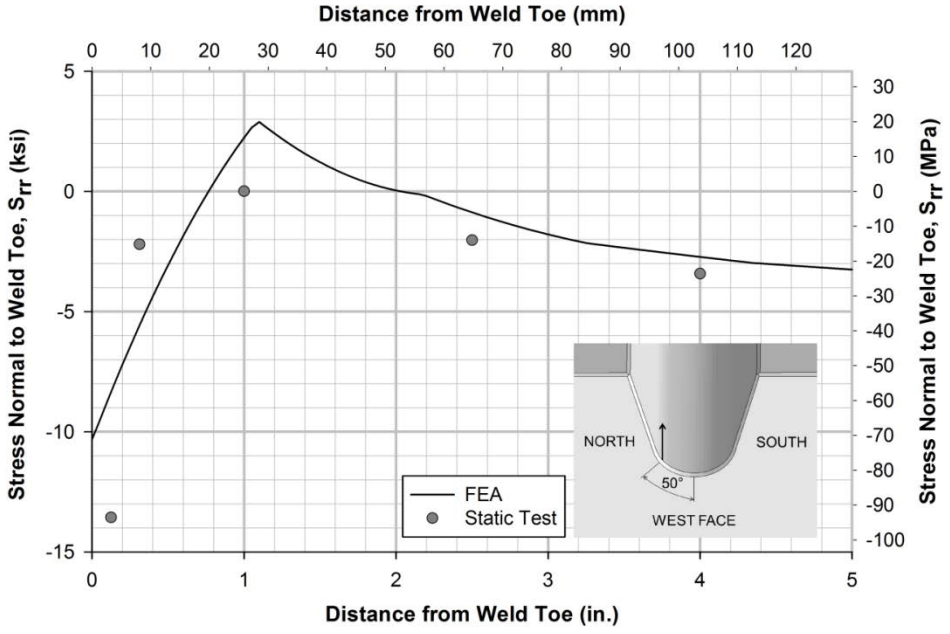

Figure 416. Radial stress range along 50 degree northwest path on rib 1

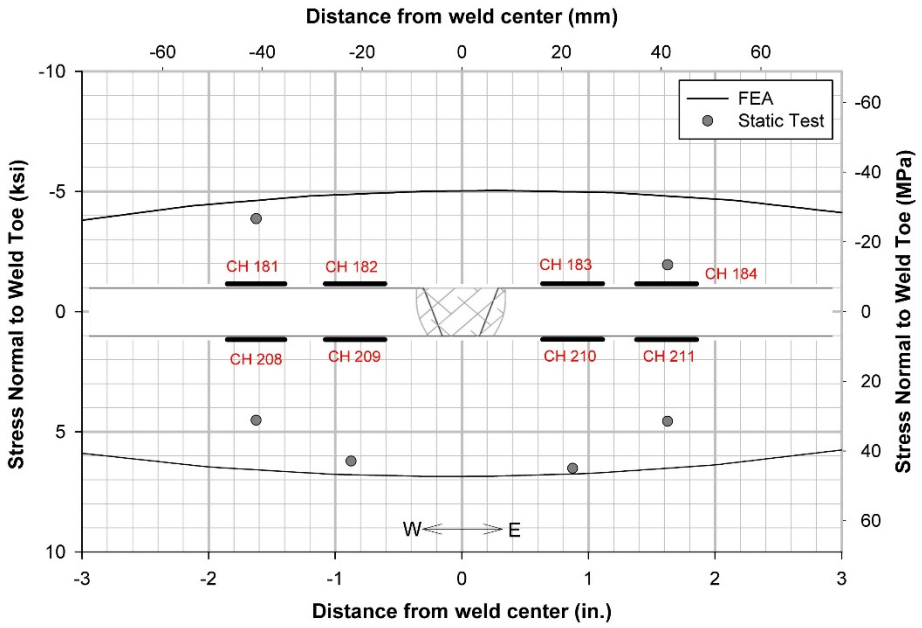

Figure 417. Stress ranges at the transverse deck splice under south-west load pads

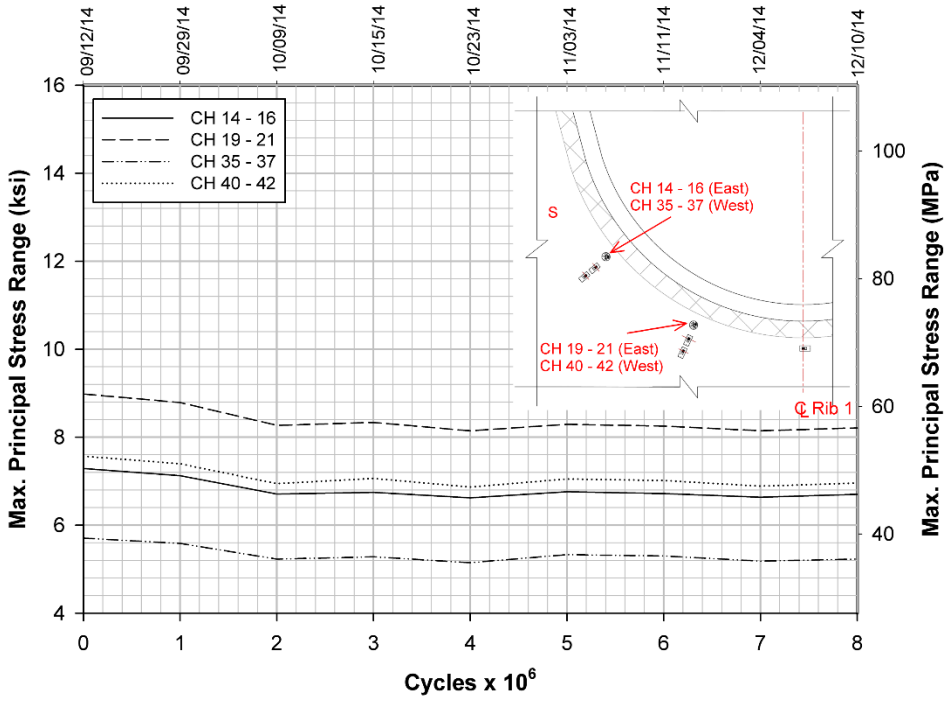

Figure 418. Changes in maximum tensile principal stress ranges at the rosettes on the inner floor beam web

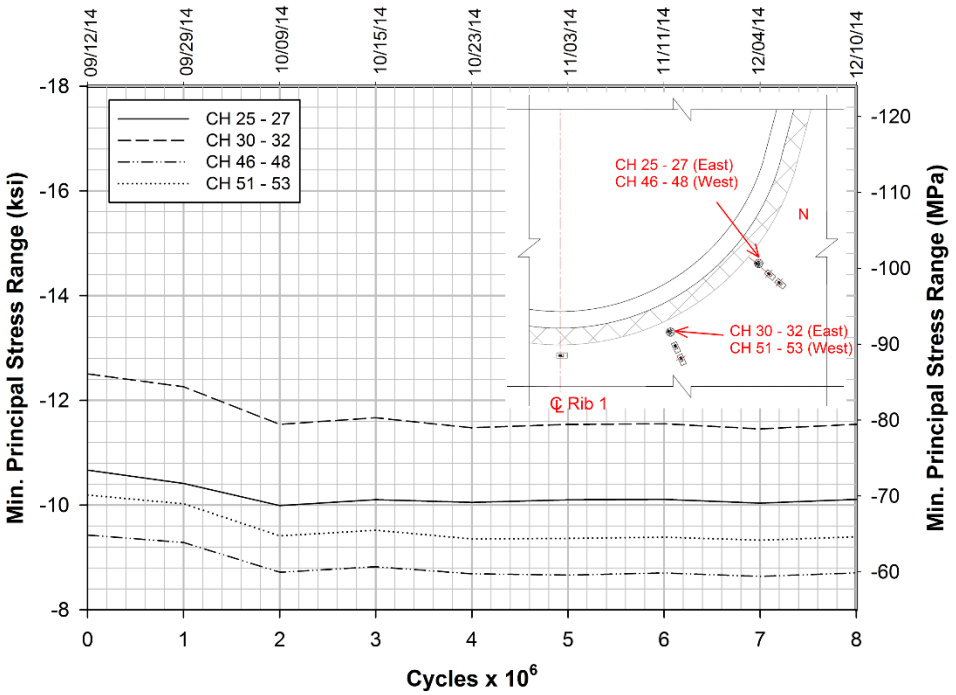

Figure 419. Changes in maximum compressive principal stress ranges at the rosettes on the inner floor beam web

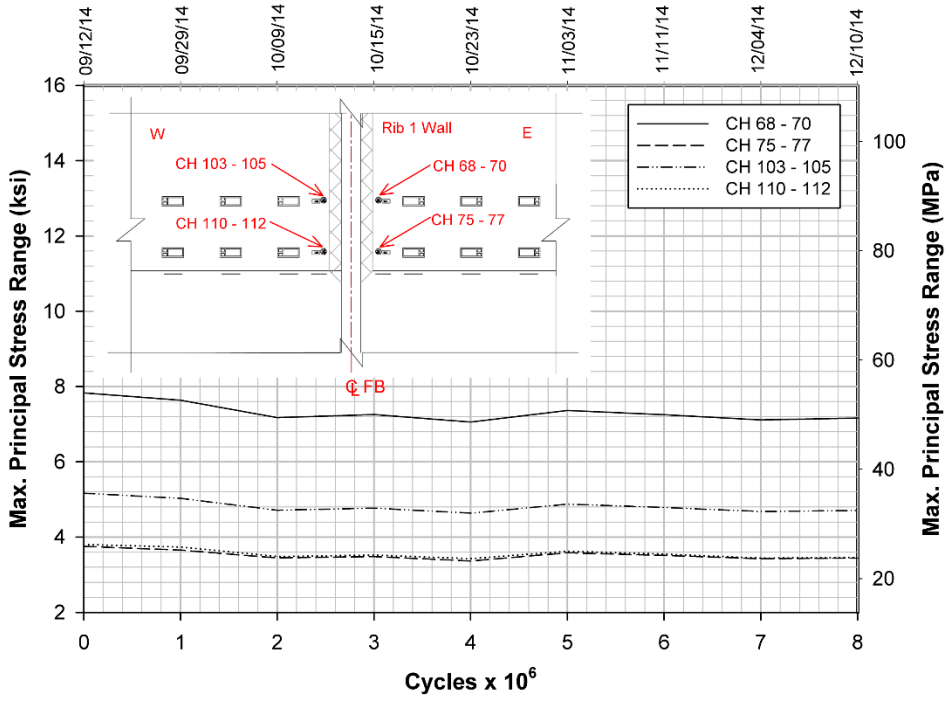

Figure 420. Changes in principal stress ranges at the rosettes on the south wall of Rib 1

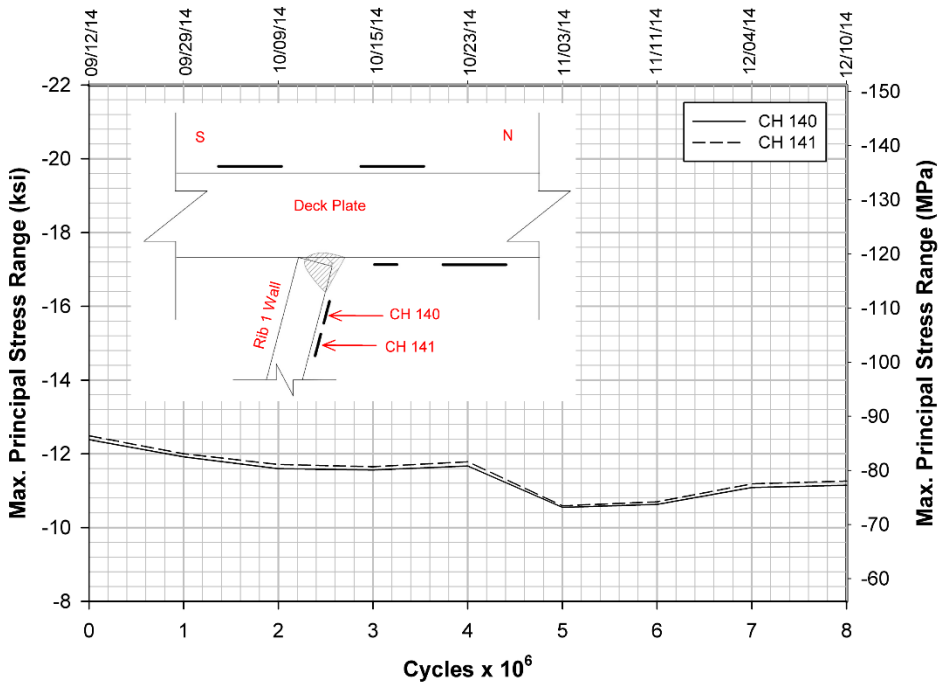

Figure 421. Changes in static test stress ranges at the gauges on north wall of Rib 1 near Rib 1-to-deck plate connection

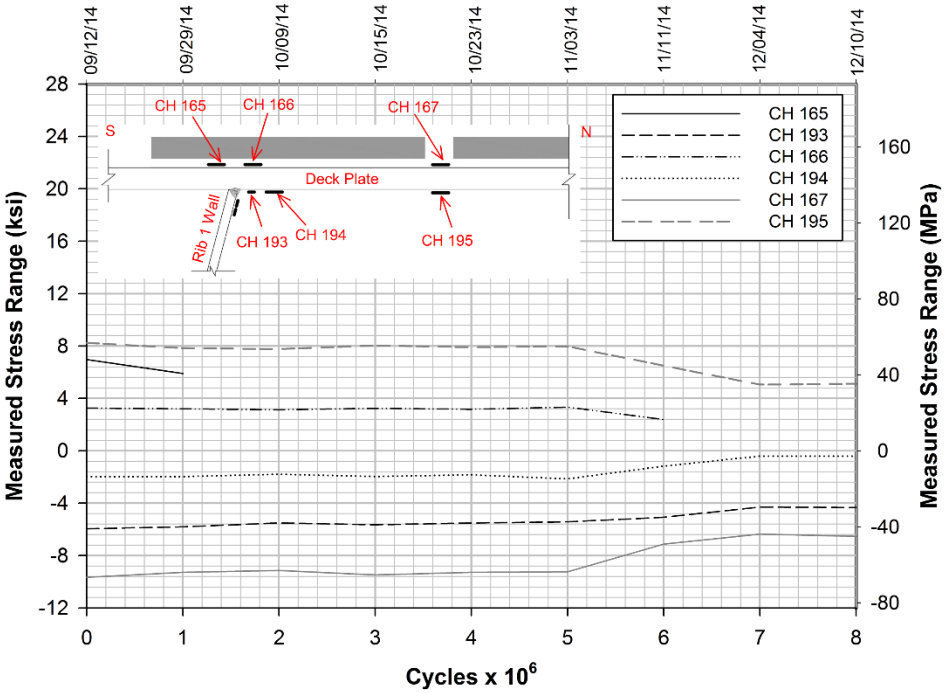

Figure 422. Changes in static test stress ranges at the deck plate gauges near Rib 1 at rib-to-deck plate connection

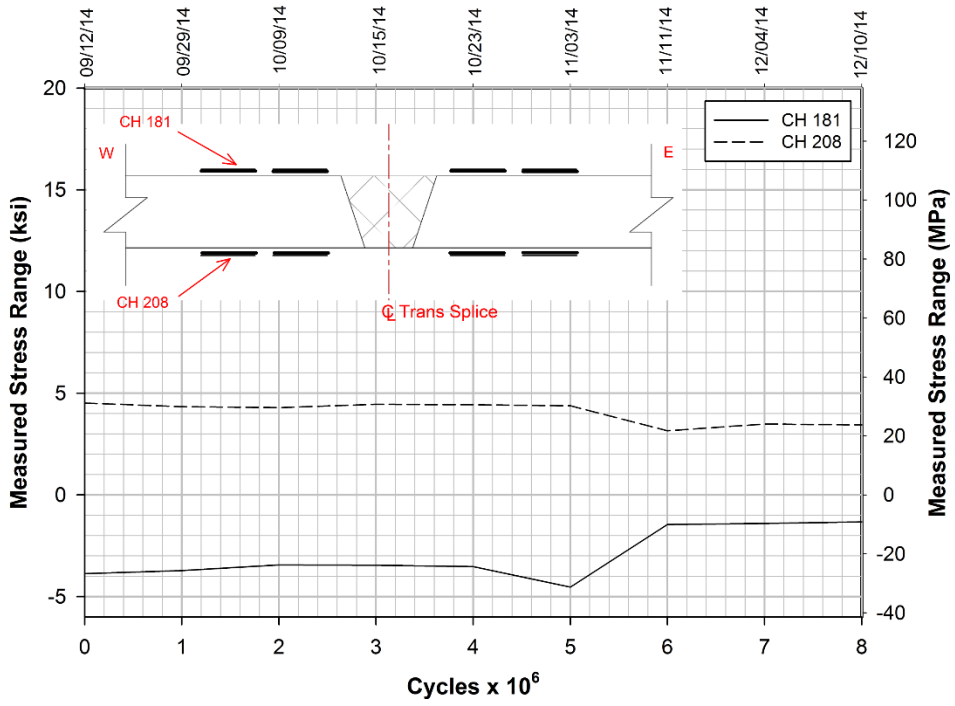

Figure 423. Changes in static test stress ranges at the gauges near the deck splice

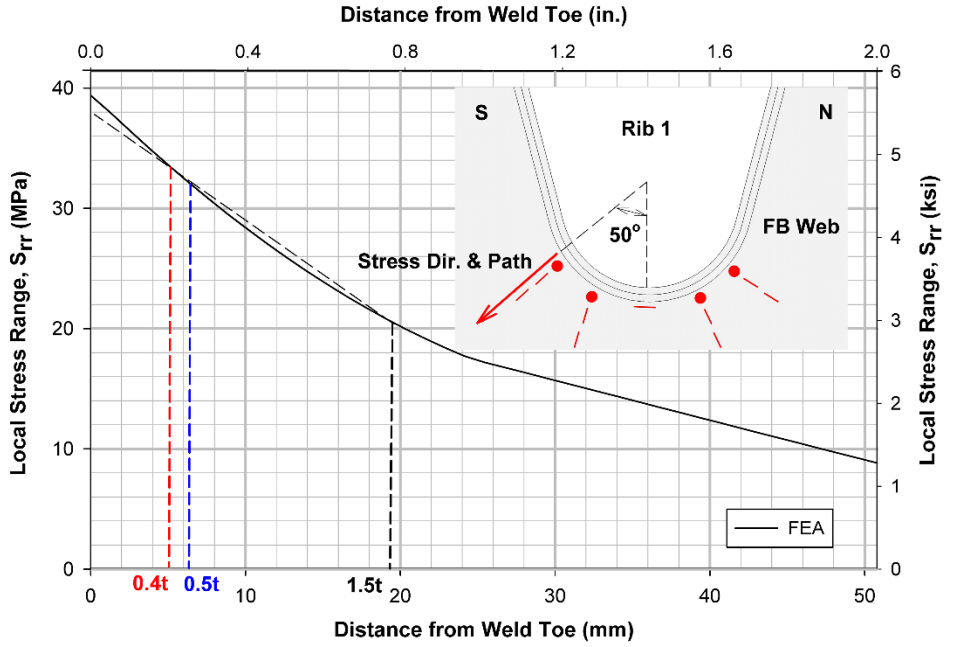

Figure 424. Reference points for extrapolation of stresses

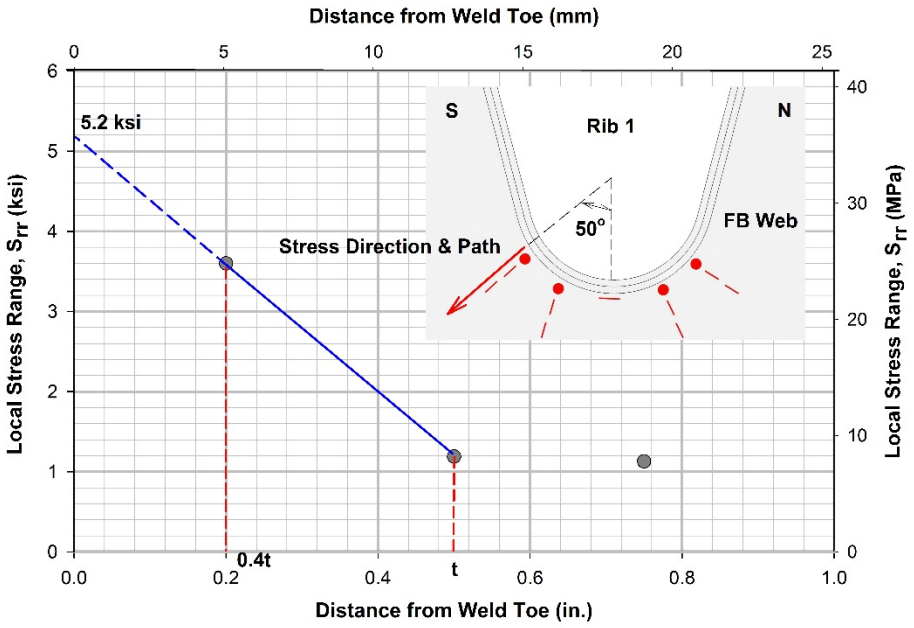

Figure 425. Method of extrapolation of stress to weld toe for rib-to-floor beam connection

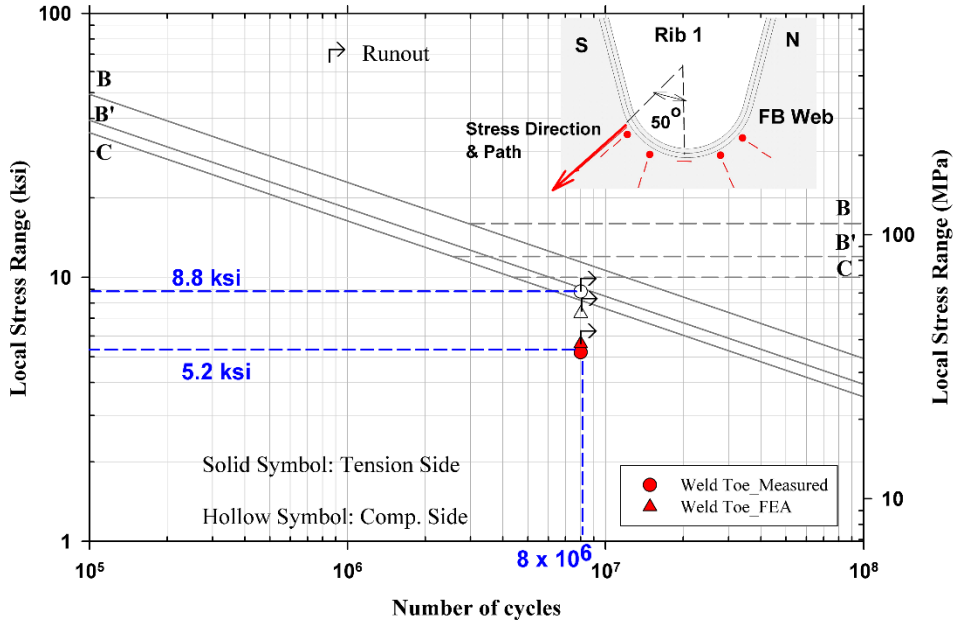

Figure 426. Assessment of fatigue performance of rib-to-floor beam connection against cracking from weld toe

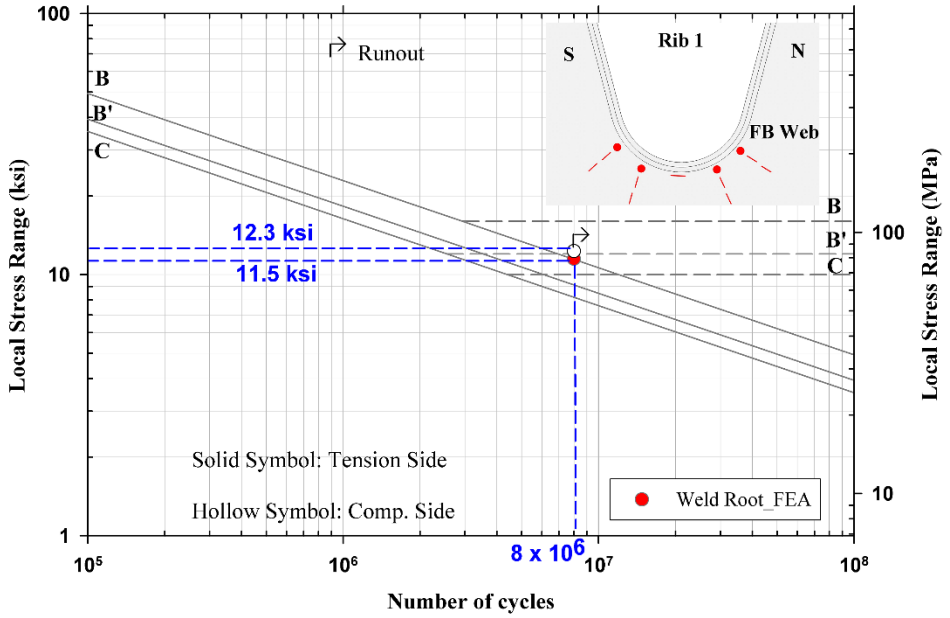

Figure 427. Assessment of fatigue performance of rib-to-floor beam connection against cracking from weld root

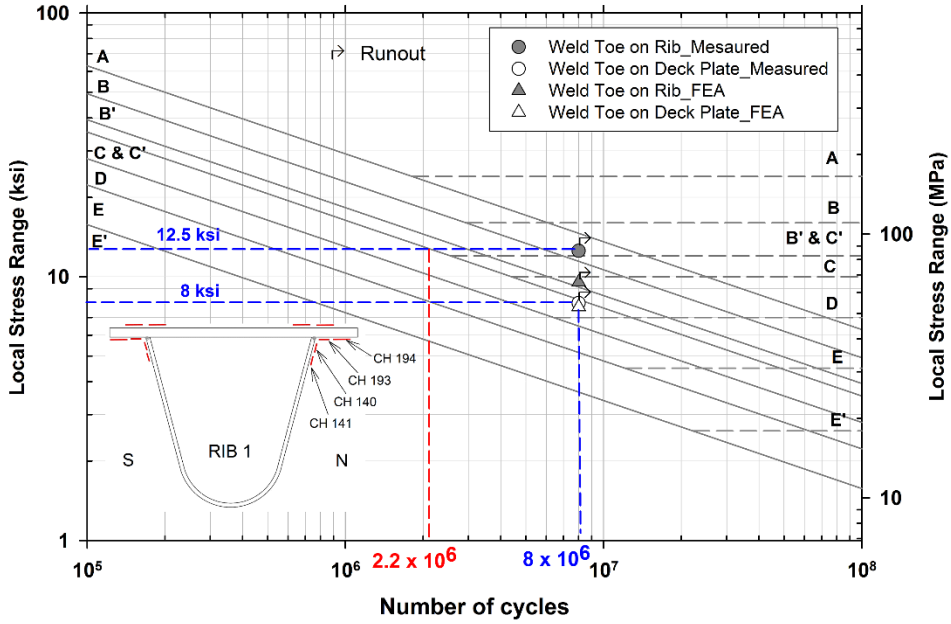

Figure 428. Assessment of fatigue performance of rib-to-deck plate connection at section Z-Z

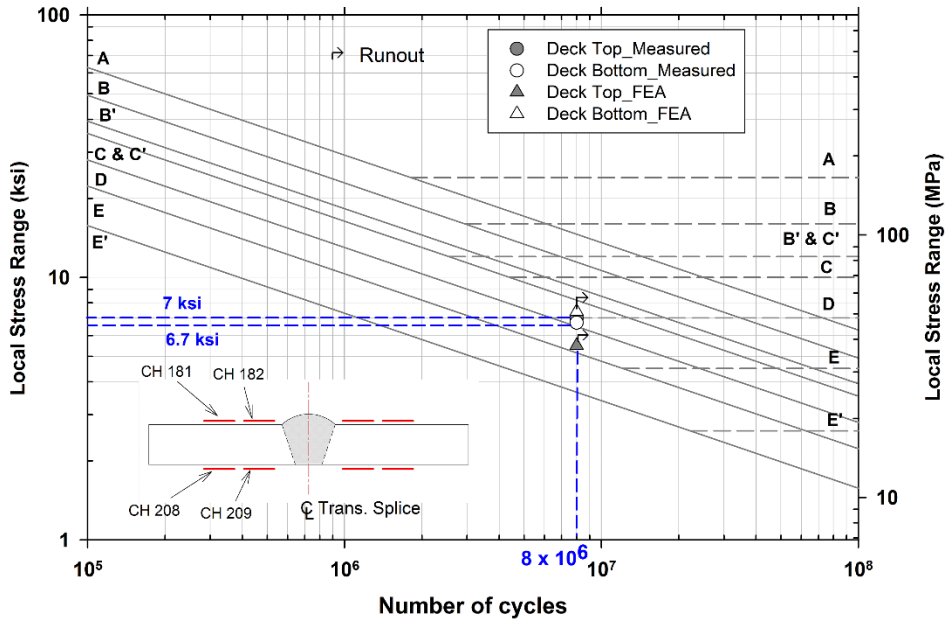

Figure 429. Assessment of fatigue performance of transverse CJP deck splice at section X-X

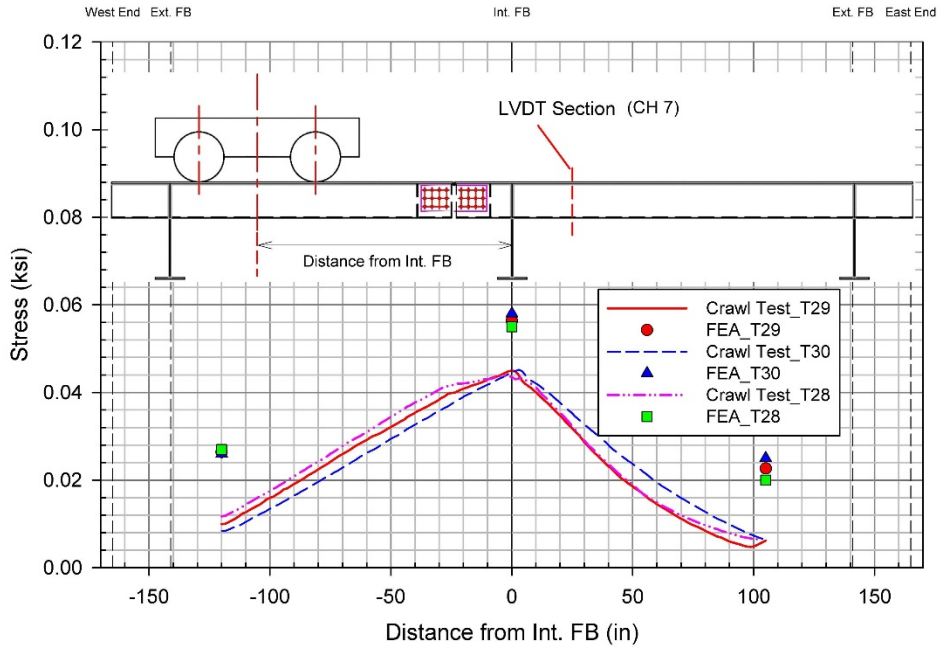

Figure 430. Displacement at LVDT under Rib 1 at section Z-Z (channel 7) for different crawl test positions

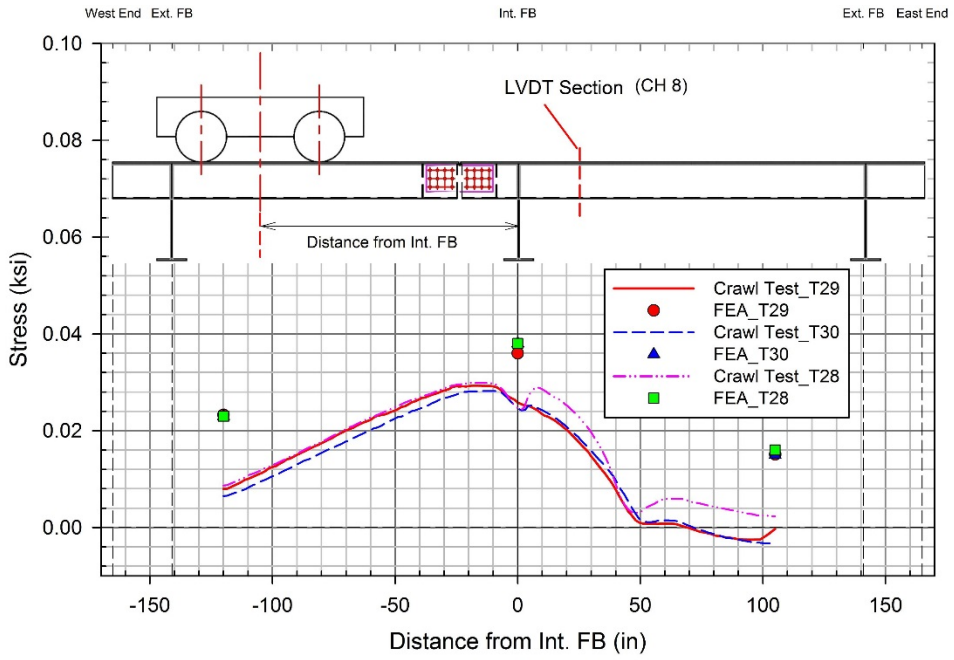

Figure 431. Displacement at LVDT under deck plate between ribs 1 and 2 at section Z-Z (channel 8) for different crawl test positions

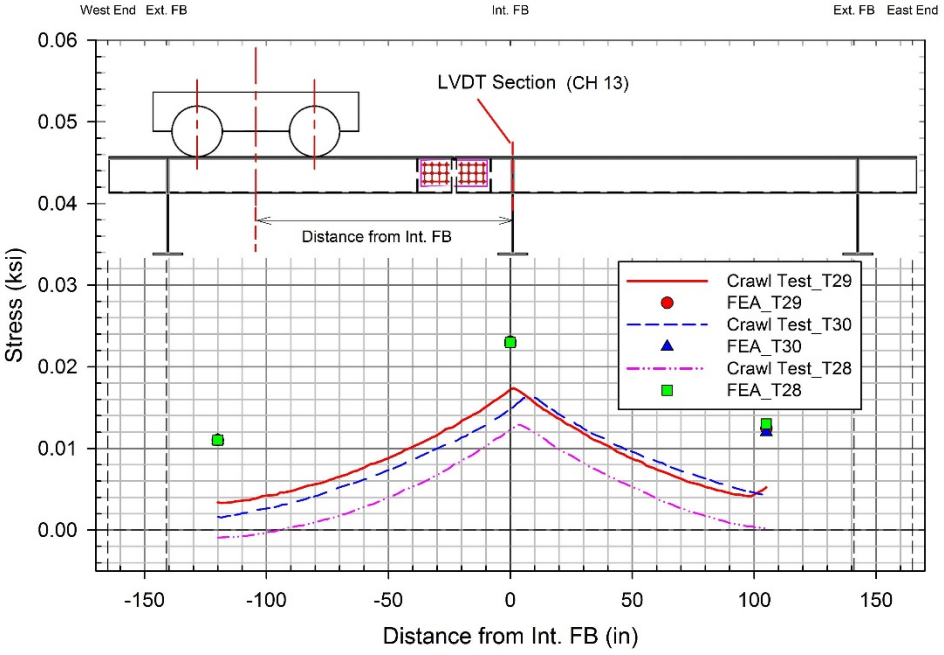

Figure 432. Displacement at LVDT under inner FB bottom flange at section Y-Y (channel 13) for different crawl test positions

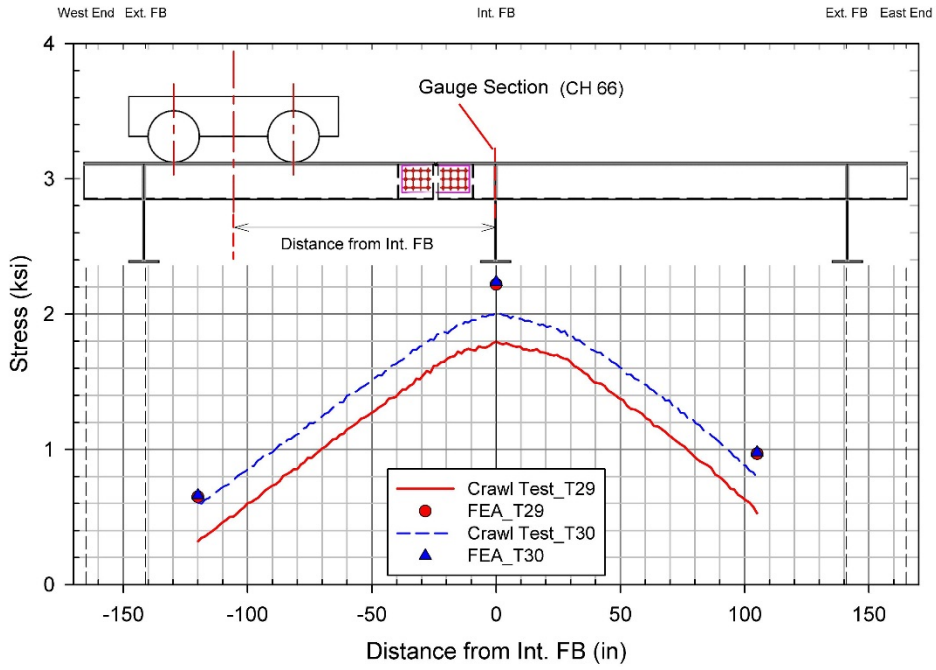

Figure 433. Transverse stress at bottom of inner FB (channel 66) at section Y-Y for different crawl test positions

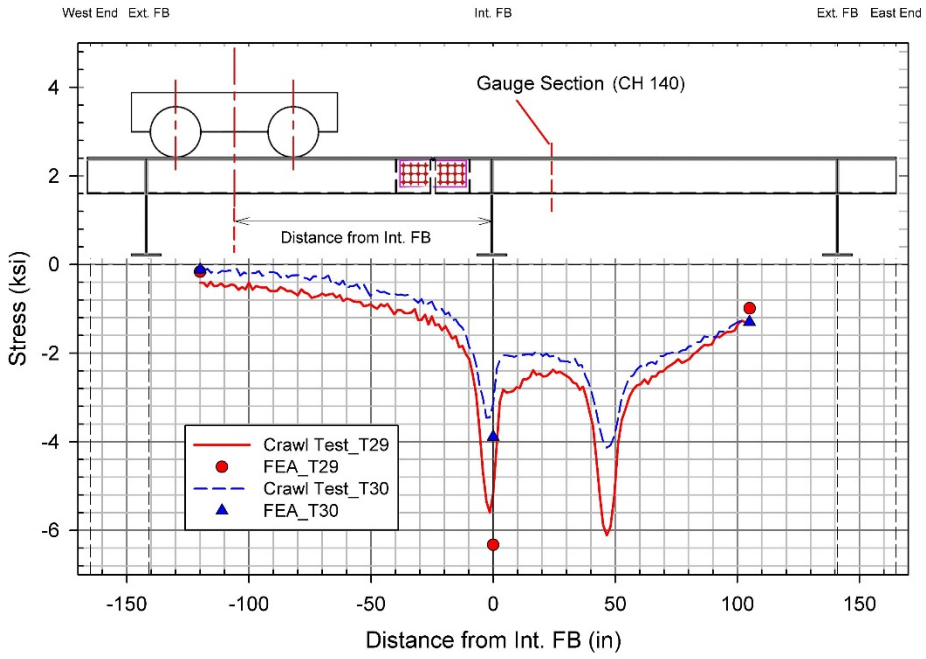

Figure 434. Transverse stress on the north wall of Rib 1 (channel 140) at section Z-Z for different crawl test positions

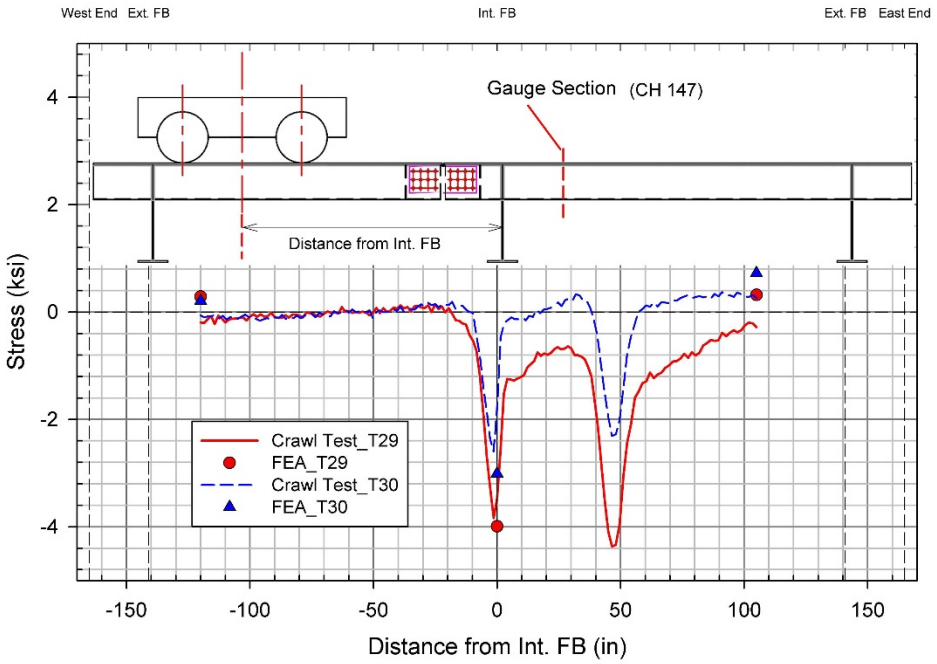

Figure 435. Transverse stress on the south wall of Rib 2 (channel 140) at section Z-Z for different crawl test positions

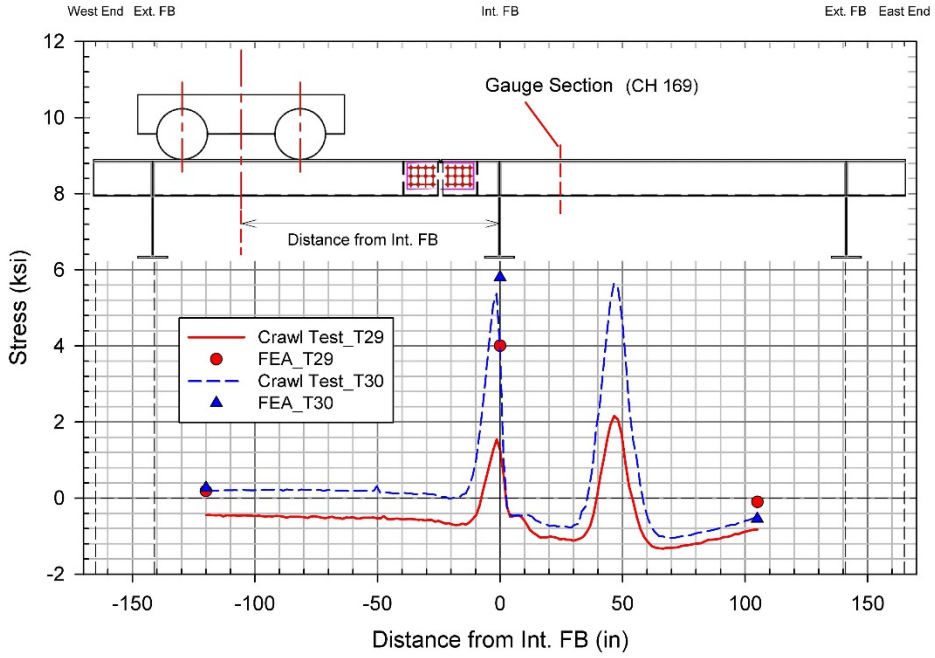

Figure 436. Transverse stress on top of deck plate to the south of Rib 2 (channel 169) for different crawl test positions

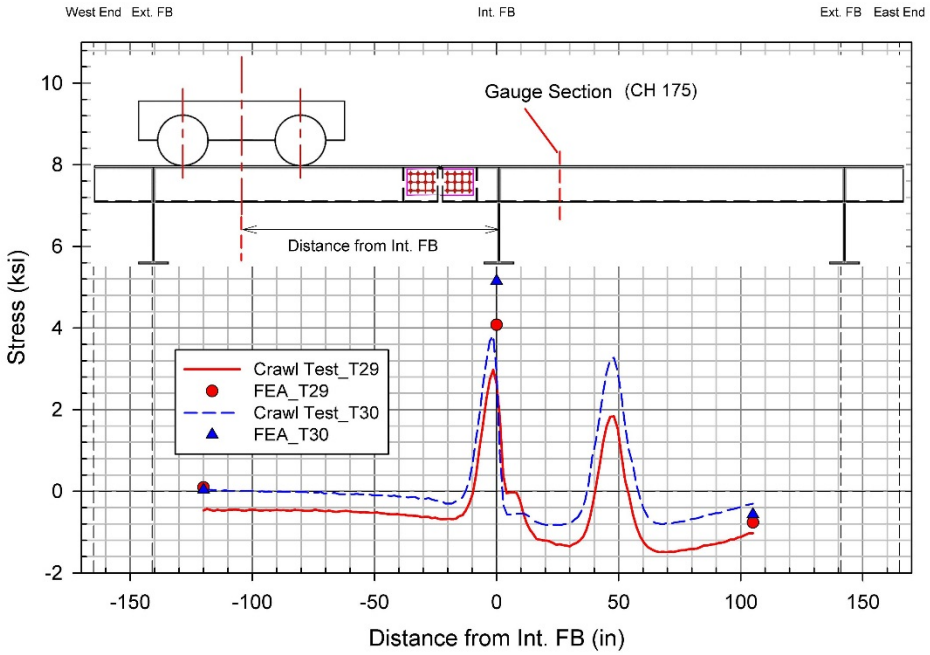

Figure 437. Transverse stress on top of deck plate to the north of Rib 4 (channel 175) for different crawl test positions

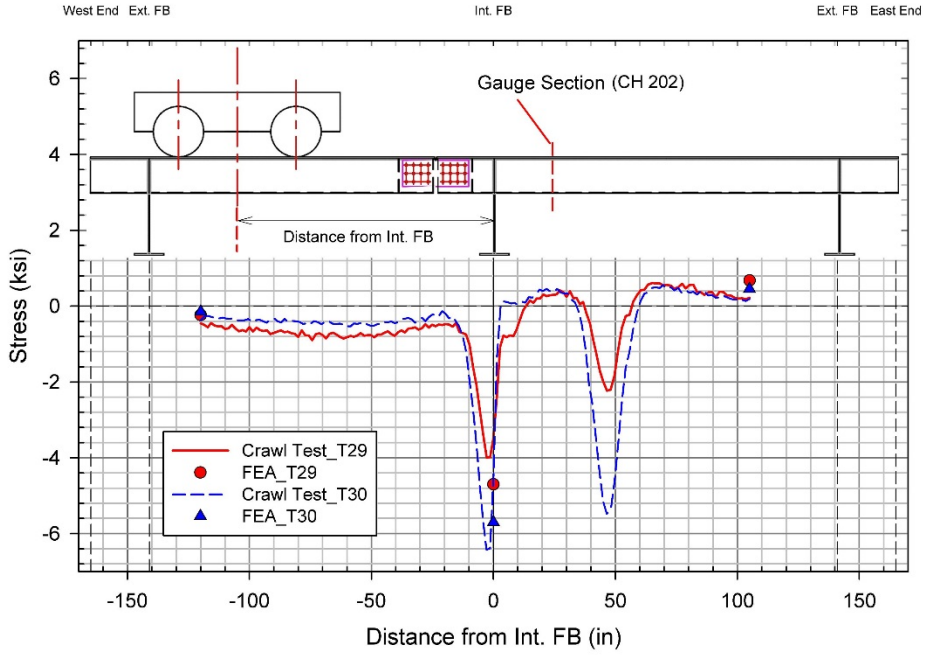

Figure 438. Transverse stress on underside of deck plate to the north of Rib 4 (channel 202) for different crawl test positions

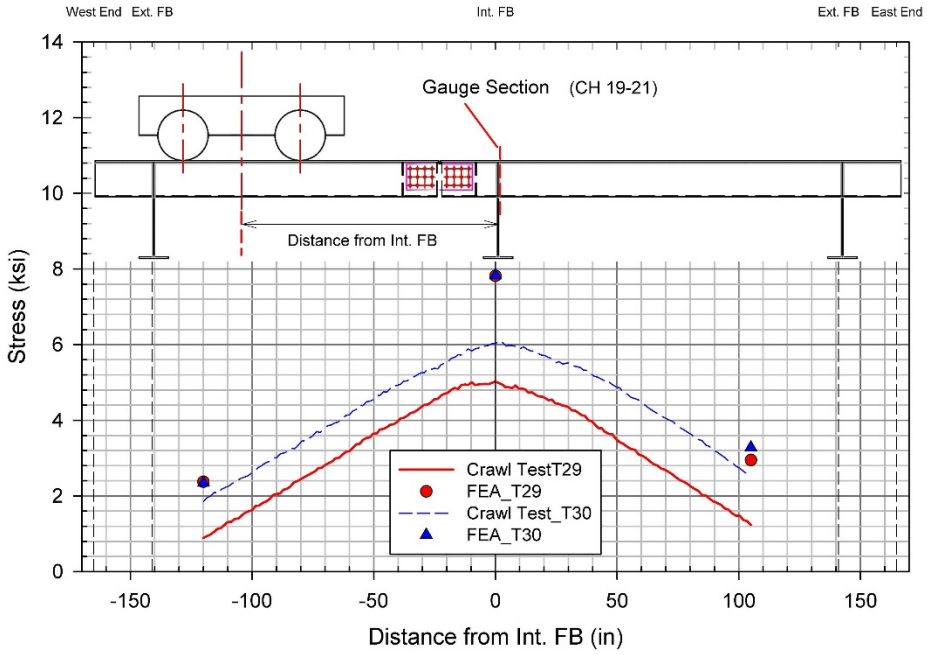

Figure 439. Principal stress at the south-east 25° rosette (channels 19-21) on the floor beam web for different crawl test positions

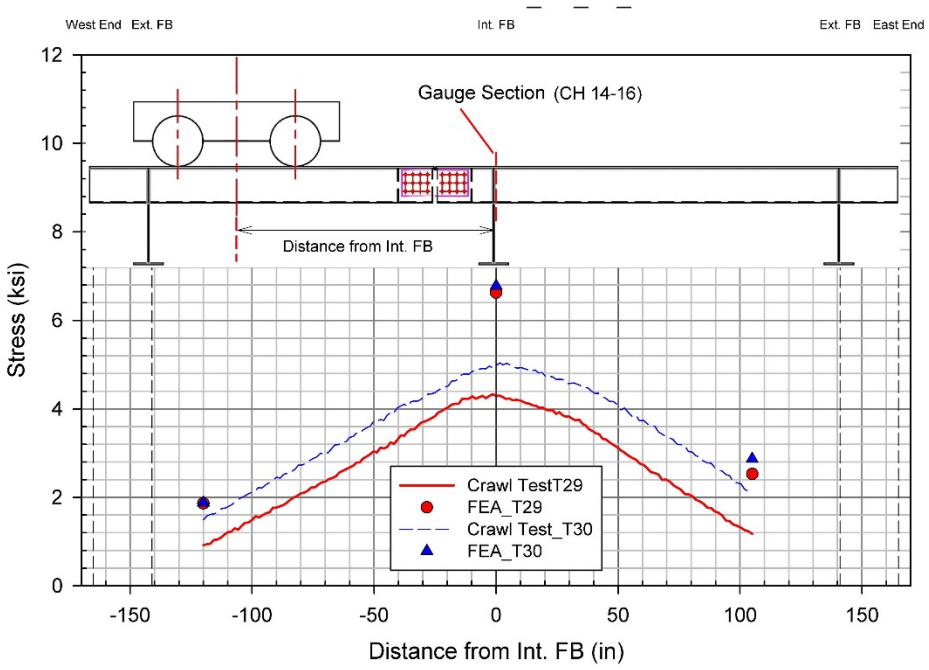

Figure 440. Principal stress at the south-east 50° rosette (channels 14-16) on the floor beam web for different crawl test positions

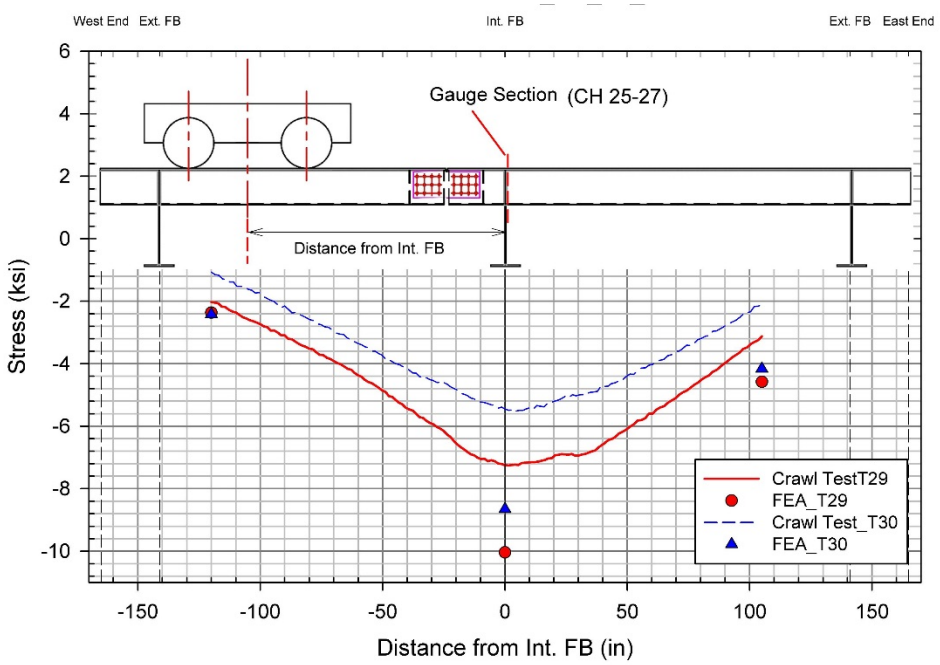

Figure 441. Principal stress at the north-east 50° rosette (channels 25-27) on the floor beam web for different crawl test positions

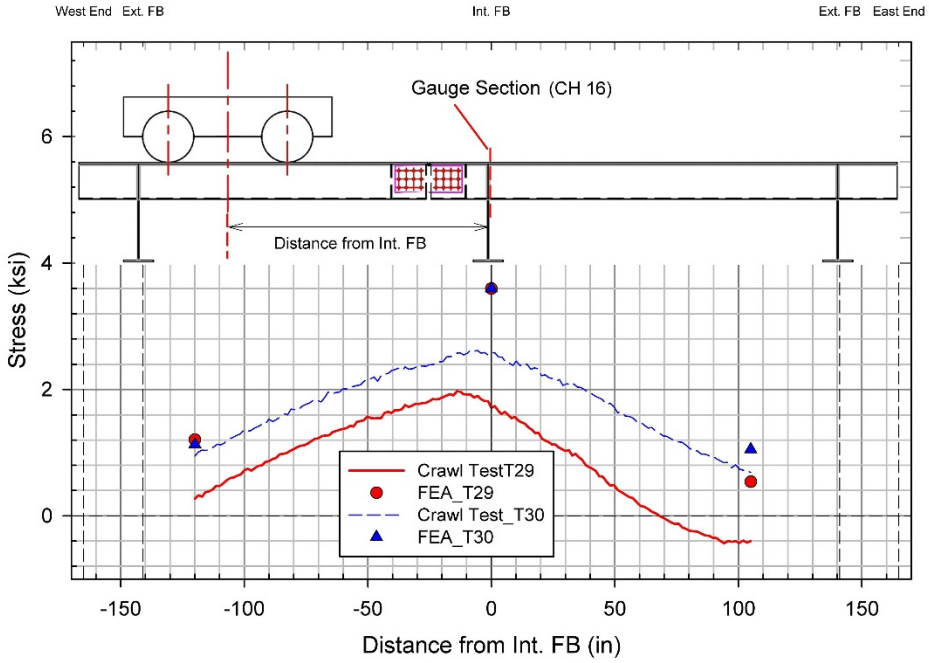

Figure 442. Stress normal to weld toe at the south-east 50° rosette (channel 16) on the floor beam web for different crawl test positions

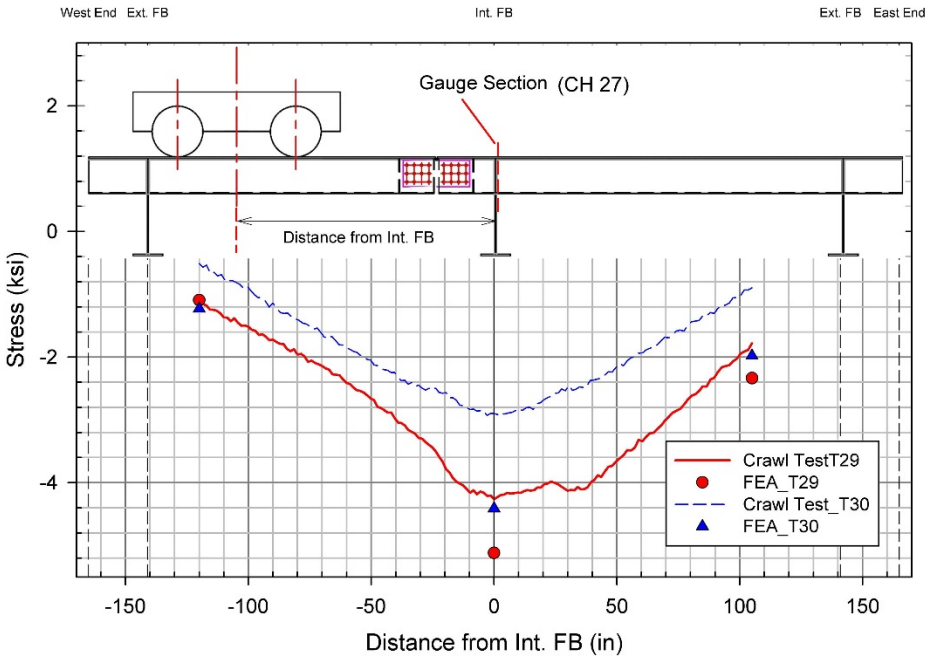

Figure 443. Stress normal to weld toe at the north-east 50° rosette (channel 27) on the floor beam web for different crawl test positions

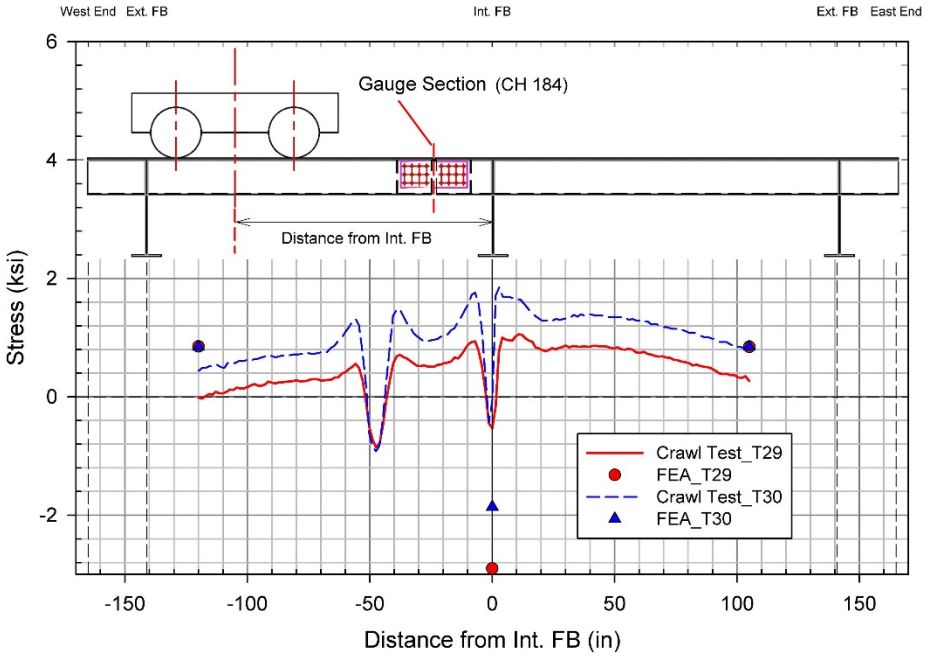

Figure 444. Longitudinal stress on top of deck plate below south-west wheel pair (channel 184) at the deck plate splice for different crawl test positions

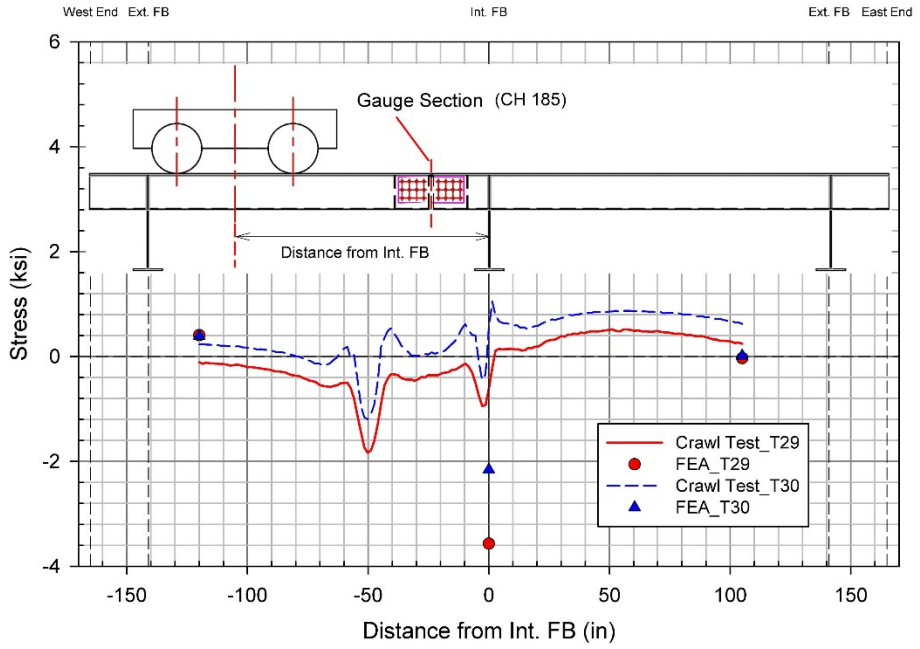

Figure 445. Longitudinal stress on top of deck plate below north-west wheel pair (channel 185) at the deck plate splice for different crawl test positions

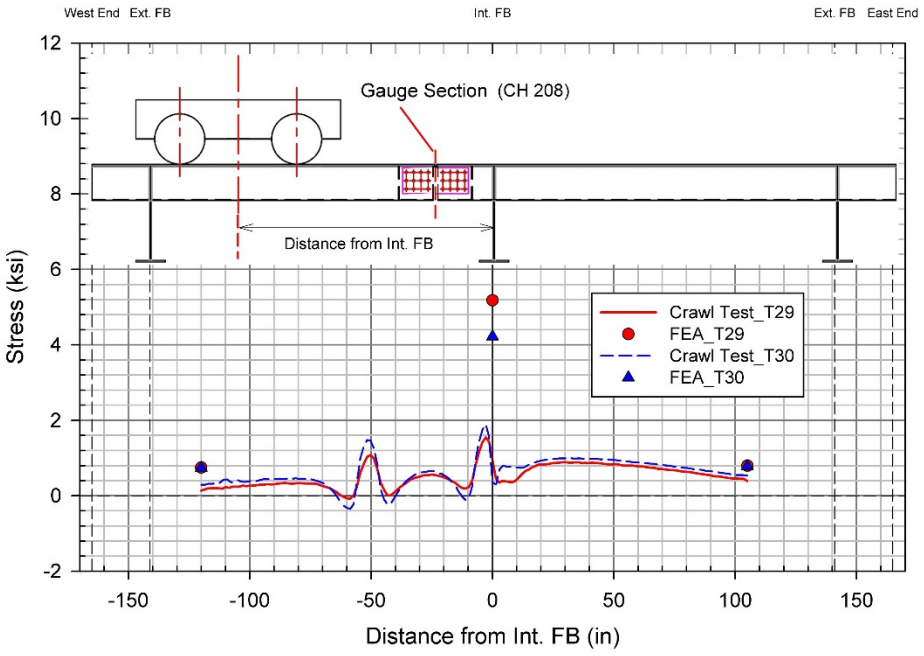

Figure 446. Longitudinal stress on underside of deck plate at the south-west wheel pair (channel 208) at the deck plate splice for different crawl test positions